2013

An Analysis of Synaptotagmins in Caenorhabditis Elegans

Laura Winzenread

AN ANALYSIS OF SYNAPTOTAGMINS IN CAENORHABDITIS ELEGANS

A Thesis Presented to the Faculty of

The Rockefeller University

in Partial Fulfillment of the Requirement for

the degree of Doctor of Philosophy

by

Laura Winzenread

June 2013

AN ANALYSIS OF SYNAPTOTAGMINS IN *CAENORHABDITIS ELEGANS*

Laura Winzenread, Ph.D.

The Rockefeller University 2013

Neurotransmission involves the release of neurotransmitters from a pre-synaptic neuron, followed by the reuptake of the protein components of the synaptic vesicle. The basic steps of synaptic vesicle exocytosis and endocytosis have been elucidated, and a number of components of the neurotransmission machinery have been identified. The exact function of each component, however, has been difficult to ascertain as many components act in multiple steps of neurotransmission.

In my thesis, I describe the identification of a mutation in the *snt-1* gene, which encodes a member of the synaptotagmin family in *Caenorhabditis elegans*. Synaptotagmins are best known as the calcium-sensing proteins for regulated synaptic vesicle exocytosis. I examined the effects of this lesion on a number of sensory neurons and motor neurons, in order to ascertain the uniformity of the phenotype between different regions of the nervous system. I utilized known synaptic vesicle markers to visualize synaptic vesicle distribution and to quantify the effect of a *snt-1* mutation *in vivo*. I found that *snt-1* reduced synaptic clustering of the SV marker RAB-3 in multiple cell types.

SNT-1 has previously been implicated in both exocytosis and endocytosis in GABAergic motor neurons of *C. elegans*. To extend these results, I examined the effect of SNT-1 on sensory neurons and used mutations to critically test the endocytosis-exocytosis model. To this end, I examined endocytosis and exocytosis mutants alone and in the *snt-1* mutant background. Blocking exocytosis in the *snt-1* mutant partially restores synaptic clustering of synaptic vesicle marker RAB-3. The suppression of the *snt-1* mutant phenotype is consistent with SNT-1 playing a key role in endocytosis downstream of regulated exocytosis.

The *C. elegans* genome contains seven identified synaptotagmin family members, of which only *snt-1* has previously been studied. I characterized the phenotypes of null mutations of *snt-2, snt-4, snt-5,* and *snt-6* in several sensory neurons, and found that some of the synaptotagmin family members affect synaptic vesicle distribution. The increased SV clustering in *snt-2, snt-4,* and *snt-5* mutants suggests that these synaptotagmins may promote SV exocytosis, inhibit endocytosis, or regulate the size of vesicle pools at the active zone. I also executed an analysis of a set of *snt* double mutants to determine which SNT family members were acting in shared or parallel pathways.

Acknowledgements

The work of this thesis would not have been possible without the support and encouragement of many, many people.

First, my incredible advisor, Cori Bargmann, whose mentorship and guidance led me through graduate school and my twenties, should be thanked every day. She is a very talented and passionate scientist, and the world has already benefitted greatly from her work. But more than that, she cultivates a lab of intelligent, generous, and funny people. Being under Cori Bargmann's wing is a privileged and prized place, and I look forward to years of trying to repay the favor that she has shown me.

My committee chair Leslie Vosshall, who talked me through important decisions, is owed a debt of gratitude. She showed me firsthand, what life as a high-achieving woman in science is like, with our adventure to Lawrence, Kansas. Leslie's frank advice and approachability made her a wonderful confidante and mentor, and her faith in my potential was unwavering.

My committee member Mike Young offered me the wisest and shortest advice in graduate school that became a mantra during the final years: "Persist." Mike's calming presence and logical, rational thought process contributed elementally to this work.

My labmates past and present, whose generosity with valuable reagents, including time and brain power, have both shaped and spoiled me as a young scientist: (In alphabetical order) Sara Abrahamsson, Dirk Albrecht, Manoush

Ardzivian, Sarah Bauer Huang, Andres Bendesky, Sreekanth Chalisani, Andy Chang, Christine Cho, Nikos Chronis, Chiou-Fen Chuang, Margaret Ebert, Evan Feinberg, Steven Flavell, Jennifer Garrison, Elizabeth Glater, Josh Greene, Andrew Gordus, Massimo Hilliard, Holly Hunnicut, Heeun Jang, Hernan Jaramillo, Xin Jin, Saul Kato, Alex Katsov, Jason Kennerdell, Priscilla Kong, Johannes Larsch, Greg Lee, Bibi Lesch, Sagi Levy, Meghan Lockard, Evan Macosko, Tapan Maniar, Patrick McGrath, Navin Pokala, Yasunori Saheki, Makoto Tsunozaki, Christian Woods, Yifan Xu, Manuel Zimmer, and Yun Zhang.

I also could not have completed this work without the support of my friends and family. My mother and father, Anne and Michael, have watched with pride as I've struggled and developed as a scientist. My brother, Guy, has encouraged me to take the breaks needed to increase productivity, and also has never once stopped believing in me. My friends Kate Hurley, Sam Weinger, Julia Gaston, Estelle Montgomery, Kelly Jones, and Nicole Creanza have always been ready with a pick-me-up on the days when no experiments were working.

The fantastic people in the Dean's Office have also been instrumental in their support. They make graduate school as bureaucracy-free as possible; they serve to alleviate the pain of all of the students and to facilitate our success.

I will be eternally grateful for the support of Team Laura.

Table of Contents

List of Figures

List of Tables

Introduction

An Introduction to Neurotransmission and Its Molecular Components

Neurons communicate with each other via specialized regions at points of cell contact known as synapses. Typically, when a pre-synaptic neuron releases neurotransmitters, the neurotransmitter receptor of the post-synaptic neuron binds to the released ligand and opens to allow depolarizing cations or hyperpolarizing ions into the neuron; these individual synaptic events (miniEPSCs) on the dendrite and cell body are summed to regulate postsynaptic action potentials. An action potential travels along the axon to the presynaptic region of that neuron, where it leads to the opening of voltage-gated calcium channels. As calcium flows into the neuron, proteins that control synaptic vesicle release sense the local calcium influx via calcium binding domains. These calcium-sensing proteins allow the vesicle-release machinery to fuse docked vesicles with the cell membrane, driving neurotransmitter release into the synaptic cleft and the transfer of information through a new set of synapses (Figure 1).

Before a vesicle fuses with the membrane to release neurotransmitter, the vesicle must first be trafficked correctly to the active zone of the presynaptic neuron and then docked close to the plasma membrane. A docked vesicle is recognized by its proximity to the active zone in electron micrographs. After docking, vesicles have to be primed, a process that makes them release-

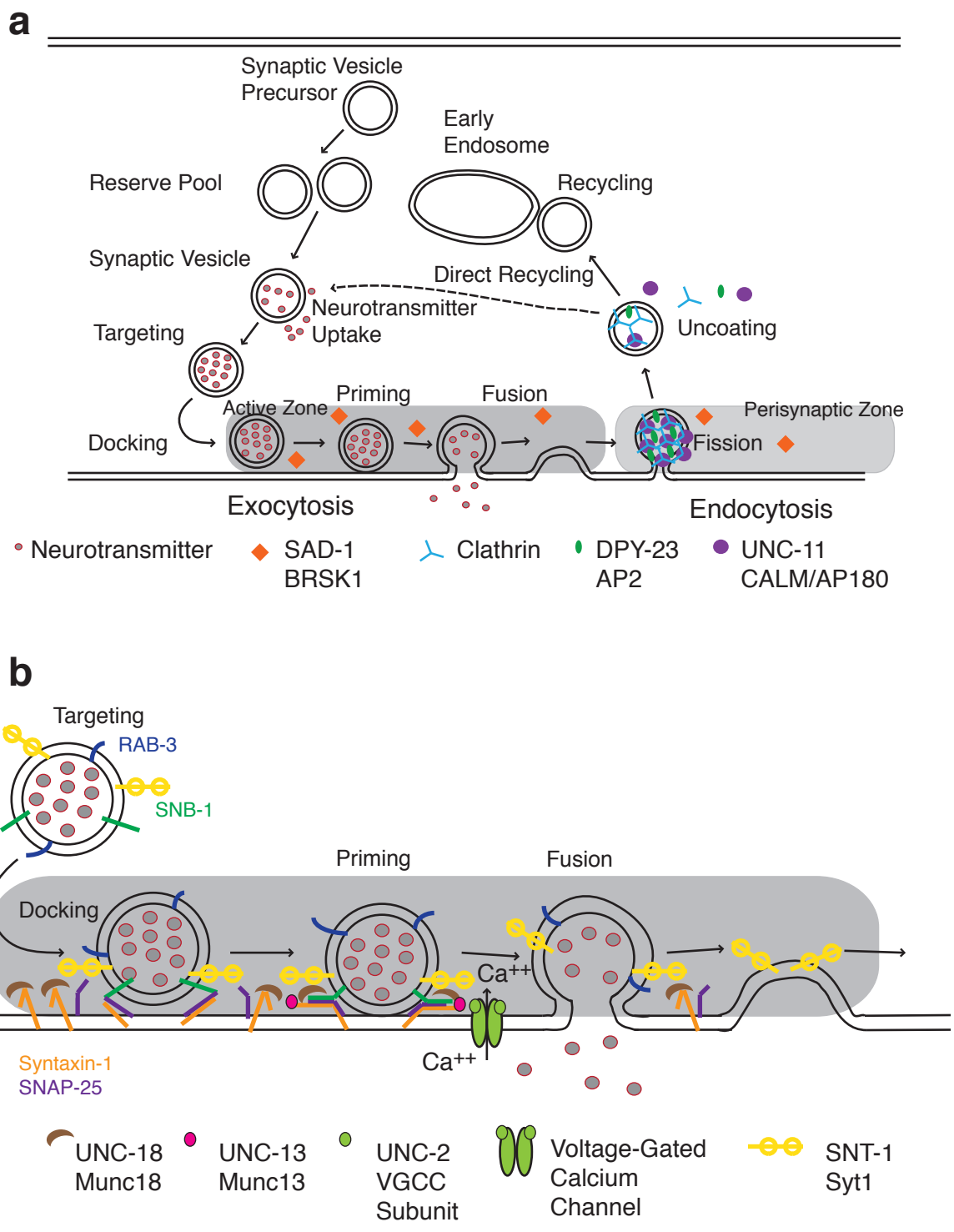

Figure 1. A simple model of neurotransmission (a) The life cycle of a synaptic vesicle as it undergoes exocytosis and endocytosis. (b) A closer view of the steps of synaptic vesicle exocytosis, with the formation of the SNARE complex and some associated proteins represented.

competent, but still blocked from full fusion until they receive the appropriate signal to fuse (reviewed in Barclay *et al.,* 2012).

Active zones are regions in the presynaptic neuron where the calcium channels, synaptic vesicles, and vesicle release machinery can be collectively confined, thus facilitating rapid neurotransmission in response to calcium signals (reviewed in Sudhof and Rizo, 2011). The calcium signals within the active zone are highly transient, on the order of less than one msec, because the calcium ion itself is promptly buffered (Meinrenken *et al.,* 2003). This rapid signal is sufficient for neurotransmitter release (Augustine *et al.,* 2003). In *Caenorhabditis elegans*, *unc-2* encodes the corresponding calcium channel alpha subunit (Schafer and Kenyon, 1995).

The SNAREs, or soluble N-ethylmalemide-sensitive factor attachment protein receptors, are essential for vesicle fusion and comprised of three parts: synaptobrevin, syntaxin, and SNAP-25 (Sudhof *et al.,* 2009). The vSNARE synaptobrevin is a component of synaptic vesicles, and the tSNARE components syntaxin and SNAP-25 are localized to the target plasma membrane. The matchup of vSNARE and tSNAREs leads to a formation of a SNARE complex, a four-helix coiled-coil bundle competent for fusion (Sudhof and Rizo, 2011). As well as being directly involved in fusion, SNAREs play some role in docking and priming steps. In mammals, SNARE complexes lacking synaptobrevin have severely impaired vesicle docking (de Wit *et al.,* 2009), and in *Caenorhabditis elegans*, the syntaxin homolog *unc-64* has a role in vesicle docking (Hammarlund

et al., 2007). The SNARE complex is disassembled by NSF, the N-ethylmalemide-sensitive factor, which functions as an ATPase (Sollner *et al.,*1993). All three of the SNARE protein homologs are essential for nervous system function in *Caenorhabditis elegans* (Brenner, 1974). Neurotoxin experiments conducted in 1992 and 1993 showed that all three SNARE proteins are necessary for synaptic vesicle fusion (Reviewed in Sudhof and Rizo, 2011). Briefly, the studied neurotoxins infiltrate the presynaptic active zone and behave as proteases that target either synaptobrevin, syntaxin, or SNAP-25, specifically impeding presynaptic membrane fusion without perturbing the morphology of the axon (Link *et al.,* 1992; Schiavo *et al.,* 1992**;** Blasi *et al,* 1993 a, b).

The amount of SNARE complex assembly is correlated with the size of the readily releasable pool of vesicles (Lonart and Sudhof, 2000). The readily releasable pool of vesicles consists of docked vesicles in the active zone; these are the first vesicles to undergo fusion upon stimulation (Neher, 1998; Pieribone *et al.,* 1995; Stevens and Tsujimoto, *et al.* 1995).

The entire recycling vesicle pool is comprised of both the readily-releasable and reserve pool of vesicles (Fernandez-Alfonso and Ryan, 2008). The proportion of the total vesicle pool that recycles fluctuates from synapse to synapse and from neuron to neuron in hippocampal cell culture. This variation is not dependent on the age of the culture, but high vesicle number in a bouton is correlated with a higher percentage of recycling vesicles. Recycling and resting

pools of vesicles both seem to shuttle between synaptic boutons (Fernandez-Alfonso and Ryan, 2008).

Generally, there are three recognized types of synaptic exocytosis: evoked neurotransmitter release, asynchronous release (Pang and Sudhof, 2010), and spontaneous mini release (Reviewed in Sudhof, 2012a). Evoked release is triggered by calcium influx. Asynchronous release is difficult to detect unless the principal calcium sensor for evoked release is ablated **(**Geppert *et al.,* 1994). Spontaneous release was first uncovered by Fatt and Katz and may or may not use an alternative vesicle pool than is used during evoked release (Sara *et al.,* 2005).

UNC-13/Munc13 is an active zone localized protein (Brose *et al.,* 1995). UNC-13/Munc13 facilitates SNARE complex formation most likely through via its interactions with syntaxin (Betz *et al.,* 1997; Brose *et al.,* 2000), and UNC-13/Munc13 proteins are essential for priming of synaptic vesicles **(**Augustin *et al.,* 1999). In an *unc-13* mutant background, vesicles appear to contact the plasma membrane, but synaptic vesicle release is blocked **(**Augustin *et al.,* 1999). *unc-13* mutants were assayed for their spontaneous miniPSC rate, to determine if synaptic vesicles were still primed in the absence of functional UNC-13. The spontaneous miniPSC rate was decreased if not absent for all alleles tested, indicating a lack of primed vesicles. In addition, *unc-13* mutant animals had more synaptic vesicles docked, but this was due to an overall increase in SV number as the percentage of docked vesicles was the same in wild type animals as in

unc-13 mutants (Richmond, *et al.,* 1999). UNC-13 is required at a step after docking, and may actually be required for more than one step. Without functional UNC-13, which normally primes synaptic vesicles for fusion, the readily-releasable pool of synaptic vesicles decreases, in spite of an increase in the number of docked vesicles. UNC-13 is proposed to play a role in priming by promoting the opening of syntaxin (reviewed in Weimer and Richmond *et al.,* 2005). In fact, UNC-13 must bind to syntaxin in order for SV exocytosis to proceed properly (Madison *et al.,* 2005). *unc-13* encodes a protein with C1 and C2 homology domains (Maruyama and Brenner, 1991), that binds diacylglycerol (DAG), phorbol esters, calcium ions, and phospholipids (Burns and Bell, 1991; Kaibuchi *et al.,* 1989). These and other results are among the arguments that SNARE complex formation facilitated by UNC-13 is the biochemical instantiation of priming.

UNC-18/Munc18 is a member of the SM (Sec1/Munc18 like) family of proteins that function as partners of the SNARE complex (Jahn and Fasshauer, 2012). *unc-18* is expressed in all neurons, and *unc-18* mutants are severely uncoordinated in their locomotion, a phenotype referred to as Unc (Weimer and Richmond, 2005; Hosono and Kamiya, 1991). Fusion of synaptic vesicles is severely diminished in the absence of either SM proteins or SNARE proteins (reviewed in Sudhof, 2012b). Munc18 was isolated bound to the t-SNARE syntaxin-1 (Hata *et al.,* 1993). SM protein binding to syntaxin-1 is proposed to recruit the SM protein to the site of SV fusion. SM proteins are then thought to

interact with the components of the SNARE complex and to promote SNARE complex assembly (Jahn and Fasshauer, 2012). Munc18 protein is shaped like an arch, with a central crevice that binds to syntaxin-1 (Burkhardt *et al.,* 2008; Misura *et al.,* 2000). Munc18 may keep syntaxin closed to prevent premature SNARE assembly (Jahn and Fasshauer, 2012). Munc13 is required for Munc18 to disengage from the closed syntaxin-1 protein; Munc18 then binds to synaptobrevin in the SNARE complex (reviewed in Parisotto *et al*., 2012). The pool of primed vesicles is reduced in *unc-18* mutants, hinting that UNC-18 plays a role in either vesicle priming, vesicle docking, or both stages of vesicle fusion. *unc-18* mutants contain more synaptic vesicles than wildtype animals, but the proportion of docked vesicles is reduced, suggesting that UNC-18 promotes vesicle docking (reviewed in Weimer and Richmond, 2005). In addition, some reports in *C. elegans unc-18 (e81)* null mutants show decreased number of synaptic vesicles docked at the plasma membrane (Weimer *et al.,* 2003) and decreased number of synaptic vesicles tethered within one vesicle diameter (0nm to <25nm) from the plasma membrane (Gracheva *et al.,* 2010). Munc18 binds Rab3 in mammalian cell culture, suggesting one means of Munc18 interacting with synaptic vesicles **(**Graham *et al.,* 2008).

Rab proteins are GTP-binding proteins that are thought to play various roles in vesicular membrane trafficking (reviewed in Stahl *et al.,* 1996). Rab3 proteins specifically associate with synaptic vesicles in mammalian brain (Fischer von Mollard *et al*., 1991). Because Rab3 proteins disassociate from synaptic vesicles

during exocytosis, they are believed to play a role in the release of neurotransmitters (Fischer von Mollard *et al.,* 1991). The mammalian homolog of RAB-3, Rab3A, associates with synaptic vesicles after Golgi transport and dissociates from SVs during recycling. Rab3A protein remains associated with SV membranes during the fusion step of exocytosis (Matteoli *et al.,* 1991). Rab3A appears to dissociate from synaptic vesicles after nerve terminal stimulation (Fisher v Mollard *et al.,* 1991). In *C. elegans rab-3* mutants, the distribution of synaptic vesicles in the presynaptic terminals is diffuse with fewer vesicles clustered near the active zone, hinting at a defect in SV docking (Nonet *et al.,* 1997). The strong association of RAB-3 with synaptic vesicles makes it a widely-used marker of synaptic vesicles *in vivo*.

Another protein thought to be an accurate marker of presynaptic vesicle clusters is synaptobrevin (Nonet,1999). Alterations of the distribution of GFP::SNB-1 can be utilized to identify defects in SV recycling. Accumulation of GFP::SNB-1 in the plasma membrane indicates endocytic defects; abnormal accumulation of GFP::SNB-1 in puncta in the axon, whether by increased puncta number, larger puncta, or brighter puncta often indicates exocytic defects (Sieburth *et al.,* 2005). Synaptic proteins distribute in a punctate pattern in *C. elegans* axons because neurons form *en passant* synapses (Ch'ng *et al.,* 2008). Fluorescent puncta created by tagged SV-associated proteins such as SNB-1 and RAB-3 correspond to pre-synaptic vesicle clusters (Sieburth *et al.,* 2005). The brightness of GFP::SNB-1 punctal fluorescence correlates with SV numbers

in the presynaptic regions; the brightness of diffuse GFP::SNB-1 in the axon correlates with the amount of synaptobrevin in the plasma membrane (Sieburth *et al.,* 2005; Dittman and Kaplan, 2006; Fernandez-Alfonso *et al.,* 2006; Ch'ng *et al.,* 2008).

sad-1 encodes a serine/threonine kinase that localizes to regions of the axon enriched in synapses. *sad-1* mutant animals have disorganized clusters of synaptic vesicles and axon termination defects in some sensory neurons. Overexpression of SAD-1 results in the formation of ectopic SV clusters in the dendrite. SAD-1 is necessary for presynaptic vesicle clustering, and it regulates the size, shape and position of the SV clusters (Crump *et al.,* 2001).

unc-104 encodes a member of the kinesin family, and UNC-104 functions as a microtubule-based motor in the nervous system. *unc-104* expression is restricted to neurons; UNC-104 transports synaptic vesicles anterogradely along the axon to the active zone (Hall and Hedgecock, 1991).

Synaptic vesicle endocytosis occurs at the perisynaptic zone, which is adjacent to the active zone (Brodin and Shupliakov, 2006). Clathrin-mediated endocytosis is considered the dominant endocytic pathway and requires the clathrin adaptor proteins AP2 and AP180. AP2 and AP180 are recruited to the SV fusion site, potentially via interactions with synaptotagmin and synaptobrevin (Reviewed in Richmond, 2007). In *C. elegans, dpy-23* encodes the μ2 (AP50) subunit of the AP2 complex (Harris *et al.,* 2001). *dpy-23* mutants have fewer SVs, suggesting that DPY-23 plays a role in synaptic endocytosis (Gu *et al.,* 2008).

UNC-11 is the CALM/AP180 homolog in *C. elegans*. UNC-11 accumulates at synapses, and synaptobrevin is mislocalized in *unc-11* mutants (Nonet *et al.,* 1999). After clathrin is recruited to the site where vesicle fusion occurred, clathrin accumulation and formation initiates vesicle budding (reviewed in Richmond, 2007).

Dynamin DYN-1 separates the budding vesicle from the plasma membrane in a step called fission. Dynamin interacts with UNC-57 endophilin (Ringstad *et al.,* 1997), but it is unclear how this interaction impacts fission. UNC-57 endophilin acts with UNC-26 synaptojanin to encourage budding of endocytosing vesicles (Schuske *et al.,* 2003 and Harris *et al.,* 2000**;** reviewed in Richmond, 2007).

After fission of the endocytosing vesicle from the plasma membrane, the clathrin cage disassembles in a process referred to as uncoating. Following uncoating, vesicles may be sorted to the pool of vesicles localized to the active zone for re-release or they may be transported to early endosomes for total disassembly preceding repacking into a new synaptic vesicle (reviewed in Richmond, 2007).

Interestingly, calcium is believed to play a role in regulating endocytosis in addition to its critical role in triggering exocytosis. For example, in hippocampal neuronal cell culture, the rate of endocytosis has been shown to increase to a "saturated" level as intracellular calcium increases (Balaji *et al.,* 2008). Furthermore, P/Q-type voltage-gated calcium channels, such as the VGCC with

the UNC-2 subunit that is involved in triggering exocytosis, appear to provide the calcium influx that also elicits endocytosis (Xue *et al.,* 2012).

Synaptotagmin is a synaptic calcium sensor

One of the proteins expressed in presynaptic neurons is synaptotagmin, a transmembrane protein with a single membrane-spanning domain that is localized to the presynaptic membrane near and often within the active zone. Synaptotagmins were first found through a genome-wide search for neuronal genes encoding proteins with calcium binding domains **(**Brose *et al.*, 1992). In general, members of the synaptotagmin family contain six domains: an amino-terminal intravesicular domain, a transmembrane domain, a spacer domain, two C2 domains that may or may not bind calcium depending on the amino acid sequence in that particular isoform, and a short carboxy-terminal domain (Nonet *et al.,* 1993; Perin *et al.,* 1991). Mammalian Syt1 has been shown to bind to multiple components of the synapse such as syntaxin **(**Kee and Scheller, 1996), neurexin adhesion molecules **(**Hata *et al.,* 1993), the β-SNAP cofactor for the NSF ATPase that dismantles SNARE complexes (Schiavo *et al.,* 1995), and the endocytosis adaptor AP2 **(**Zhang et al., 1994).

In mammals, there are 17 identified synaptotagmin genes (Dean *et al.,* 2012a). Not all synaptotagmin isoforms bind calcium; in fact, is has been estimated that half of the calcium-binding or C2-domains lack the residues required for calcium ion binding (von Poser *et al.,* 1997). C2 is a calcium- and

lipid-binding domain, so the isoforms lacking the calcium-binding residues may be acting as lipid-associated synaptotagmins. In mammals, the eight calcium-binding synaptotagmins have a range of apparent calcium-binding affinities, which hints that they may respond to different cellular calcium signals (Sugita *et al.,* 2002). The calcium binding kinetics of each synaptotagmin isoform may be useful predictors of their individual expression patterns (Sudhof and Rizo, 2011). All of the calcium-binding isoforms appear to bind SNARE proteins and to phospholipids in a calcium-dependent manner (Li *et al.,* 1995; Sutton *et al.,* 1999; Sugita *et al.,* 2002; Hui *et al.,* 2005).

The best-studied member of the mammalian synaptotagmin family is Syt1*,* which binds calcium as well as syntaxin (Kee and Scheller, 1996). These properties first suggested that Synaptotagmin-1 controls synaptic vesicle release from neurons by linking Ca^{2+} with the SNARE complex, the dominant model in the field. Human Syt1 cycles through many conformations, both calcium bound and unbound, that could contribute its many functions such as membrane insertion, calcium ion sensing, and neuronal plasticity mediation (Gauer *et al.,* 2012).

Some structure-function studies have been performed on rat Syt1. X-ray crystallography revealed that the three aspartic acid residues in C2A are the key calcium-binding amino acids (Sutton *et al.,* 1995). NMR studies showed that the C2A domain binds three calcium ions, and the C2B domain binds two calcium ions (reviewed in Rizo *et al., 2012*).

Although the Syt1 C2-domains have somewhat low Ca^{2+} affinity (on the millimolar level), their apparent Ca^{2+} affinity increases one hundred to one thousand fold when negatively charged phosopholipids are present (Zhang *et al.,* 1998). In order for Syt1 to bind to phospholipids, both calcium and negatively charged phospholipids, such as phosphatidyl-inositolphosphates must be present **(**Pang *et al.,* 2006). Recent reports have suggested that Syt1, when tethered to membrane, can promote vesicle docking and fusion in the absence of calcium (Lee, *et al.,* 2010). Using an *in vitro* vesicle mixing assay, Kim and colleagues concluded that Syt1 binds t-SNARE and PIP_2, resulting in vesicle tethering in the absence of calcium. Upon synaptobrevin interacting with tSNARE and forming the SNARE complex, Syt1 detaches from the complex. Once calcium is added to the assay, however, Syt1 reassociates with the SNARE complex in a PIP_2-dependent step (Kim *et al.,* 2012). It has been estimated from these *in vitro* assays that Syt1 promotes docking of vesicles one thousand fold, compared to vesicle mixing assay controls containing only vSNARE and tSNARE proteins.

Cryo-Electronmicroscopy results suggested that the C2B domain may act to bring two membranes into close proximity (Arac *et al.,* 2006). The proposed model was that Syt1 C2B domain bridged the vesicle bilayer and the plasma membrane in a calcium-dependent manner (Arac *et al.,* 2006). Two arginines in the C2B domain were later identified to be critical for this membrane linking, and additional experiments demonstrated that bridging was more probable if one of the bilayers contained SNARE complexes, hinting that Syt1 functions may

include bringing vesicles close to the plasma membrane (reviewed in Rizo *et al.,* 2012).

Genetic studies of synaptotagmin were first conducted in *Drosophila melanogaster* and *Caenorhabditis elegans*; analysis of *C. elegans* synaptotagmin (*snt-1*) mutants will appear in the next section. In *D. melanogaster*, synaptotagmin 1 was initially thought to act as a clamp, blocking synaptic vesicle fusion until calcium flowed into the active zone (Littleton *et al.,* 1994). Fly *syt1* is pan-neuronally expressed, and Syt1 protein is sub-cellularly localized to synapses (Littleton *et al.,* 1993a). Flies with mutations in *syt1* often arrest as first-instar larvae, hinting that Syt1 plays a major role in nervous system function (Littleton *et al.,* 1994). Partial loss of function mutation of *syt1* causes a small increase in spontaneous synaptic vesicle release and a large decrease in evoked synaptic vesicle release (Littleton *et al.,* 1993c). Intragenic complementation is evident between some *syt1* alleles, a feature that suggests Syt1 may form a multimeric complex in *Drosophila* (Littleton *et al.,* 1994).

The first C2 domain structure was determined using the C2A domain of the rat Syt1 protein (Sutton *et al.,* 1995). C2 domains contain a β-sandwich with flexible connecting loops at both sides of the sandwich; the loops emerging from the top of the C2 domain form the calcium-binding domain (Sutton *et al.,* 1995). Every subsequently studied C2 domain determined has demonstrated nearly identical loops and folds (reviewed in Sudhof, 2012a). Interestingly, disturbing the calcium-binding capability of the C2B domain of Syt1 is more disruptive to functioning

than disturbing the calcium-binding capability of the C2A domain (Mackler *et al.,* 2002; Robinson *et al.,* 2002). From these structural analyses, it was unclear whether synaptotagmins operated as clamps on vesicle fusion which were only disengaged upon calcium binding or as enhancers of membrane interaction (Chicka *et al.,* 2008).

Syt1 mutant mice have damaged evoked excitatory post-synaptic currents (EPSCs), specifically a diminished fast synchronous component of the response in hippocampal neurons (Geppert *et al.,* 1994). In cell cultures derived from mouse hippocampal neurons, overexpressing Syt1 raises the probability of evoked release (Han, *et al.,* 2004). In the cortical neurons, Syt1 mutant mice display attenuated inhibitory post synaptic currents (IPSCs) (Xu *et al.,* 2007). Of eight tested synaptotagmin proteins, only Syt1, Syt2, and Syt9 are capable of rescuing the Syt1 knockout **(**Xu *et al.,* 2007).

A recent study by Dean and colleagues surveyed many of the mammalian Syt isoforms for their cellular and subcellular localization patterns in hippocampal neurons (Dean, *et al.,* 2012a). Some synaptotagmins are trafficked to axons, some to dendrites, and some to both loci (summarized in Table 1). In addition, many of the isoforms seemed to localize to specific secretory organelles within cellular compartments. Syt isoforms were also assayed for membrane-recycling capabilities using a pH-sensitive GFP protein, pHluorin, fused to the predicted luminal end of each isoform (Miesenbock *et al.,* 1998; Diril *et al.,* 2006). If a Syt is

targeted to a vesicle that fuses to a less acidic compartment or extracellular space, fluorescent signal increases. An advantage of using this system is that the hippocampal cells in the culture can be easily stimulated by depolarization, and then each Syt-pHluorin fusion protein assessed for any changes in GFP fluorescence levels, indicating a vesicle fusion event.

Table 1. Mammalian Syt Cellular Expression Patterns

Axons	Dendrites	Both	No Response	Not in Brain
Syt1 (SV)	Syt3	Syt4	Syt10	Syt8
Syt2 (SV)	Syt11	Syt6		Syt14
Syt5		Syt9		Syt15
Syt7		Syt12		
Syt17				

(Adapted from Dean, *et al.*, 2012a) SV=Synaptic Vesicle Associated

Of the synaptotagmin isoforms tested, only Syt10-pHluorin failed to show a change in fluorescence suggesting regulated fusion. Syt1 and Syt2 both responded to the depolarization stimulus with a kinetic pattern typical of synaptic vesicle release dynamics. Because other Syt isoforms had different time scales of responses than Syt1 and Syt2, perhaps these Syt isoforms are targeted to vesicles that are not classical synaptic vesicles packaged with neurotransmitter but rather other vesicle subtypes. Syt3, for example, responded to depolarization with a decrease in fluorescence, suggesting that it is endocytosed as a result of depolarization. Perhaps Syt3 acts to modulate the amount of receptors on the cell surface and thus moderate the neuronal response. Dean and colleagues also

noted a general trend that synaptotagmins that recycle exclusively in axons displayed increased surface expression compared to other isoforms, hinting that it may be possible to predict in which region of the neuron a Syt recycles based on the fraction of surface fluorescence signal compared to the amount of internal protein signal (Dean *et al.,* 2012a). Most of the identified synaptotagmin proteins are associated with vesicles of some sort, but the contents and types of vesicles containing synaptotagmins remains unclear (reviewed in Sudhof, 2012a).

The complexities of Syt function can be exemplified by Syt4, which is thought to affect many diverse processes. Syt4 and Syt7 act together to control somatodendritic dopamine release. This release requires the SNARE complex and specific sources of calcium from N- or P/Q-type voltage-gated calcium channels. Syt1 is also present in dopaminergic cells, supporting the idea that multiple Syt isoforms can be present in a single cell, controlling distinct types of neurotransmission (Mendez *et al.,* 2011).

Syt1, Syt4, Syt7 and Syt9 associate with different sized dense core vesicles (DCVs) in PC12 neuroendocrine cell culture (Zhang *et al.,* 2011b). Syt4 is a negative regulator of exocytosis in PC12 cells (Wang *et al.* 2001), and is localized to the Golgi, on immature vesicles, and on mature DCVs (Berton, *et al.,* 2000; Ibata *et al.,* 2000; Fukuda *et al.,* 2001). Each of the other three synaptotagmin isoforms in PC12 cells, with the exception of Syt4, exhibits varying calcium sensitivities, varying divalent cation sensitivities, varying responsiveness to the inhibition by Syt4, and varying preference for full fusion

versus kiss-and-run fusion. These results suggest that a DCV of a specific size will exocytose depending on the stimulation and the proportion of Syt isoforms associated with it (Zhang *et al.,* 2011b).

In rat hippocampal neuron culture, Syt4 is associated with vesicles containing BDNF (Brain-Derived Neurotrophic Factor) in both the axons and the dendrites (Dean, *et al.,* 2009). Because Syt4 does not have the residues in its C2-domains that allow for calcium binding, it can bind SNARE proteins, but does not bind membranes upon calcium influx (Chapman *et al.,* 1998; Wang and Chapman, 2010). As a result, BDNF release is inhibited by Syt4 (Dean *et al.,* 2009). Knocking out Syt4 induces an increase of miniEPSCs and a decrease of miniEPSCs, thereby affecting modifying both excitatory and inhibitory synapses (Dean *et al.,* 2012b). In these rat hippocampal cultures, Syt4 acts via BDNF to modulate exocytosis in response to activity by synaptic scaling, potentially at highly localized sites with a fairly fast time scale (Dean *et al.,* 2012b).

In mouse hippocampal neurons, Syt4 plays multiple roles in vesicle maturation and release. In Syt4 knockout cultures, the Golgi area is approximately 40% larger in volume than in wildtype neuron culture, implicating Syt4 in synaptic vesicle biogenesis or transport. Furthermore, Syt4 knockout cultures have less synaptic vesicles compared to wildtype control culture, suggesting that Syt4 normally blocks vesicle fusion in mouse hippocampal neurons. Additional experiments showed a further decrease of synaptic vesicles in Syt4 knockout cells after stimulation compared to wildtype cells. Thus

synaptotagmin 4 in mouse hippocampal neurons functions in both early vesicle biogenesis or trafficking steps and acts to maintain a particular amount of synaptic vesicles in the active zone (Arthur *et al.,* 2010).

Another example of Syt4 inhibiting vesicle fusion comes from mouse hypothalamus (Zhang, *et al.,* 2011a). Syt4 expression in the hypothalamus neurons directly coincides with the oxytocin expression pattern. High magnification immunostaining revealed that Syt4 was present on vesicles containing oxytocin. Syt4 knockout mice maintain normal weight over a yearlong feeding period, even when fed a high-fat diet that caused obesity in wildtype littermate controls. Injecting oxytocin into the brains of wildtype mice resulted in a significant suppression of food intake in the four hours post-injection. Administering oxytocin antagonists to wildtype mice caused weight gain and an increase in food intake. Similarly, rescuing Syt4 under the oxytocin promoter in Syt4 knockout animals resulted in both weight gain and increased food intake. Oxytocin levels within the blood of Syt4 knockout were twice the concentration of oxytocin in wildtype animals, illustrating that Syt4 normally inhibits oxytocin release. In addition, wildtype mice fed the high-fat diet had a 40% reduction in oxytocin levels, demonstrating a link between oxytocin and obesity. These results show that Syt4 can inhibit neuropeptide release in specific parts of the mammalian brain, but it is unclear whether Syt4 acts directly or indirectly on these neuropeptides (Zhang *et al.,* 2011a).

An additional Syt relevant to peptide release is Syt10. In mouse olfactory bulb neurons, Syt1 and Syt10 both act to trigger exocytosis, but each protein controls the release of distinct, non-overlapping subsets of vesicles. Syt10 facilitates exocytosis of vesicles that are non-synaptic and contain IGF-1 (Insulin-like Growth Factor-1); Syt1 drives exocytosis of synaptic vesicles within the same cells (Cao *et al.,* 2011). Syt10 is one of the calcium binding synaptotagmins that is thought to dimerize (Fukuda *et al.,* 1999). Thus, two synaptotagmins can function within cells, both as calcium sensors, to control separate secretory pathways using nearly identical mechanisms. Syt10-controlled exocytosis is restricted to the cell body and dendrites of olfactory bulb neurons. Loss of Syt10 results in diminished IGF-1 secretion, which then causes smaller cell size with decreased dendritic branching. Additionally, in Syt10 knockout mice, the synaptic density of the neurons in the external plexiform layer of the olfactory bulb is decreased, but the synaptic density of the neurons in the glomerular level of the olfactory bulb remains at wildtype levels. Overall, the loss of dendrites coupled with the loss of synaptic vesicles in some neurons of the olfactory bulb contributed to an cumulative loss of synapses within the olfactory bulb in Syt10 knockout mice, rendering them slower food finders in a timed assay (Cao *et al., 2011)*. Electrophysiology results of Syt10 knockout neurons confirmed that synaptic transmission on the whole was diminished. Thus, synaptotagmins can change neurotransmission in a calcium-dependent manner, without physically controlling the release of vesicles containing neurotransmitters or neuropeptides

(Cao, *et al.* 2011). Moreover, multiple synaptotagmin isoforms can function in the same cell, regulating distinct vesicle fusion pathways.

Synaptotagmins are also expressed in non-neuronal cells. For example, Syt2 is found in mast cells of the immune system in mice (Baram *et al.,* 1999). Syt2 appears to both block and facilitate exocytosis in mast cells, depending on the intracellular calcium concentration (Nagai, *et al.,* 2011).

Synaptotagmins in *Caenorhabditis elegans*

There are seven *snt* genes predicted in the *C. elegans* genome, though only *snt-1* has been studied (Nonet *et al.,* 1993; Jorgensen *et al.,* 1995; Mathews *et al.,* 2007). *snt-1* mutants have jerky uncoordinated body movements, are constipated and starved (Raizen *et al.,* 1995), and have slower, irregular pharyngeal pumping rates (Avery, 1993 and Steger *et al.,* 2005).

Synaptic transmission mutants usually have uncoordinated locomotion due to disturbed communication at the neuromuscular junctions (Reviewed in Richmond, 2007). Specific locomotion defects in *snt-1* mutants include the "shrinker" phenotype (Nonet, *et al.,* 1993). The "shrinker" phenotype is characterized by touching animals lightly on the head or by tapping the plate on which the worms are growing. If the muscles on both the dorsal and ventral sides of the animal contract simultaneously, as opposed to in tandem, the anterior part of the worm shortens or shrinks. This "shrinker" defect is typically indicative of dysfunction of the inhibitory GABAergic motor neurons controlling sinusoidal

motion at high locomotion speeds. In spite of this locomotion defect, *snt-1* mutants often display normal body waves during slow forward movement, indicating that excitatory acetylcholine neurons retain some function.

Direct evidence that *snt-1* affects exocytosis in *C. elegans* first came from electrophysiological recordings from pharyngeal muscles, which stimulate pharynx pumping and thus play a role in *C. elegans* feeding behavior. Extracellular recordings on dissected pharynxes showed that *snt-1* mutant phanryngeal glutamatergic motor neurons have asynchronous and decreased neurotransmission compared to the wildtype (personal communication from J.A. Dent, M.W. Davis, and L. Avery reported in Jorgensen *et al.,* 1993; Steger, *et al.,* 2005). This abnormal spiking pattern was proposed to be a result of a reduction of acetylcholine release by the MC "pacemaker" neuron that coordinates pharyngeal pumping. Decreased acetylcholine release may cause the smaller excitatory post-synaptic potentials that are unable to generate full action potentials to stimulate pumping (Steger *et al.,* 2005).

Indirect but highly suggestive evidence that SNT-1 affects exocytosis in *C. elegans* came from the observation that *snt-1* mutants also show resistance to aldicarb, an acetylcholinesterase inhibitor (Nonet *et al.,* 1993). The aldicarb resistance assay is used in *C. elegans* to indirectly quantify neurotransmitter release at neuromuscular junctions. Acetylcholine is released by motor neurons at excitatory neuromuscular junctions to stimulate muscle contraction and thus locomotion. Aldicarb, an acetylcholinesterase inhibitor, causes paralysis as

normal-functioning motor neurons release acetylcholine that cannot be broken down by the aldicarb-inhibited acetylcholinesterase present in the neuromuscular junction. Overabundance of acetylcholine in the synaptic cleft leads to hypercontraction. In the aldicarb resistance assay, animals are placed in the presence of aldicarb and assayed for time to total paralysis. Animals can be classified as Ric (**R**esistors to **I**nhibitors of **C**holinesterase) or Hic (**H**ypersensitivity to **I**nhibitors of **C**holinesterase) (Reviewed in Rand, 2007). *snt-1* mutants are Ric, suggesting that acetylcholine release is decreased at neuromuscular junctions (Nonet *et al.,* 1993; Jorgensen *et al.,* 1995). However, the fact that *snt-1* mutants have contracted muscles in the presence of aldicarb indicates that some acetylcholine is released and that exocytosis of acetylcholine is not completely blocked in *snt-1* mutants (Nonet *et al.,* 1993). This result also indicates that SNT-1 is most likely not the only calcium sensor for synaptic vesicle fusion in motor neurons (Nonet *et al.,* 1993), and is supported by the evidence that other synaptic vesicle mutants such as *unc-13* exhibit more severe defects in coordinated movement than *snt-1*. While *snt-1* mutants were some of the first identified RIC mutants (they were once named *ric-2*), they did not appear in screens for resistance to the acetylcholine agonist levamisole. This suggests that the acetylcholine receptors on muscle are still active but that *snt-1* mutants release less acetylcholine from their motoneurons than wildtype animals (Avery, 1993).

Recent optogenetic tools have been utilized in *C. elegans* to probe specific neurotransmitter release at neuromuscular junctions (NMJs). A light-gated cation channel, Channelrhodopsin-2 (ChR2), was selectively expressed in motoneurons, allowing for specific and precise stimulation of neurons without the variability and damage caused by using shocks to stimulate voltage-gated calcium channels during traditional electrophysiology. An additional benefit of ChR2 in *C. elegans* is that the transparent nematode permits stimulation and response assays to be conducted in vivo, without dissection. The readout for ChR2 stimulation in motoneurons was measurement of body length (Liewald *et al.,* 2008). Neurons innervate muscles at the NMJs using both excitatory cholinergic connections and inhibitory GABAergic connections (White *et al.,* 1986). Acetylcholine is released at excitatory NMJs and results in muscle contraction; GABA is released at inhibitory NMJs and results in muscle relaxations (reviewed in Richmond, 2007). When ChR2 was expressed in GABAergic neurons, light-induced depolarization caused paralysis and body elongation that could be recovered over time after light pulses ended. Stimulating ChR2 in cholinergic neurons resulted in contraction and a decrease in body length, due to the excitation of body wall muscles. Whole cell voltage-clamp recordings performed on body wall muscles confirmed neurotransmitter release from the motoneurons by detecting evoked postsynaptic currents (ePSCs). In *snt-1* null mutants, GABA-ePSCs were severely reduced, reiterating the involvement of SNT-1 in normal GABA-ergic function as alluded to by the

“shrinker” phenotype. Acetylcholine-ePSCs were also dramatically reduced in *snt-1* null mutant worms compared to wildtype, again confirming the cellular basis for the resistance to cholinesterase phenotype. Repeated photo-stimulation of ChR2, i.e. stimulus trains, in either cholinergic or GABA-ergic neurons in a *snt-1* mutant background resulted in ePSC responses that decayed over time, indicating synaptic vesicle depletion on a faster scale than wildtype and hinting at SNT-1 acting in the vesicle recycling pathway (Liewald *et al.,* 2008).

In spite of the fact that proteins other than synaptotagmins have calcium-binding domains, only synaptotagmins have been shown to play a role as calcium-sensors in neurotransmission. For example, although rabphilin contains calcium binding domains, synaptotagmin rabphilin *snt-1*; *rbf-1* double mutants have locomotion defects, abnormal pharyngeal pumping rates, and defecation defects only as severe as *snt-1* single mutants. This experiment shows that neuronally-expressed RBF-1 does not function as an additional calcium sensor responsible for synaptic vesicle fusion beyond the synaptic vesicle fusion controlled by SNT-1 (Staunton *et al.,* 2001).

Although acetylcholine release in *snt-1* mutants is impaired, additional mutations can further limit the release of acetylcholine. *wsp-1* is epistatic to *snt-1*; the double mutant is aldicarb sensitive. A loss of function mutation in *wsp-1* enhances the aldicarb sensitivity in tomosyn *tom-1(ok 285)* mutants. WSP-1 protein localizes to the perisynaptic region, adjacent to RAB-3. *wsp-1* mutants

most likely have a slightly unstable actin cytoskeleton, aiding in SV docking and fusion (Zhang and Kubiseski, 2010).

SNT-1 and Endocytosis

In addition to its inferred role in exocytosis, Syt1 is directly involved in endocytosis (Yao, *et al.* 2012a). When examined using electron microscopy, *snt-1* mutant motor neurons had fewer synaptic vesicles in the VA, VB, and VD motor neurons (Jorgensen *et al.,* 1995). To rule out vesicle biogenesis defects, *snt-1* mutant was crossed with *unc-104*, which affects the kinesin required for SV transport to synapses. In *unc-104;snt-1* double mutants, many SVs were observed in the cell body by EM, indicating that SVs could form and accumulate in the absence of SNT-1. The synaptic vesicle-associated protein RAB-3 was also reported to be present in axons, although these data were not shown (Jorgensen *et al., 1995)*. A second vesicle-associated protein, synaptobrevin-1 tagged with GFP is reduced and diffuse in VD and DD neurons of *snt-1* mutants, dovetailing with the electron microscopy results showing fewer synaptic vesicles in the mutants (Jorgensen *et al.,* 1995).

Wildtype synaptotagmin may promote vesicle fusion, block vesicle fusion, or enhance endocytosis of fused vesicles via its interaction with the clathrin AP2 complex (Zhang *et al.,* 1994). Teasing apart the roles of synaptotagmin in exocytosis and endocytosis will add to our understanding of synaptotagmin's role in the vesicle release and recycling pathways (Yao *et al.,* 2012a). These two pathways are not necessarily tethered to each other (Dittman and Kaplan, 2006).

Cell Biology of SNT-1

Vesicle trafficking motors are critical in the correct sub-cellular distribution of SNT-1. In wildtype *C. elegans* neurons, synapses form *en passant* rather than in a restricted manner at an axon terminus (White, 1986). Kinesin motors act in neurons to transport cargo, including synaptic vesicles and many SV-associated proteins in the anterograde direction from the cell body down the axon. When the kinesin motor UNC-104/Kif1A is impaired, SNT-1 fails to distribute along the axon and remains restricted to the neuronal cell body (Nonet *et al.,* 1993). A second motor that contributes to synaptic vesicle distribution is dynein, which acts to carry cargo, including synaptic vesicle proteins retrogradely. The dynein-dynactin complex is considered the major retrograde motor (Goldstein and Yang, 2000). In *dhc-1(js319)* dynein mutants and *dnc-1(or404ts)* dynactin adaptor mutants, synaptotagmin accumulates in the terminal tip of the mechanosensory neuron AVM, bypassing its normal site (Koushika *et al.,* 2004). This same misaccumulation happens in the absence of either UNC-116 kinesin heavy chain or UNC-16 JIP3 homolog, that acts as a cargo adaptor for kinesin motors. Although UNC-116 is an anterograde motor, it targets dynein as cargo to the nerve terminus where it begins its retrograde, cargo-laden journey to the soma (Arimoto *et al.,* 2011).

Molecular Biology of *C. elegans snt-1*

The *C. elegans snt-1* gene is located on chromosome II (Nonet *et al.,* 1993) and encodes two isoforms, A and B. The A isoform is strongly expressed in most

neurons, and the SNT-1A protein is sub-cellularly localized to synaptic-rich regions of the neurons (Nonet *et al.,* 1993; Mathews *et al.,* 2007). SNT-1A protein was also observed in secretory uterine cells in *C. elegans* (Nonet *et al.,* 1993). SNT-1B protein was detected at lower levels than SNT-1A, and in fewer neurons (Mathews *et al.,* 2007).

The genetic difference between the two isoforms lies in the alternative forms of the sixth exon (Fig. 2) (Craxton, 2001). This alternative splicing of the sixth exon of synaptotagmin is conserved in Aplysia (Nakhost, *et al.,* 2004). *C. elegans* exon 6A is 134 nucleotides long and encodes 45 amino acids, and the non-overlapping exon 6B is 140 nucleotides long and encodes 47 amino acids (Mathews, *et al.,* 2007). The sixth exon in *C. elegans* lies within the highly conserved C2B calcium-binding domain (Mathews *et al.,* 2007). *C. elegans* SNT-1A has 78% amino acid identity to rat synaptotagmin I (Nonet *et al.,* 1993).

Elimination of SNT-1A results in uncoordinated movement defects, slowed growth and defecation defects; elimination of SNT-1B results in no behavioral defects (Nonet *et al.,* 1993; Mathews *et al.,* 2007). However, expressing either *snt-1A* or *snt-1B* isoform under a strong pan-neuronal promoter in null mutants fully rescues pharyngeal pumping rates, thrashing in liquid, and defecation completion frequency (Mathews *et al.,* 2007). Thus both isoforms are capable of some measure of phenotypic rescue if widely expressed, and the most important difference between them is their cellular expression patterns.

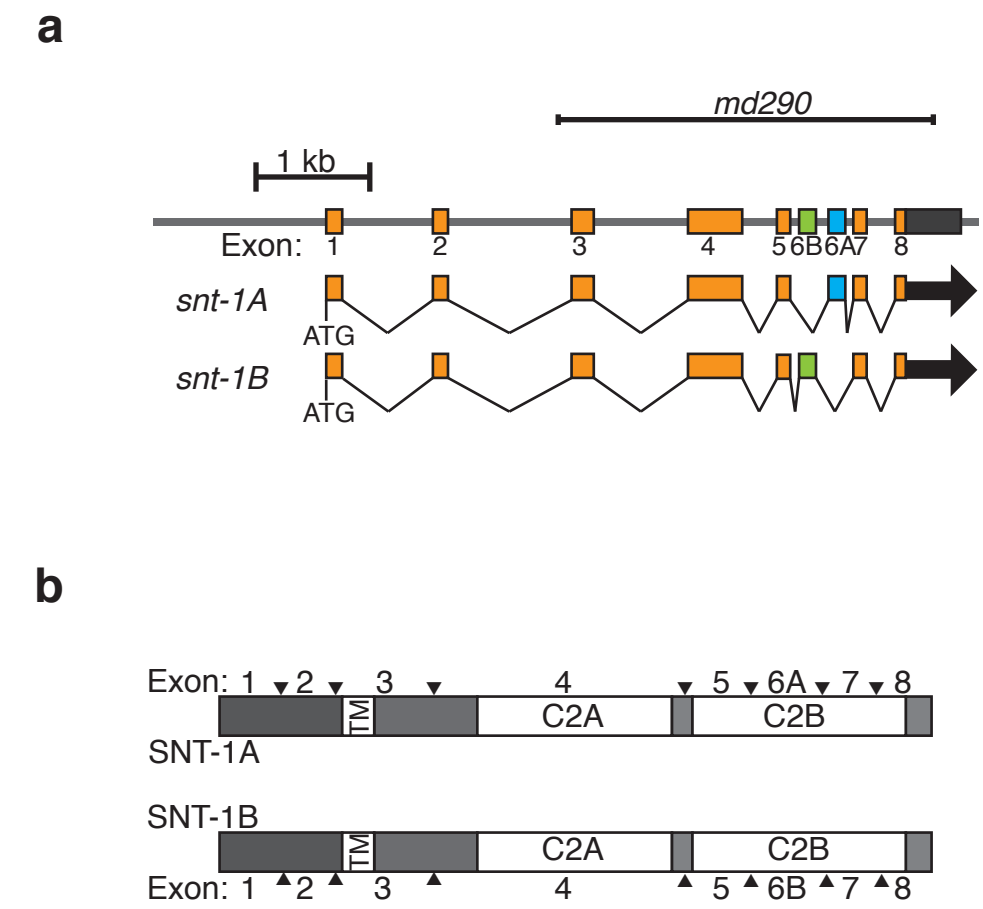

Figure 2. *snt-1* encodes two isoforms, SNT-1A and SNT-1B (a) Gene and mRNA models for *snt-1* (b) Proteins produced by *snt-1*. TM indicates transmembrane domain; C2A and C2B indicate the two C2 domains; and arrowheads indicate splice sites.

An analysis of the available alleles of *snt-1* was performed by Mathews and colleagues in 2007. Alleles of *snt-1* have been isolated from screens for aldicarb resistance, a screen for feeding mutants, and a screen for defecation-defective mutants. Two of these studied alleles are relevant in this work: *md290* and *md257*. *snt-1(md290)* is a 3.3 kilobase deletion that eliminates ~85% of the coding sequence, leaving some of the intravesicular N-terminus, and is considered the canonical null allele (Mathews *et al.,* 2007). *snt-1(md257)* is a 2 base pair deletion in exon 6A that only affects the SNT-1A isoform, and these mutants have intact defecation behavior but defective locomotory behavior (Mathews *et al.,* 2007). When *snt-1* alleles have been assayed for protein production using anti-SNT antibodies, most lines show no immunoreactivity, and the lines that do have some detectable signal have reduced immuno-staining compared to wildtype (Nonet *et al.,* 1993; Mathews *et al.,* 2007). The only published structure-function analysis experiment of SNT-1 to date revealed that a VIL motif in exon 5 is necessary for trafficking SNT-1 from the cell body to the synapse (Mathews *et al.,* 2007). As this motif is in the fifth exon, it affects both A & B isoforms; VIL deletion most likely results in protein misfolding, and thus retention in the cell body secretory pathway by chaperone proteins (Mathews *et al.,* 2007). In general, mutations in the C2B domain have a more severe impact on neurotransmission than mutations in the C2A domain (Koch and Holt, 2012).

To further the studies of SNT-1 in *C. elegans*, we analyzed the effects of a *snt-1* mutation in four classes of neurons. I will first describe the isolation of the

ky1002 allele of *snt-1* and its mapping and characterization. I will then go on to describe the phenotype of *snt-1(ky1002)* mutant animals, by examining RAB-3 distribution in three classes of sensory neurons and one class of motor neurons. Then I will describe experiments that confirm that SNT-1 plays a key role in endocytosis in *C. elegans*. Next, I will present an analysis of the phenotypes resulting from null mutations of *snt-2*, *snt-4*, *snt-5,* or *snt-6*. I will then describe the quantification of phenotypes of double mutants in which two synaptotagmin genes are mutated. Finally, I will discuss future directions for study.

Glossary of Most-Referenced Genes (Mammalian Homologs in Parentheses)

dpy-23 *(AP50)* Encodes DPY-23, the μ2 subunit of the AP2 clathrin adaptor protein required for endocytosis. *dpy-23* mutants have fewer synaptic vesicles in the axon compared to wildtype animals. SV endocytosis in *dpy-23* mutant animals is impaired, but not eliminated.

rab-3 *(rab3A)* Encodes RAB-3, a GTP-binding protein that is believed to associate with synaptic vesicles at the time that they are transported from the Golgi to the active zone and to disassociate from SVs before their return to the Golgi during the recycling steps after endocytosis. RAB-3 is considered a synaptic vesicle marker.

sad-1 *(BRSK1)* Encodes a serine/threonine kinase, SAD-1, which localizes to synapse-rich regions of axons. *sad-1* mutants have disorganized clusters of synaptic vesicles; SAD-1 is regulates the pattern of the distribution of synaptic vesicles in the active zone. For the purposes of this thesis, SAD-1 is used as a marker for the active zone and perisynaptic region of axons.

snb-1 *(VAMP1 and VAMP2)* Encodes synaptobrevin, the vesicle-associated vSNARE that, when complexed with syntaxin and SNAP-25, bundles to form the SNARE complex. SNB-1 is considered a synaptic vesicle marker.

snt-1 *(syt1)* Encodes synaptotagmin, a vesicle-associated protein with two C2 domains that may bind calcium. *snt-1* mutants appear to be both exocytosis and endocytosis defective.

unc-2 *(alpha subunit)* Encodes the alpha subunit of a voltage-gated calcium channel. For the purposes of this thesis, UNC-2 is considered a marker of voltage-gated calcium channels.

unc-11 *(CALM/AP180)* Encodes UNC-11, the clathrin adaptor protein AP180. SNB-1 (synaptobrevin), but not SNT-1 or RAB-3, is mislocalized in *unc-11* mutants. UNC-11 is thought to regulate clathrin-cage assembly during endocytosis. UNC-11 is not required for endocytosis, but endocytosis is abnormal in *unc-11* mutant animals.

unc-13 *(Munc13)* Encodes UNC-13, a protein localized to the active zone, where SV exocytosis occurs. UNC-13 interacts with the tSNARE syntaxin to facilitate SV exocytosis. *unc-13* mutants have more SVs docked at the plasma membrane, indicating that UNC-13 is required for SV priming and may play an additional role in subsequent steps of exocytosis. SV exocytosis is severely blocked in *unc-13* mutants.

unc-18 *(Munc18)* Encodes UNC-18, a chaperone protein that regulates the transport of syntaxin from the endoplasmic reticulum to the active zone. UNC-18 also promotes SV docking and may play an additional role in other steps of exocytosis. SV exocytosis is severely blocked in *unc-18* mutants.

unc-104 *(KIF1a)* Encodes UNC-104, a microtubule-based kinesin motor that transports SVs anterogradely along the axon to the active zone. *unc-104* mutants have fewer synaptic vesicles in the axon compared to wildtype animals.

Results

A Screen for Mutants Affecting Synapses in PQR Neurons

To identify genes that affect synapse distribution or synaptic connectivity, we designed an EMS-based screen using the integrated marker *kyIs512*, which reports GRASP (GFP Reconstituted Across Synaptic Partners) signals between the PQR sensory neuron and the AVA backward command neurons.

The use of the split GFP is a technique developed by Evan Feinberg known as GRASP, or GFP Reconstitution Across Synaptic Partners. Two fragments of the split GFP are expressed in non-overlapping subsets of cells. These GFP fragments alone are not fluorescent. When the two parts are fused to synaptic transmembrane proteins, synapses between cells are marked with an extracellular GFP signal. GRASP specifically marks a small number of synapses in areas of the worm, such as the nerve ring and ventral nerve cord, that are synaptically enriched (Feinberg *et al.*, 2008).

The *kyIs512* transgene combines four elements: *gcy-36::ptp-3A::spGFP11*, a fusion protein of a receptor tyrosine phosphatase (PTP-3A) with an extracellular domain conjugated to a portion of the GFP molecule, expressed in PQR, AQR, and URX neurons; *flp-18::nlg-1::spGFP1-10*, a fusion protein of neuroligin, a synaptically-associated molecule conjugated to the remaining portion of the GFP molecule, expressed specifically in the AVA command interneurons; *flp-17::mCherry*, a co-injection marker that marks the pair of BAG head neurons

brightly enough to be seen under a fluorescent dissecting microscope; and *gcy-36::mCherry::rab-3*, which marks the RAB-3 synaptic vesicle associated GTPase in the PQR, AQR, and URX neurons (Fig. 3)

I performed a clonal screen by examining the F2 progeny of F1 animals (Supp. Fig. 1). I screened the progeny of 500 F1 worms, which represents ~1000 heterozygous mutagenized genomes, for the absence of either mCherry or GFP. 118 potential candidate mutants were pulled out of the screen. 72 candidates were deficient in the GRASP GFP signal, 28 candidates were deficient in the mCherry::RAB-3 signal, and 18 candidates had mixed phenotypes (some animals had a mutant mCherry::RAB-3 phenotype and some had mutant GRASP phenotype) (Fig. 4a). Approximately twenty worms were examined per line; each potential mutant line had between one and four mutant animals in this pool of twenty (Fig. 4b). Any animals with a mutant phenotype were then picked from the slide to a new plate, for further examination in subsequent generations.

In the second screen through these 118 potential mutant lines, 58% showed transmission of a mutant phenotype to subsequent generations. Interestingly, some lines that had previously shown GRASP defects now showed mCherry defects and vice versa (Fig. 4c). At this time, the penetrances of the mutant phenotypes were also determined for each line (Fig. 4d). The thirteen lines with the highest penetrance (15% and above) were selected to be outcrossed to the *kyIs512* starting strain, in order to facilitate future mapping of mutations.

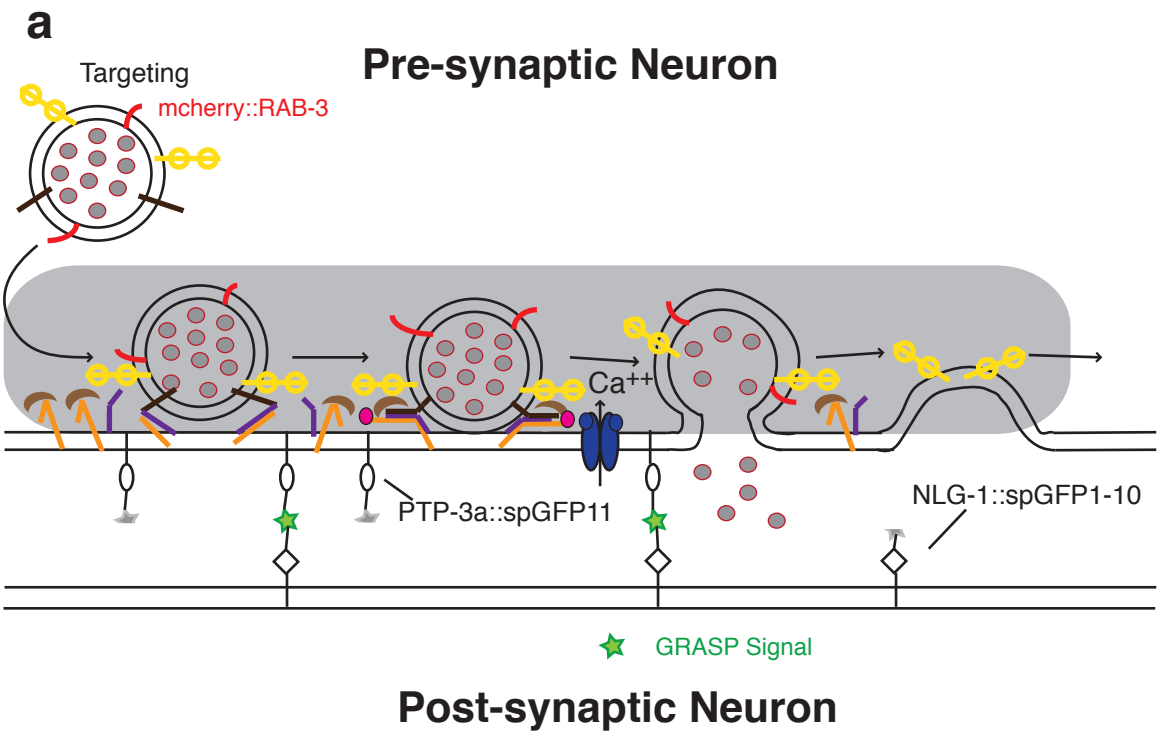

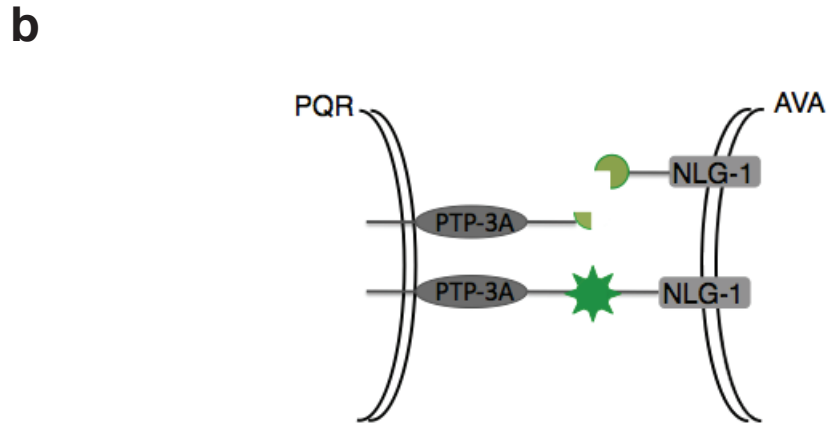

Figure 3. A simple model of the *kyIs512* transgene products. (a) mCherry::RAB-3 and PTP-3a::spGFP11 are expressed in the pre-synaptic neurons. NLG-1::spGFP1-10 is expressed in the post-synaptic neurons. (b) GFP signal is seen when the pre-synaptic PTP-3a::spGFP11 and the post-synaptic NLG-1::spGFP1-10 components come in close enough proximity to each other, a small distance indicating that the two neurons are synaptic partners.

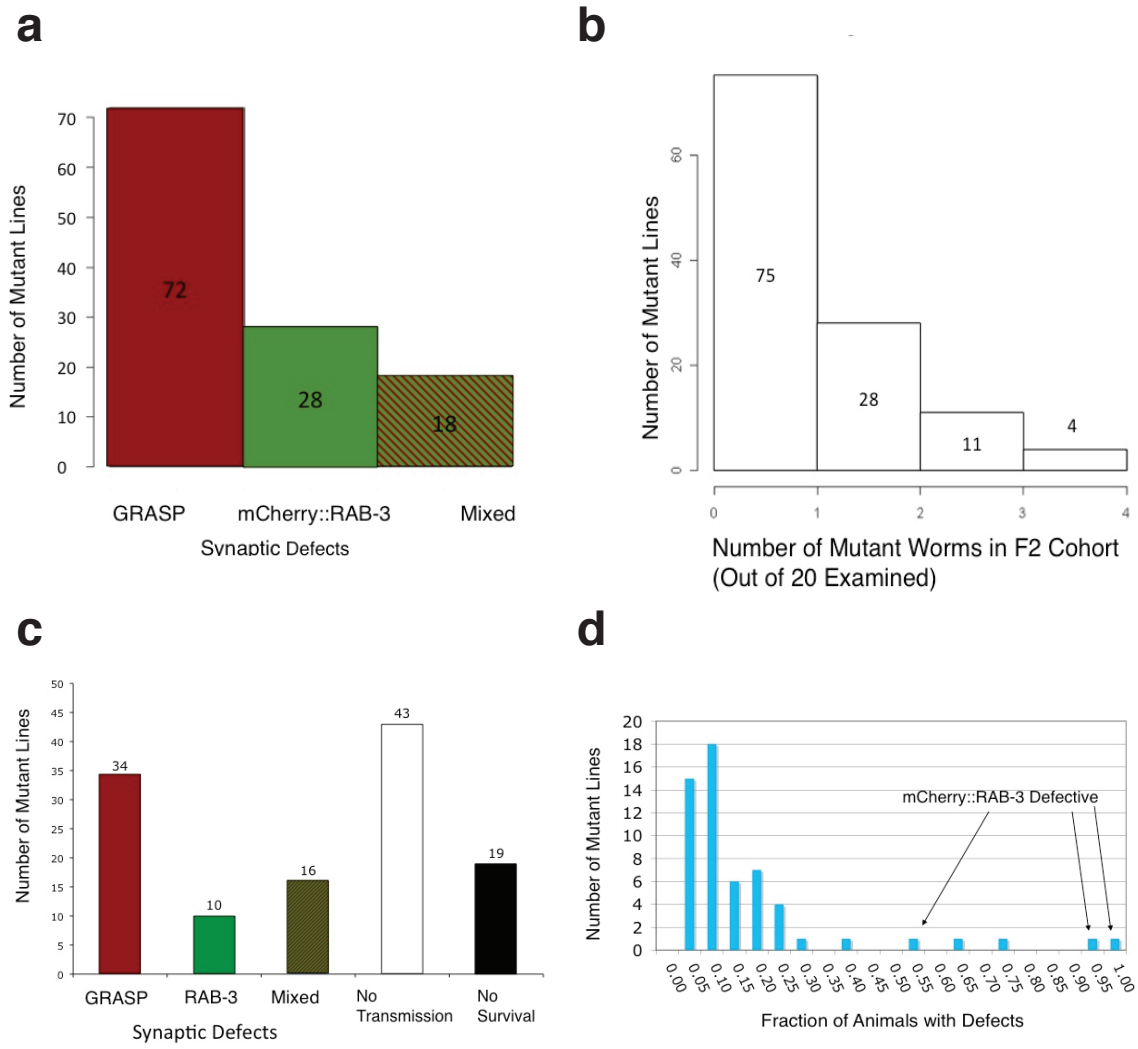

Figure 4. Screen Results. 118 potential mutant lines were identified in the initial screen and then screened a second time for phenotype transmission to subsequent generations and for phenotype penetrance. (a) Histogram of phenotypes displayed in the initial screen. (b) Histogram of the number of mutant animals found within a single group of twenty sibling F2 animals. For a recessive mutation, five mutant F2s are expected if the mutation is 100% penetrant. (c) Histogram of the phenotypes displayed by the potential mutant lines when examined in F3 or later generations. (d) Histogram of penetrance of mutant phenotypes in F3 or later generations.

The outcrossing strategy entails crossing each mutant line to the *kyIs512* starting strain, then examining the progeny of the cross progeny to identify F2 animals that retain the mutant phenotype. F2 animals that display the mutant phenotype are believed to still carry the mutation of interest, but also to have exchanged approximately 50% of their genome, which has been exposed to EMS, with the wildtype starting strain genome. Initially, eleven of the 13 potential mutant strains were crossed to the starting strain. (Strain 10.6 was not outcrossed at that time because it grew slowly; strain 11.11 was not outcrossed at that time because the plate contained contaminating bacteria.) Of the eleven outcrossed lines, three lines, 27.2, 21.1, and 26. 7 did not produce F2 progeny with any detectible mutant phenotype. The eight outcrossed lines that did have progeny displaying a mutant phenotype all displayed mCherry::RAB-3 defects, regardless of whether they had previously been GRASP defective or mCherry::RAB-3 defective. The mutation in line 9.19 appeared to be linked to the X chromosome. After four outcrosses, the mutation in line 26.11 appeared to be dominant or X-linked. Also, after four outcrosses, line 12.2, which had animals with GRASP defects and animals with mCherry::RAB-3 defects before the outcrossing, produced animals with mCherry::RAB-3 defects, but no F2 animals with GRASP defects, in a ratio that suggested that the mutation in line 12.2 was dominant. This shift in phenotype and penetrance after outcrossing raised the possibility that several of the mutations in the outcrossed lines may be linked to the *kyIs512* transgene itself.

To sidestep this possibility, I chose to focus on the potential mutant line with the highest penetrance, line 10.6, which also happened to be slow growing and uncoordinated (Unc).

Table 2. Thirteen Potential Mutant Lines Before and After Backcrossing

Line	Phenotype	Penetrance	Number of Times Backcrossed	Phenotype After Backcrossing
10.6	RAB-3 Defective	100%	0	
30.5	RAB-3 Defective	94%	4	RAB-3 Defective
27.2	Mixed Defects	61%	0	
37.2	RAB-3 Defective	35%	2	RAB-3 Defective
9.19	RAB-3 Defective	25%	4	RAB-3 Defective
26.11	RAB-3 Defective	24%	4	RAB-3 Defective
21.12	GRASP Defective	22%	2	RAB-3 Defective
19.3	Mixed Defects	17%	2	RAB-3 Defective
20.6	GRASP Defective	17%	2	RAB-3 Defective
21.1	GRASP Defective	17%	0	
12.2	Mixed Defects	16%	4	RAB-3 Defective
26.7	Mixed Defects	15%	0	
11.11	Mixed Defects	75%	0	

The potential mutant line that I had identified as line 10.6 was mCherry::RAB-3 defective (Fig. 3). The mutation that caused this defect was named *ky1002*,

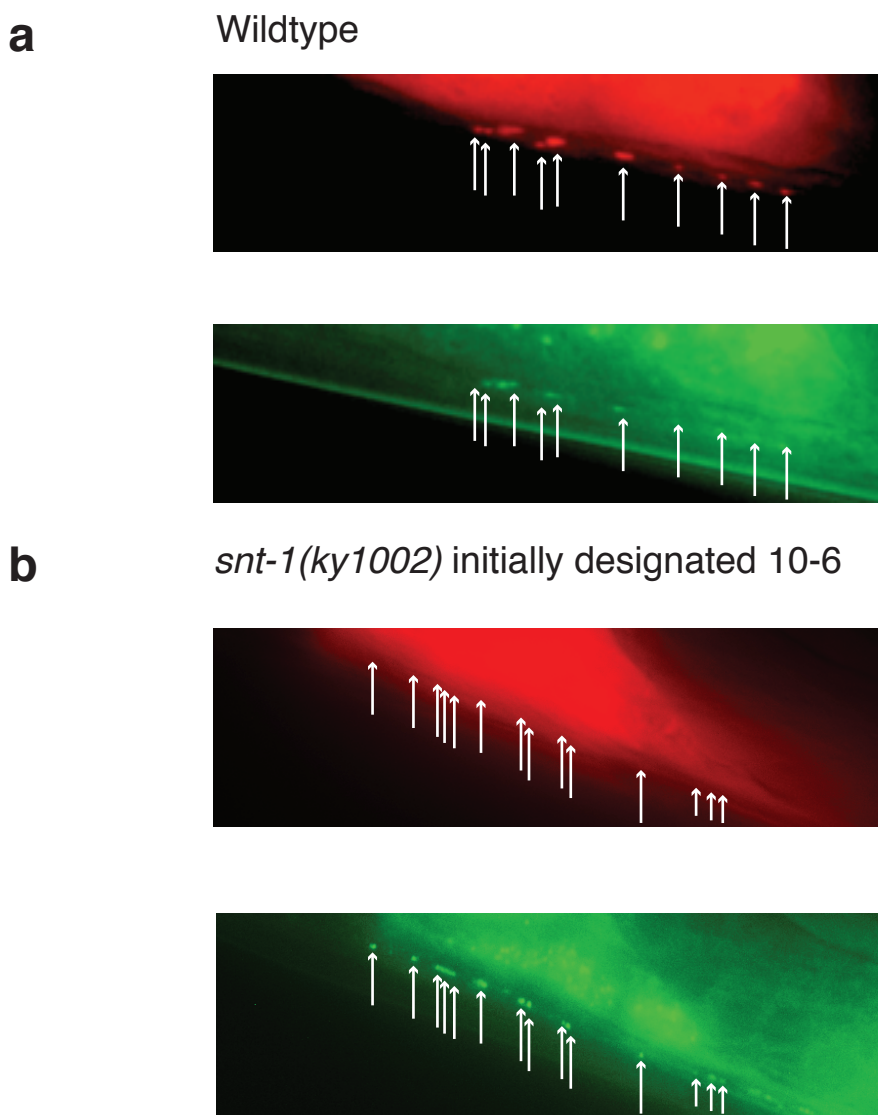

Figure 5. WT and *snt-1(ky1002)* animals in the *kyIs512* marked background. (a) Wildtype. Top panel shows mCherry::RAB-3 expression in PQR; bottom panel shows GRASP expression between PQR and AVA neurons. (b) *snt-1(ky1002).* Top panel shows mCherry::RAB-3 expression in PQR; bottom panel shows GRASP expression between PQR and AVA neurons. White arrows indicate fluorescent puncta examined in the screen.

indicating that it was the 1002nd mutant allele to be generated and catalogued in the lab.

To verify that the *ky1002* mutation was not specific to the *kyIs512* integrated marker, the *ky1002*; *kyIs512* line was crossed to another line containing a YFP::RAB-3 fusion protein expressed in the PQR neuron, *kyIs403*. In the *kyIs403* background, the *ky1002* phenotype resulted in a reduced YFP::RAB-3 signal, with a diffuse, rather than punctate distribution (Fig. 6).

As the *ky1002* mutation was outcrossed, it appeared that the YFP::RAB-3 defect was highly linked to an uncoordinated (Unc) locomotion phenotype. This linkage facilitated the mapping of the *ky1002* mutation.

Mapping of *ky1002*

A common method of mapping mutations in *C. elegans* involves using a highly divergent wild strain isolated in a pineapple field in Hawaii, CB4856 (Jakubowski and Kornfeld, 1999). The standard lab strain N2 and CB4856 differ from each other at many sites, including insertions and deletions. PCR primer sets flanking 5879 predicted insertions or deletions were designed by Andres Bendesky to generate genotypic markers that could be easily scored with a single PCR reaction.

Coarse mapping of *ky1002*, was conducted using three primer pairs detecting deletions per chromosome—one on the left arm, one in the center of the chromosome, and one on the right arm; *ky1002* displayed linkage to the markers on chromosome II (Fig. 7a, b)

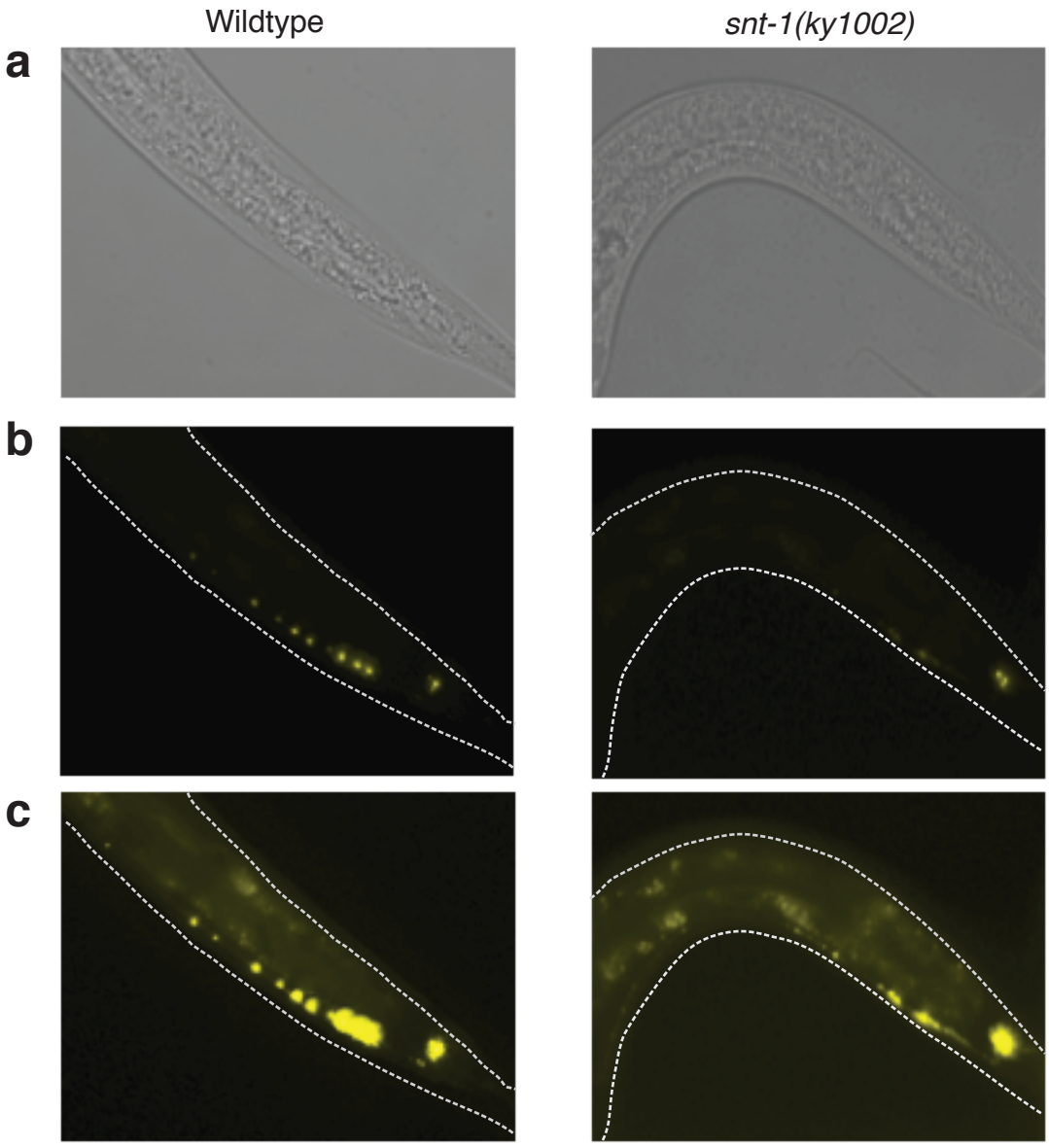

Figure 6. WT and *snt-1(ky1002)* animals in the *kyIs403* marked background. (a) Brightfield illumination. Left column of panels are all from the same wildtype animal; right column of panels are from the same *snt-1(ky1002)* animal. (b) YFP::RAB-3 expression. (c)YFP::RAB-3 expression with brightness increased. Note that YFP::RAB-3 puncta that were not visible in panel (b) are now visible in panel (c) in the *snt-1(ky1002)* animal.

Figure 7. Mapping Strategy and Mapping Results. (a) The genetic crossing scheme, set up to generate mapping lines containing the *ky1002* mutation in a CB4856 background. (b) Coarse mapping results. White boxes in the table indicate that the genotyping reaction failed or was uninterpretable. (c) Finer mapping results. White boxes in the table indicate that the genotyping reaction failed or was uninterpretable. Expected result: enrichment of N2 DNA (blue) compared to CB4856/HW DNA (red) near gene of interest.

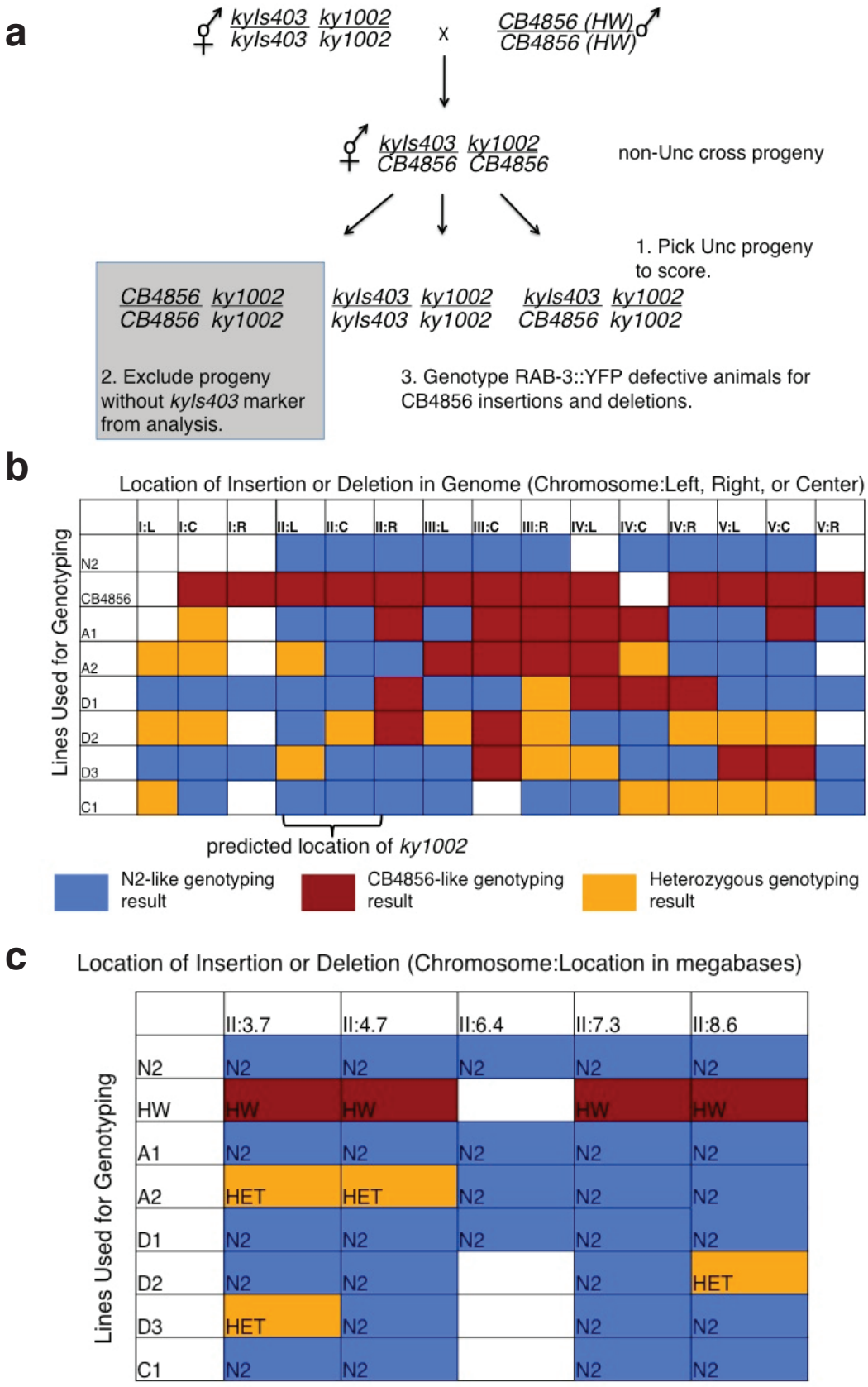
a
kyIs403 ky1002 / kyIs403 ky1002
x
CB4856 (HW) / CB4856 (HW)
kyIs403 ky1002 / CB4856 CB4856
non-Unc cross progeny
1. Pick Unc progeny to score.
CB4856 ky1002 / CB4856 ky1002
kyIs403 ky1002 / kyIs403 ky1002
kyIs403 ky1002 / CB4856 ky1002
2. Exclude progeny without kyIs403 marker from analysis.
3. Genotype RAB-3::YFP defective animals for CB4856 insertions and deletions.
b
Location of Insertion or Deletion in Genome (Chromosome:Left, Right, or Center)
I:L I:C I:R II:L II:C II:R III:L III:C III:R IV:L IV:C IV:R V:L V:C V:R
Lines Used for Genotyping
N2
CB4856
A1
A2
D1
D2
D3
C1
predicted location of ky1002
N2-like genotyping result
CB4856-like genotyping result
Heterozygous genotyping result
c
Location of Insertion or Deletion (Chromosome:Location in megabases)
II:3.7 II:4.7 II:6.4 II:7.3 II:8.6
Lines Used for Genotyping
N2 N2 N2 N2 N2 N2
HW HW HW HW HW
A1 N2 N2 N2 N2 N2
A2 HET HET N2 N2 N2
D1 N2 N2 N2 N2 N2
D2 N2 N2 N2 HET
D3 HET N2 N2 N2
C1 N2 N2 N2 N2

Figure 7

To further map the locus of *ky1002,* three more primer pairs were selected on the left arm of chromosome II (Fig. 7c), and 26 additional F2 lines were assayed for the presence of Hawaiian DNA in this region (data not shown). These results confirmed that *ky1002* most likely was within a 4.9 megabase region on the left arm of chromosome II between the insertion or deletion at 4.7 megabases and the insertion or deletion at 8.6 megabases.

_ky1002_ is not an allele of _unc-104_

The uncoordinated (Unc) phenotype of the *ky1002* line combined with the mapping data suggested a candidate gene, *unc-104*, as a promising locus for the *ky1002* mutation. *unc-104*, which is homologous to Kif-1A, encodes a kinesin-like motor protein that is required for anterograde axonal transport of synaptic vesicles (Hall and Hedgecock, 1991). Synaptic vesicle-associated proteins like RAB-3, SNB-1, and SNT-1 all require UNC-104/Kif1A to correctly localize at the synaptic terminal (Nonet *et al.,* 1993, 1997, 1998). The abnormal and dim RAB-3::YFP phenotype in *ky1002* is related to but milder than that of an *unc-104* null mutant, in which all YFP::RAB-3 would be lost from synapses and axons.

Primers were designed to sequence the coding regions of *unc-104* in the *ky1002* line. One tyrosine to adenine transversion was identified in the ninth exon that was predicted to change a valine to a glutamic acid residue. When the same region was also sequenced in the non-EMS-treated *CX11472* starting strain, however, this same base change was present. Furthermore, Patrick McGrath had identified this base change in his work mapping the differences

between the lab wildtype strain and the published worm genome, indicating that it was present in the starting strain.

In conjunction with this sequencing, a number of other experiments were performed that supported the hypothesis that *ky1002* was not a mutation in *unc-104*. *ky1002* and *unc-104(e1265)* complemented each other for the YFP::RAB-3 phenotype. Additionally, *kyIs403; unc-104(e1265)* and *kyIs403; ky1002* had different YFP::RAB-3 phenotypes; *unc-104(e1265)* had YFP::RAB-3 signal only in the PQR cell body, unlike the diffuse signal in the axon of *ky1002*. This was also the case in the *kyIs512* background. These results suggest that *ky1002* is not an allele of *unc-104*.

_ky1002_ is an allele of _snt-1_

Another candidate gene, *snt-1*, was tested as the locus of the *ky1002* allele while further outcrossing and mapping continued. Primers were designed to sequence the entire coding region of *snt-1*. A mutation in *ky1002* changing a guanine to an adenine was identified at the splice junction preceding exon 6A (Fig. 8). This mutation was not present in the starting strain, and matched the most common change caused by EMS mutagenesis.

The canonical *snt-1* allele, *md290,* failed to complement *ky1002* for both the YFP::RAB-3 phenotype and for the Unc locomotion defect. Furthermore, a *kyIs403; snt-1(md290)* strain closely resembled the *kyIs403; ky1002* line in YFP::RAB-3 distribution and dimness (Fig. 9, Fig. 10, Supp. Fig. 2). Microinjection of two separate fosmids, each containing the full *snt-1* gene,

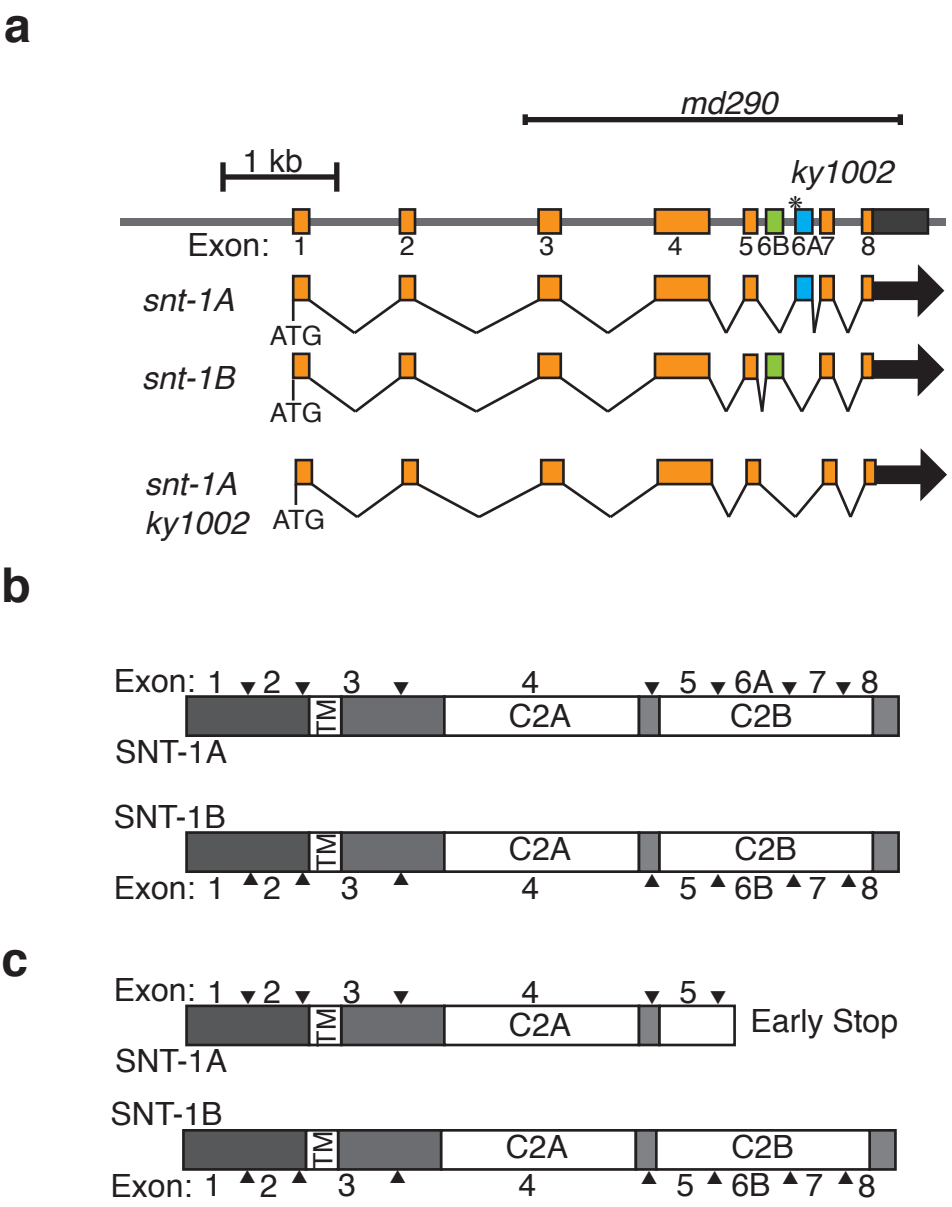

Figure 8. *snt-1(ky1002)* encodes a G to A transition immediately preceding exon 6A. (a) Gene and mRNA models for *snt-1.* (b) Proteins produced by *snt-1*. TM indicates transmembrane domain; C2A and C2B indicate the two C2 domains; and arrowheads indicate splice sites.(c) Proteins predicted to be produced in *snt-1(ky1002)* mutant background. SNT-1A would be truncated 11 amino acids after the 5th exon; SNT-1B would be produced normally.

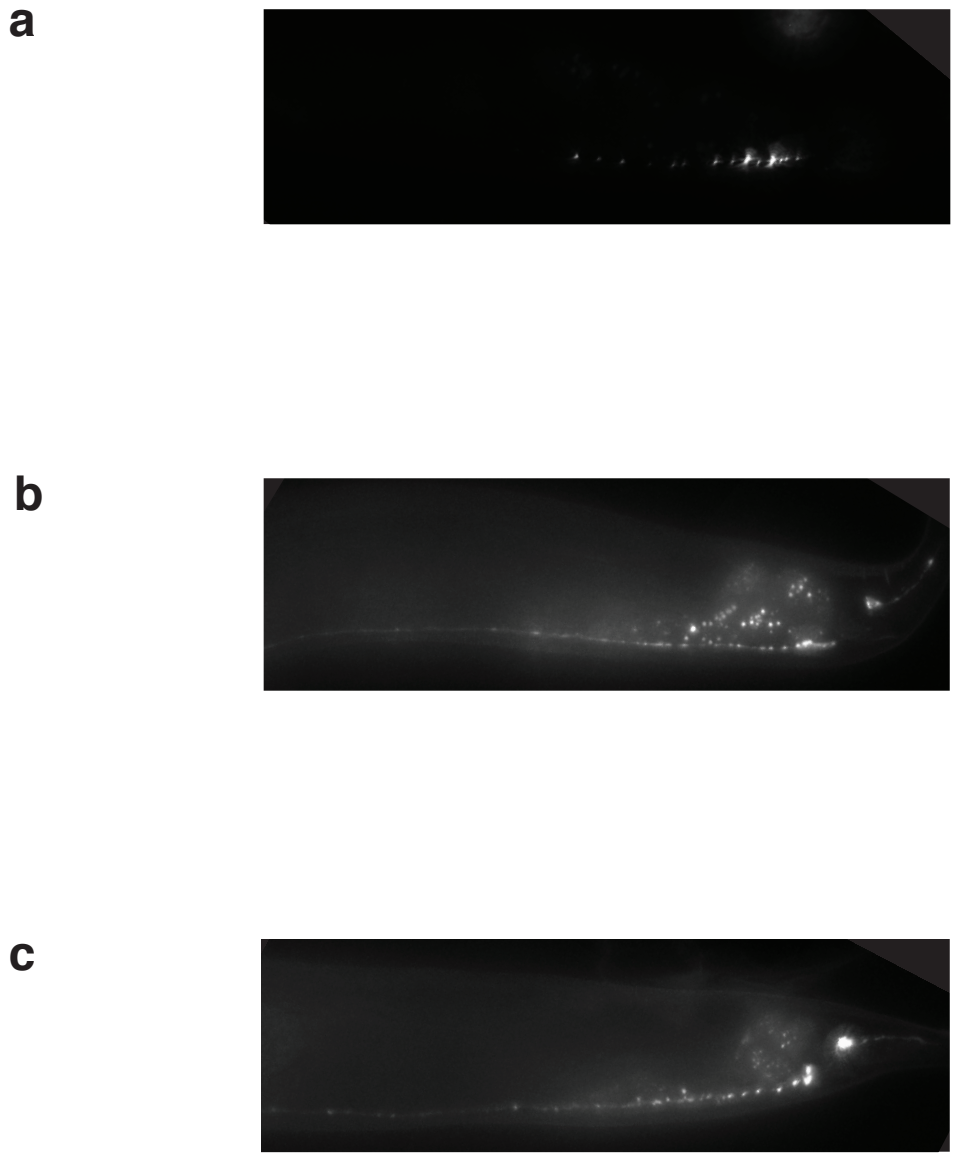

Figure 9. *snt-1(ky1002)* and *snt-1(md290)* both have diffuse, dim YFP::RAB-3 clusters in PQR. (a) Wildtype. (b) *snt-1(ky1002).* (c) *snt-1(md290)*. All images are the same magnification. (b) and (c) images have brightness increased so that YFP::RAB-3 puncta are as bright as wildtype puncta. Note puncta in (b) and (c) are close in brightness to the background fluorescence in the gut of the worm.

Figure 10. *snt-1(ky1002)* and *snt-1(md290)* affect YFP::RAB-3 fluorescence in PQR (a) Total fluorescence in the region of interest in PQR in each worm. (***p<0.001 versus wildtype, unpaired t-test) (b) Total fluorescence value divided by the number of pixels above the noise threshold, indicating the brightness of the fluorescent signal. (***p<0.001 versus wildtype, unpaired t-test) (c) Number of fluorescent puncta in the region of interest in each worm. (n.s. is not statistically significant). (a-c) Wildtype data were collected using the same strain on different days. (d) Representation of YFP::RAB-3 puncta in PQR neuron and model of YFP::RAB-3 associated with a synaptic vesicle.

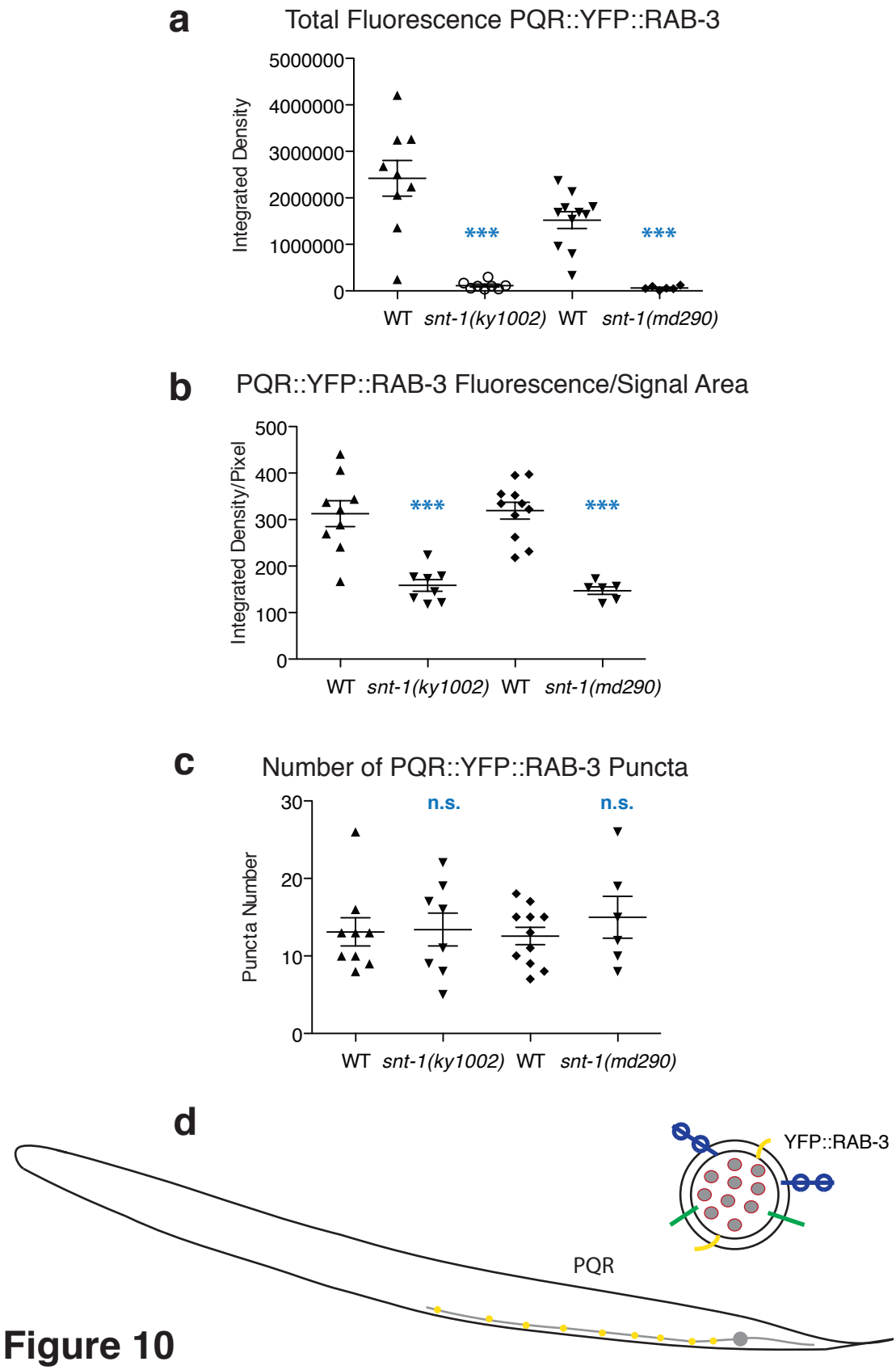
a
Total Fluorescence PQR::YFP::RAB-3
Integrated Density
5000000
4000000
3000000
2000000
1000000
0
***
***
WT
snt-1(ky1002)
WT
snt-1(md290)
b
PQR::YFP::RAB-3 Fluorescence/Signal Area
Integrated Density/Pixel
500
400
300
200
100
0
***
***
WT
snt-1(ky1002)
WT
snt-1(md290)
c
Number of PQR::YFP::RAB-3 Puncta
Puncta Number
30
20
10
0
n.s.
n.s.
WT
snt-1(ky1002)
WT
snt-1(md290)
d
YFP::RAB-3
PQR

Figure 10

rescued the YFP::RAB-3 fluorescence to wild-type levels **(**Fig. 11). These molecular and genetic results identify *snt-1* as the gene affected by the *ky1002* mutation (Fig. 12). *snt-1(ky1002)* mutation causes a G to T transition in the nucleotide immediately preceding exon 6A, which suggested that the *snt-1(ky1002)* mutant phenotype may be caused by a mis-splicing of SNT-1A.

To understand how the nucleotide change in *snt-1(ky1002)* in the splice site preceding exon 6A affected *snt-1* function, rtPCR was performed (Fig. 13). Total RNA was isolated from four N2 wildtype samples and four *snt-1(ky1002)* mutant samples, and reverse transcribed to a cDNA library. PCR with a primer pair that recognized exon 1 and exon 8 was performed to detect all snt-1 mRNA. These primers amplified a single band from wild-type cDNA, but amplified two bands differing by approximately 100 base pairs from the *snt-1(ky1002)* cDNA samples. Spliced *snt-1A* mRNA is predicted to yield a fragment 1326 nucleotides in length, whereas *snt-1B* mRNA should yield a fragment 1332 nucleotides in length, and exon 6A is 134 nucleotides long. Both bands amplified from *snt-1(ky1002)* samples were cut out of the gel and sequenced. The larger of the two bands contained exon 6B, representing *snt-1B* spliced cDNA, but the smaller of the two bands skipped exon 6, splicing from exon 5 to exon 7. Thus, the *snt-1(ky1002)* mutation indeed causes a mis-splicing of the *snt-1A* transcript, excluding exon 6A. This exclusion of 6A is predicted to cause a frameshift that results in an early stop 11 amino acids after exon 5. This truncation would occur within the C2B calcium-binding domain. Some studies suggest that disturbing the calcium-

Figure 11. Map of Contents of Fosmid WRM 0625cD08.

Figure 12. *snt-1(ky1002)* and *snt-1(md290)* alleles are both rescued by injection of the fosmid WRM 0625cD08. (a) Total fluorescence in the region of interest in PQR in each worm. (b) Total fluorescence value divided by the number of pixels above the noise threshold, indicating the brightness of the fluorescent signal. (c) Number of fluorescent puncta in the region of interest in each worm. (d) Representation of YFP::RAB-3 puncta in PQR neuron and model of YFP::RAB-3 associated with a synaptic vesicle.

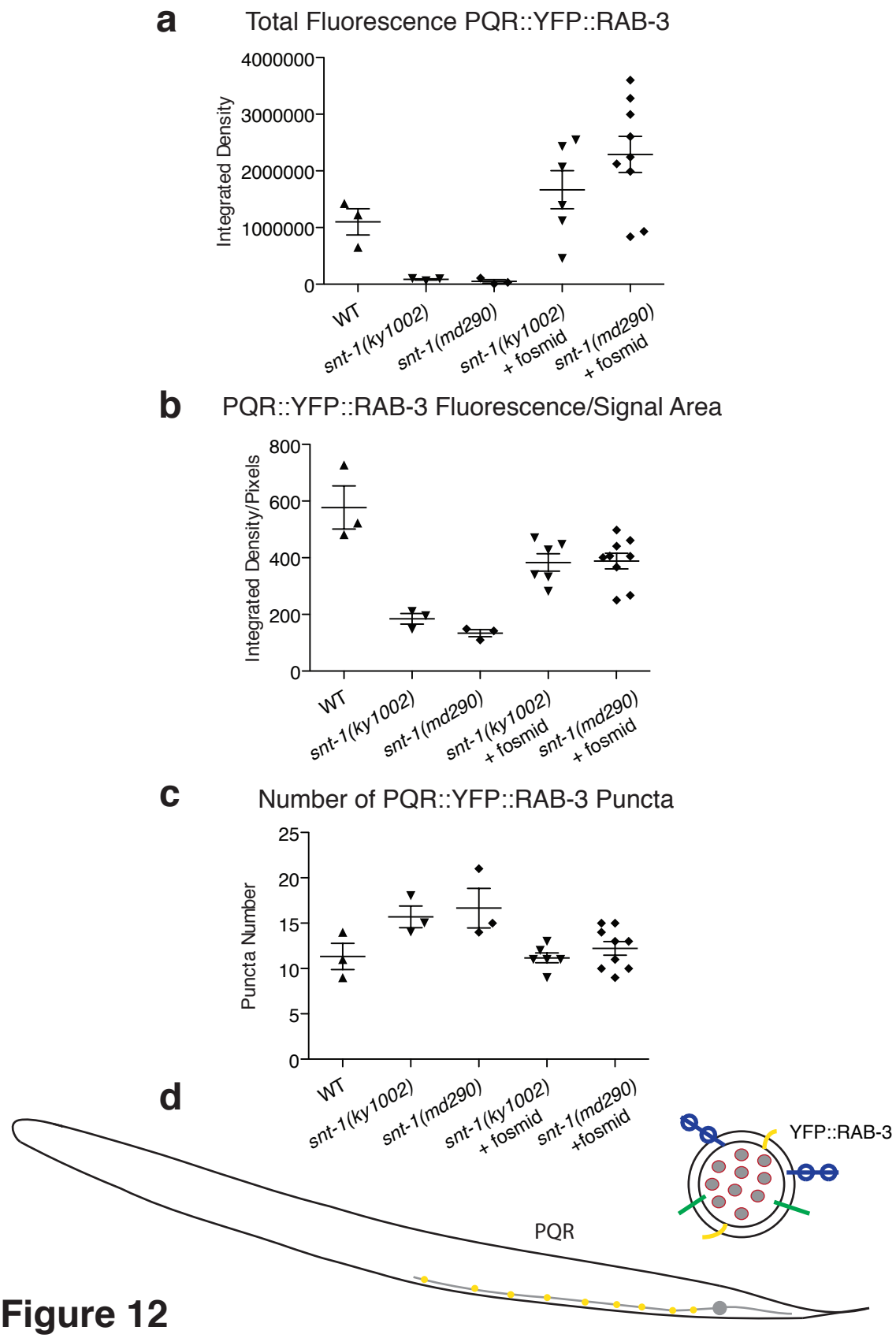
a
Total Fluorescence PQR::YFP::RAB-3
Integrated Density
4000000
3000000
2000000
1000000
0
WT
snt-1(ky1002)
snt-1(md290)
snt-1(ky1002) + fosmid
snt-1(md290) + fosmid
b
PQR::YFP::RAB-3 Fluorescence/Signal Area
Integrated Density/Pixels
800
600
400
200
0
WT
snt-1(ky1002)
snt-1(md290)
snt-1(ky1002) + fosmid
snt-1(md290) + fosmid
c
Number of PQR::YFP::RAB-3 Puncta
Puncta Number
25
20
15
10
5
0
WT
snt-1(ky1002)
snt-1(md290)
snt-1(ky1002) + fosmid
snt-1(md290) +fosmid
d
YFP::RAB-3
PQR

Figure 12

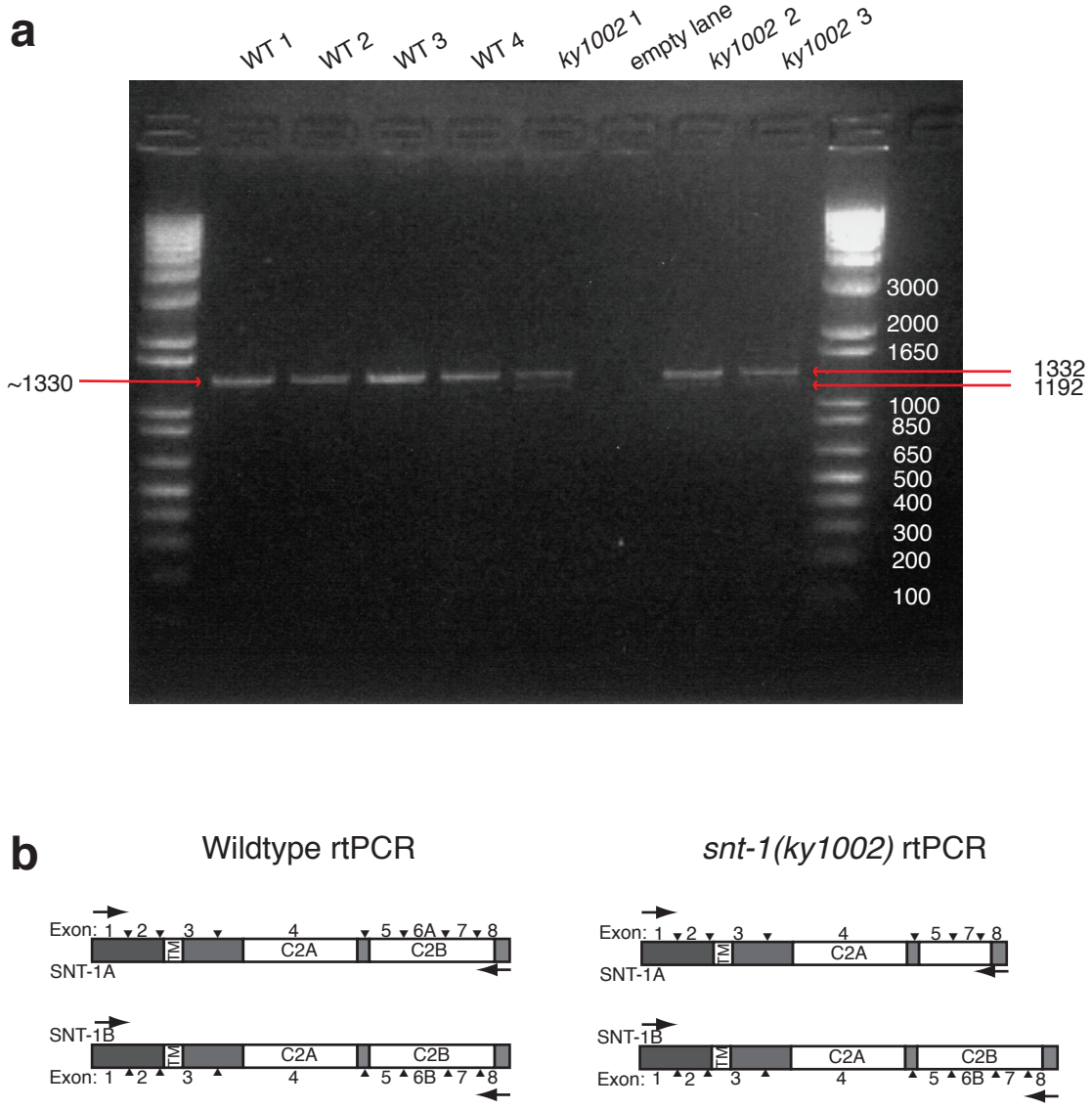

Figure 13. The *snt-1(ky1002)* mutations causes a mis-splicing of the *snt-1A* transcript. (a) Image of gel from rtPCR. Wildtype lanes have a single band that is approximately 1330 nucleotides in length. *ky1002* lanes have two bands: one that is 1332 nucleotides and encodes a complete *snt-1B* mRNA and one that is 1192 nucleotides and encodes a truncated *snt-1A* mRNA (b) Schematic of rtPCR with primers. Arrows approximate predicted primer annealing loci.

binding capability of the C2B domain of Syt1 is more disruptive to functioning than disturbing the calcium-binding capability of the C2A domain (Mackler *et al.,* 2002; Robinson *et al.,* 2002). Thus, a truncated SNT-1A protein lacking a C2B domain, as would be produced in a *snt-1(ky1002)* mutant, would be severely defective.

_ky1002_ Affects Other Synaptic Markers in PQR

In mammals, RAB3A seems to detach from SV membranes after vesicle fusion (Fischer v. Mollard *et al.,* 1991). RAB-3 reversibly associates with synaptic vesicles, depending on the nucleotide bound to RAB-3 (Stahl, *et al.,* 1996). In general, mutations that affect RAB-3 usually also affect SNB-1 and vice versa (Ch'ng *et al.,* 2008). However, at least one mutation in *sng-1*, the *C. elegans* synaptogyrin homolog, alters SNB-1 patterns in the nerve cord, but not RAB-3 patterns (Abraham *et al.,* 2011). Thus, both SNB-1 and RAB-3 markers should be examined in mutant backgrounds. To ask whether *snt-1(ky1002)* was affecting synaptic vesicle distribution versus affecting the RAB-3 fusion protein markers in the *kyIs403* and *kyIs512* marked backgrounds, *snt-1(ky1002)* was crossed into PQR-marked background carrying an extrachromosomal array containing a synaptobrevin fluorophore fusion protein, SNB-1::YFP (Fig. 14). *ky1002* mutant animals had the same number of SNB-1::YFP puncta as wild-type animals, but their SNB-1::YFP puncta were dimmer in the mutant background, resulting in a significantly reduced total fluorescence in the mutant line. This result indicates that *snt-1(ky1002)* lesion produces a reduction in multiple synaptic vesicle

Figure 14. *snt-1(ky1002)* affects SNB-1::YFP fluorescence in PQR. (a) Total fluorescence in the region of interest in PQR in each worm. (**p<0.01 versus wildtype, unpaired t-test) (b) Total fluorescence value divided by the number of pixels above the noise threshold, indicating the brightness of the fluorescent signal. (***p<0.001 versus wildtype, unpaired t-test) (c) Number of fluorescent puncta in the region of interest. (n.s. is not statistically significant) (d) Representation of SNB-1::YFP puncta in PQR neuron and model of SNB-1::YFP associated with a synaptic vesicle.

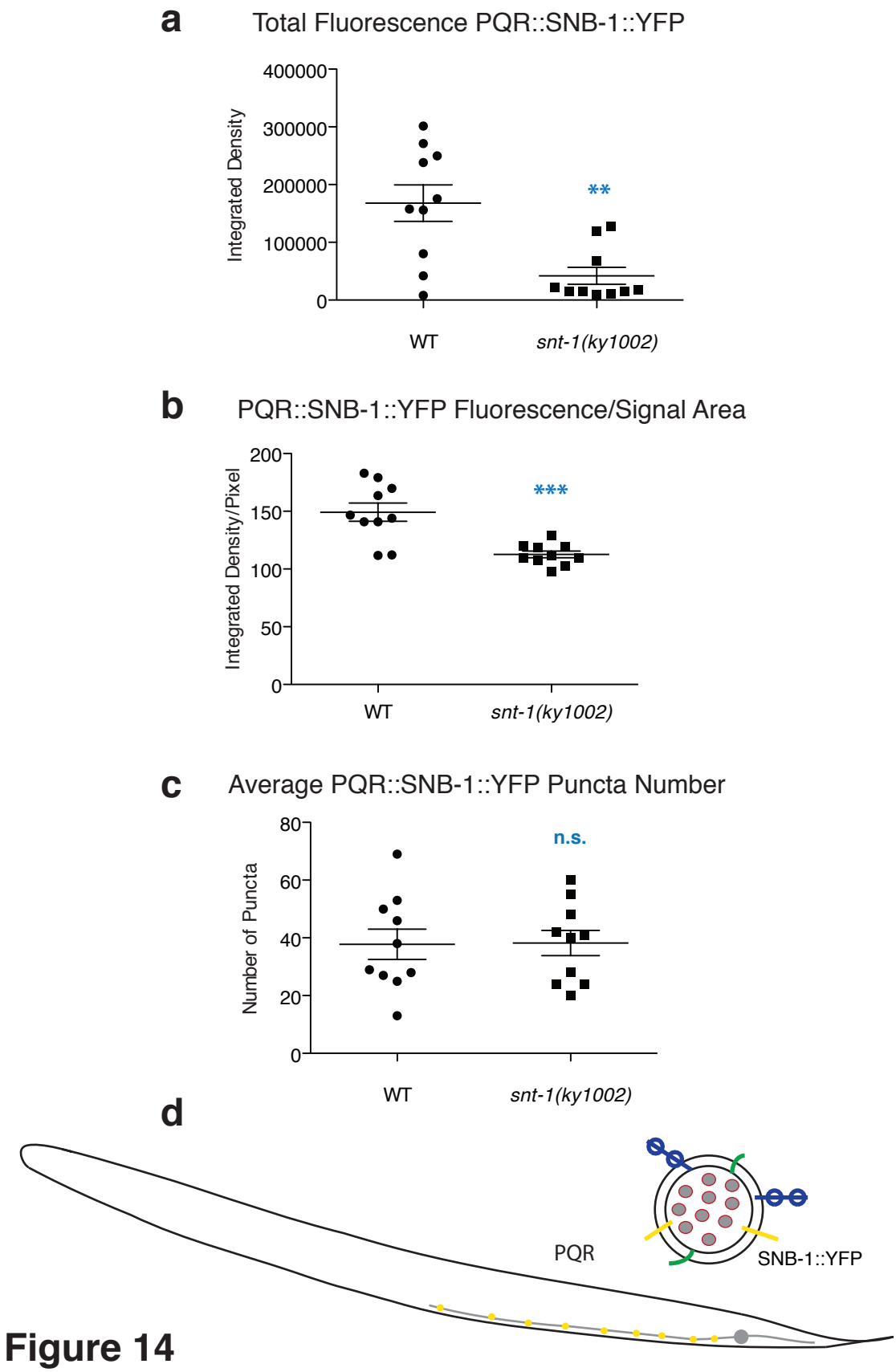
a
Total Fluorescence PQR::SNB-1::YFP
Integrated Density
400000
300000
200000
100000
0
**
WT
snt-1(ky1002)
b
PQR::SNB-1::YFP Fluorescence/Signal Area
Integrated Density/Pixel
200
150
100
50
0
***
WT
snt-1(ky1002)
c
Average PQR::SNB-1::YFP Puncta Number
Number of Puncta
80
60
40
20
0
n.s.
WT
snt-1(ky1002)
d
PQR
SNB-1::YFP

Figure 14

markers, suggesting that SNT-1 plays a role in determining the amount of synaptic vesicles in the axon.

Characterizing *ky1002* in AWC, PVD, and DD Neurons

The screen, rescue, and initial characterization of *snt-1(ky1002)* mutation were all performed in a single sensory neuron, PQR. Previous studies had examined the effects of *snt-1(md290)* on SNB-1 in VD and DD neurons and on synaptic vesicles in the ventral nerve cord (Jorgensen *et al.,* 1995). In addition, the SNT-1A isoform is reported to be expressed in most neurons (Mathews *et al.,* 2007). If *snt-1(ky1002)* affects the SNT-1A isoform, then *snt-1(ky1002)* mutation is likely to cause synaptic vesicle aberrations within many different neurons, not just PQR. I tested this hypothesis by examining a variety of sensory and motor neurons.

AWC

In order to determine whether *ky1002* affected sensory neurons besides PQR, the *ky1002* allele was crossed into the *kyIs442* background, which labels AWC synapses. *kyIs442* is an integrated marker containing three constructs: *odr-3::mCherry::rab-3*, which marks RAB-3 synaptic vesicle associated protein in AWC sensory neuron; *odr-3::GFP::unc-2*, which marks UNC-2 alpha subunit of a voltage-gated calcium channel (VGCC) in AWC; and *unc-122::dsRed,* a co-injection marker.

ky1002 contained significantly dimmer and significantly fewer mCherry::RAB-3 puncta in AWC as well as an overall lower mCherry::RAB-3 fluorescence than in

wild-type (Fig. 15). This result demonstrates that *snt-1(ky1002)* affects both the AWC sensory neurons and the PQR sensory neuron.

The GFP::UNC-2 signal was also examined and quantified in AWC. UNC-2 forms the alpha subunit of presynaptic voltage-gated calcium channels that increase the local calcium concentration near vesicles to trigger fusion (reviewed in Richmond *et al*., 2007). The number of UNC-2 puncta was similar in both wild-type and *snt-1(ky1002)* mutant backgrounds, but the UNC-2 puncta were somewhat brighter, resulting in an increased, statistically significant GFP::UNC-2 fluorescence signal in the mutant background (Fig. 16).

The presentation of a normal number and spacing of UNC-2 puncta suggests that AWC still has presynaptic active zone specializations in the *snt-1(ky1002)* mutant. The increased UNC-2 fluorescence could be an indicator that the AWC sensory neurons have undergone homeostatic plasticity. For example, the neurons could be attempting to compensate for the lack of the canonical SNT-1 calcium sensor by allowing for more calcium influx during a depolarization. Indeed, calcium channels and synaptotagmin are proposed to interact with each other in neurons (reviewed in Augustine *et al.,* 2003). This interaction is possibly due to direct binding or through indirect binding with SNARE as the adaptor. Theoretically, positioning calcium complex and synaptotagmins closely would increase the probability of synaptotagmin sensing calcium before it is buffered away (reviewed in Augustine *et al.,* 2003). Thus, the effect of *snt-1(ky1002)* on

Figure 15. *snt-1(ky1002)* reduces mCherry::RAB-3 fluorescence in AWC. (a) Total fluorescence in the region of interest in AWC in each worm. (***p<0.0001 versus wildtype, unpaired t-test) (b) Total fluorescence value divided by the number of pixels above the noise threshold, indicating the brightness of the fluorescent signal. (***p<0.001 versus wildtype, unpaired t-test) (c) Number of fluorescent puncta in the region of interest in each worm. (**p<0.01 versus wildtype, unpaired t-test) (d) Representation of mCherry::RAB-3 puncta in AWC neuron and model of mCherry::RAB-3 associated with a synaptic vesicle.

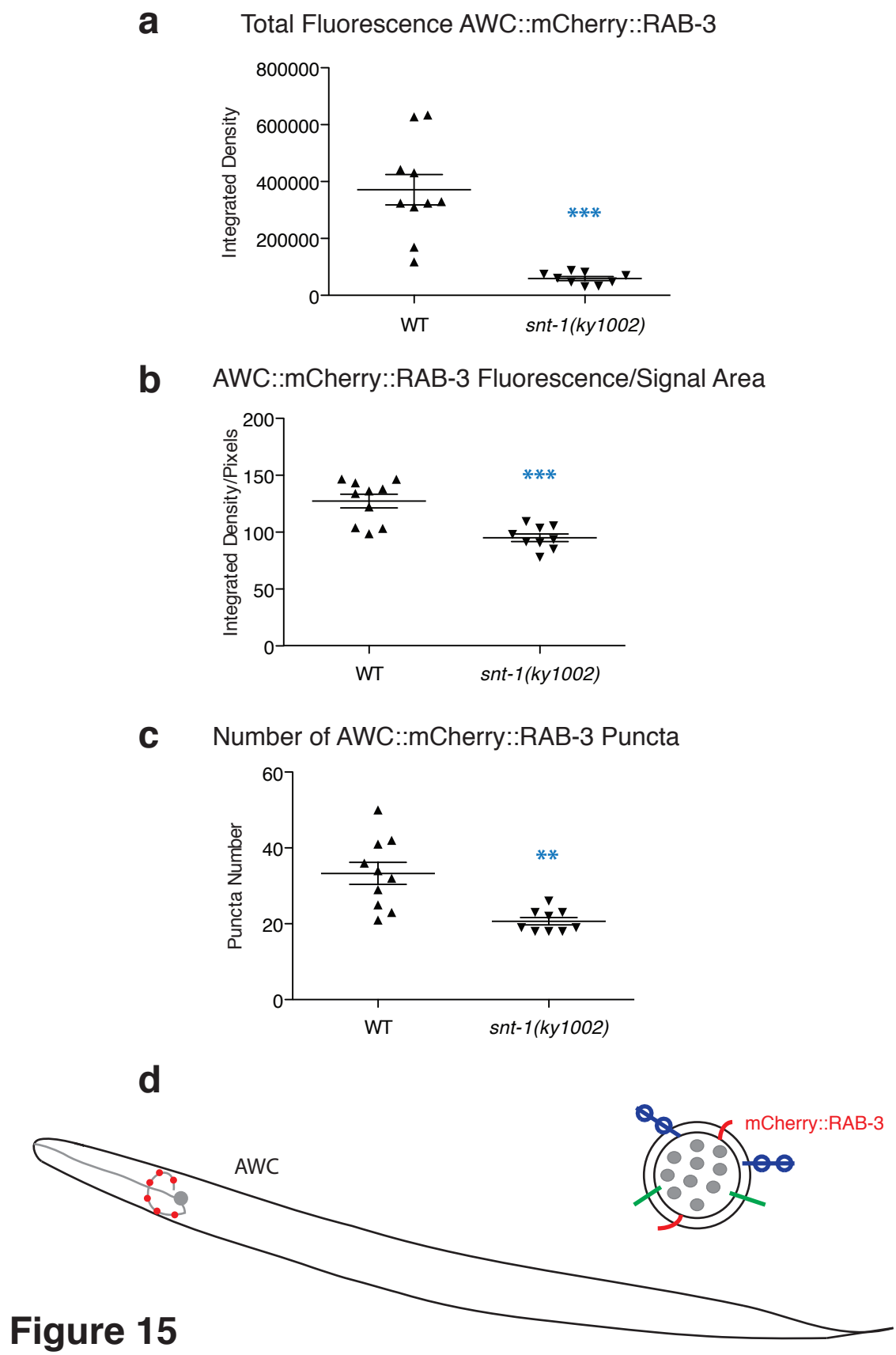
a
Total Fluorescence AWC::mCherry::RAB-3
Integrated Density
800000
600000
400000
200000
0
***
WT
snt-1(ky1002)
b
AWC::mCherry::RAB-3 Fluorescence/Signal Area
Integrated Density/Pixels
200
150
100
50
0
***
WT
snt-1(ky1002)
c
Number of AWC::mCherry::RAB-3 Puncta
Puncta Number
60
40
20
0
**
WT
snt-1(ky1002)
d
AWC
mCherry::RAB-3

Figure 15

Figure 16. *snt-1(ky1002)* brightens GFP::UNC-2 puncta in AWC. (a) Total fluorescence in the region of interest in AWC in each worm. (**p<0.01 versus wildtype, unpaired t-test) (b) Total fluorescence value divided by the number of pixels above the noise threshold, indicating the brightness of the fluorescent signal. (n.s., not statistically significant) (c) Number of fluorescent puncta in the region of interest in each worm. (n.s., not statistically significant) (d) Representation of GFP::UNC-2 puncta in AWC neuron and model of GFP::UNC-2 subunit assembled into a Voltage-Gated Calcium Channel.

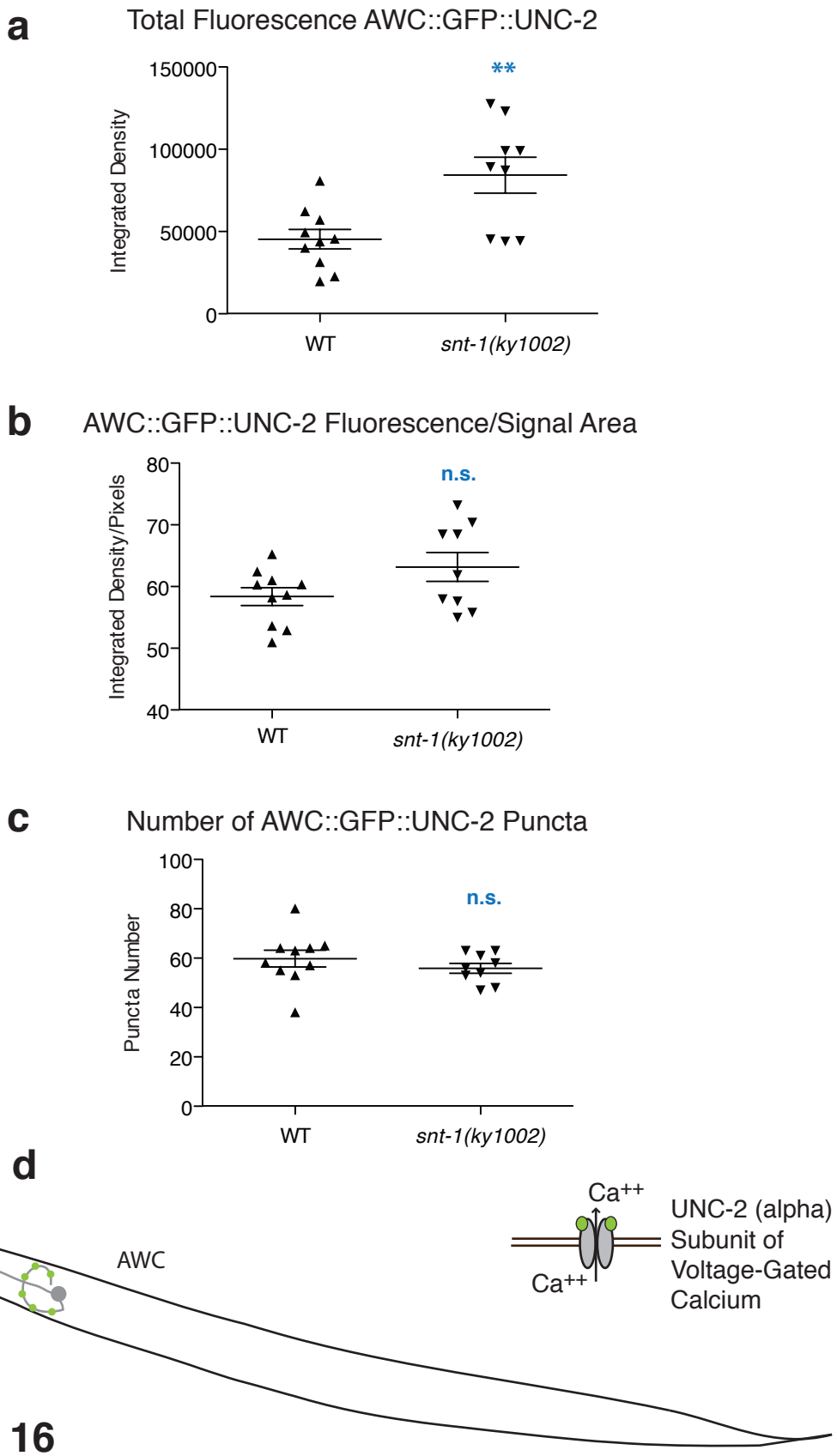
a
Total Fluorescence AWC::GFP::UNC-2
Integrated Density
150000
100000
50000
0
**
WT
snt-1(ky1002)
b
AWC::GFP::UNC-2 Fluorescence/Signal Area
Integrated Density/Pixels
80
70
60
50
40
n.s.
WT
snt-1(ky1002)
c
Number of AWC::GFP::UNC-2 Puncta
Puncta Number
100
80
60
40
20
0
n.s.
WT
snt-1(ky1002)
d
AWC
Ca++
Ca++
UNC-2 (alpha)
Subunit of
Voltage-Gated
Calcium

Figure 16

UNC-2 in AWC may hint at a conserved functional interaction between SNT-1 and voltage-gated calcium channels.

Moreover, previous studies in *Drosophila melanogaster* have shown that such a homeostatic mechanism of modulation pre-synaptic vesicle release exists and that it occurs primarily through the UNC-2 homolog Cacophony (Frank *et al.,* 2006). Impairing the post-synaptic receptor function at the neuromuscular junction results in a compensating increase of pre-synaptic vesicles referred to as synaptic homeostasis (Frank *et al.,* 2006). Parts of the pathway leading to synaptic homeostasis have been uncovered; signals in the pre-synaptic neuron ultimately converge on the Cacophony protein, an UNC-2 homolog (Frank *et al.,* 2009). This homeostatic signaling system that originates in the post-synaptic muscle and then feeds back to the pre-synaptic neuron appears to be a very rapid (on the order of ~10 minutes) means of conferring plasticity on the circuit (Frank *et al.,* 2006). The increased UNC-2 protein in the AWC neuron is hinting that the synaptic homeostasis found in *Drosophila melanogaster* may also be conserved in *C. elegans*, and may even use the same protein pathways.

PVD

Synapses in the PVD sensory neuron, which mediates responses to light, cold, and harsh touch, were examined using the *kyIs445* integrated marker. *kyIs445* consists of three plasmids: *des-2::mCherry::rab-3*, which marks RAB-3 synaptic vesicle associated protein in PVD sensory neuron; *des-2::sad-1::GFP*,

which marks SAD-1 serine/threonine kinase in PVD; and *odr-1::dsRed,* a co-injection marker.

The *ky1002* allele significantly reduced the number, but did not affect the peak brightness of mCherry::RAB-3 puncta. The overall total fluorescent signal of mCherry::RAB-3 was significantly reduced, however, indicating that the size of these puncta was also smaller in the mutant background in wildtype (Fig. 17). This result suggests that *snt-1(ky1002)* affects synaptic vesicles in PVD as well as in AWC and PQR.

The SAD-1::GFP marker was also present in the *kyIs445* PVD-marked background; *sad-1* encodes a conserved serine/threonine kinase that is localized near, but not on synaptic vesicles. SAD-1 helps establish neuronal polarity, promotes synapse formation, and maintains SV clustering patterns in later larval stages (Crump *et al.,* 2001; Kim *et al.,* 2008). *sad-1* mutants have diffuse clusters of synaptic vesicles, overextended axons, and dendritically mislocalized synaptic vesicles (Crump *et al.,* 2001). The *snt-1(ky1002)* mutation did not affect on the SAD-1::GFP marker in PVD neurons, indicating that this perisynaptic protein does not relocalize in concert with synaptic vesicles (Fig. 18).

DD

Synapses in the six DD GABAergic motor neurons, which mediate sinusoidal locomotion, were examined using the *kyIs476* integrated marker. *kyIs476* consists of three plasmids: *unc-25::mCherry::rab-3*, which marks RAB-3 synaptic vesicle associated protein in GABAergic neurons, including DD neurons; *unc-*

Figure 17. *snt-1(ky1002)* affects mCherry::RAB-3 in PVD. (a) Total fluorescence in the region of interest in PVD in each worm. (**p<0.01 versus wildtype, unpaired t-test) (b) Total fluorescence value divided by the number of pixels above the noise threshold, indicating the brightness of the fluorescent signal. (n.s., not statistically significant) (c) Number of fluorescent puncta in the region of interest in each worm. (*p<0.05 versus wildtype, unpaired t-test) (d) Representation of mCherry::RAB-3 puncta in PVD neuron and model of mCherry::RAB-3 associated with a synaptic vesicle.

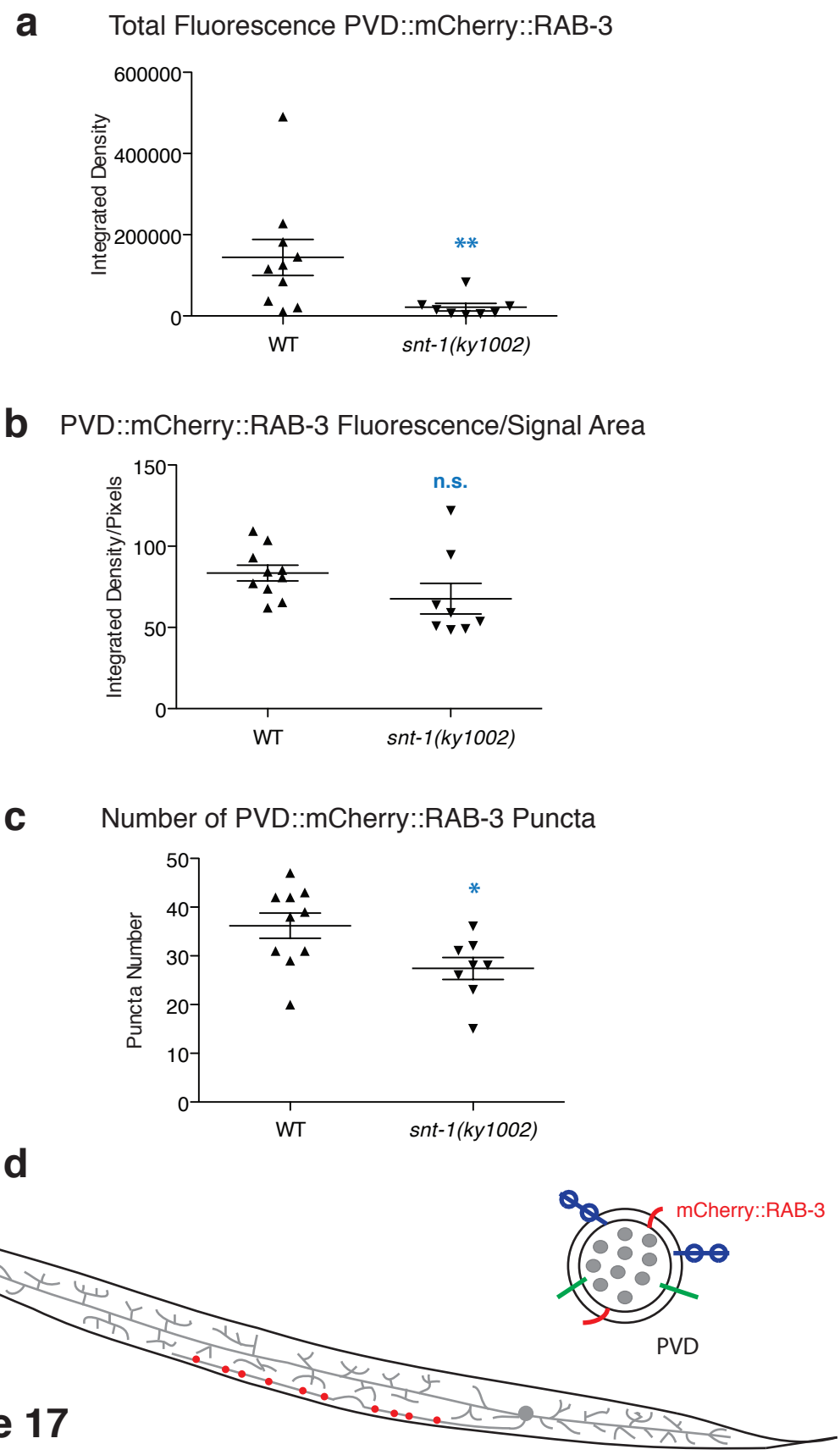
a
Total Fluorescence PVD::mCherry::RAB-3
Integrated Density
600000
400000
200000
0
**
WT
snt-1(ky1002)
b
PVD::mCherry::RAB-3 Fluorescence/Signal Area
Integrated Density/Pixels
150
100
50
0
n.s.
WT
snt-1(ky1002)
c
Number of PVD::mCherry::RAB-3 Puncta
Puncta Number
50
40
30
20
10
0
*
WT
snt-1(ky1002)
d
mCherry::RAB-3
PVD

Figure 17

Figure 18**.** *snt-1(ky1002)* has no significant effect on SAD-1:GFP fluorescence in PVD. (a) Total fluorescence in the region of interest in PVD in each worm. (n.s., not statistically significant) (b) Total fluorescence value divided by the number of pixels above the noise threshold, indicating the brightness of the fluorescent signal. (n.s., not statistically significant) (c) Number of fluorescent puncta in the region of interest in each worm. (n.s., not statistically significant) (d) Representation of SAD-1::GFP puncta in PVD neuron and model of SAD-1::GFP in the cytoplasm near the synaptic vesicles.

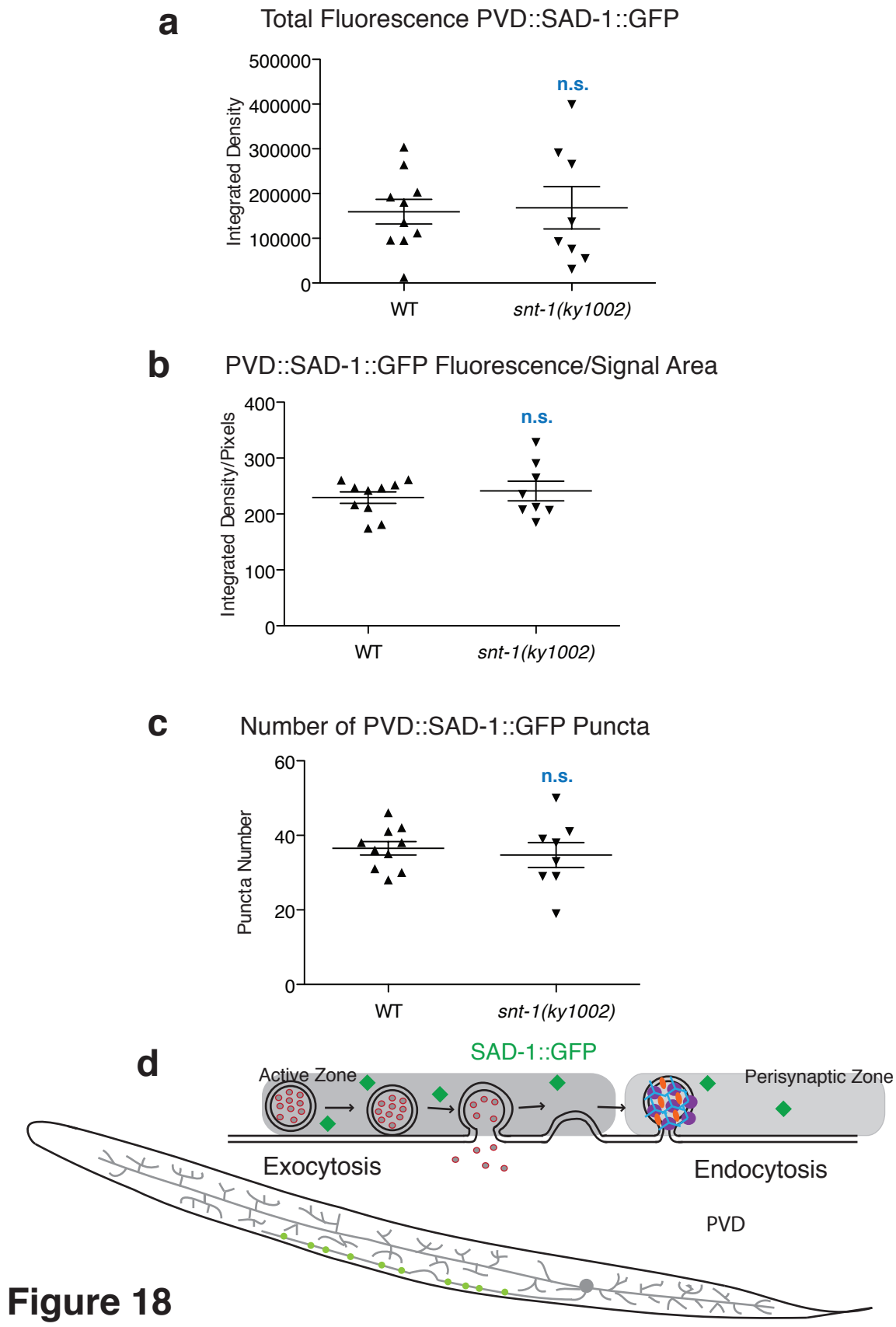
a
Total Fluorescence PVD::SAD-1::GFP
Integrated Density
500000
400000
300000
200000
100000
0
n.s.
WT
snt-1(ky1002)
b
PVD::SAD-1::GFP Fluorescence/Signal Area
Integrated Density/Pixels
400
300
200
100
0
n.s.
WT
snt-1(ky1002)
c
Number of PVD::SAD-1::GFP Puncta
Puncta Number
60
40
20
0
n.s.
WT
snt-1(ky1002)
d
SAD-1::GFP
Active Zone
Perisynaptic Zone
Exocytosis
Endocytosis
PVD

Figure 18

Figure 19. *snt-1(ky1002)* affects mCherry::RAB-3 puncta number in DD neurons. (a) Total fluorescence in the region of interest in DD in each worm. (n.s., not statistically significant) (b) Total fluorescence value divided by the number of pixels above the noise threshold, indicating the brightness of the fluorescent signal. (n.s., not statistically significant) (c) Number of fluorescent puncta in the region of interest in each worm. (*$p<0.05$ versus wildtype, unpaired t-test) (d) Representation of mCherry::RAB-3 puncta in DD neurons and model of mCherry::RAB-3 associated with a synaptic vesicle.

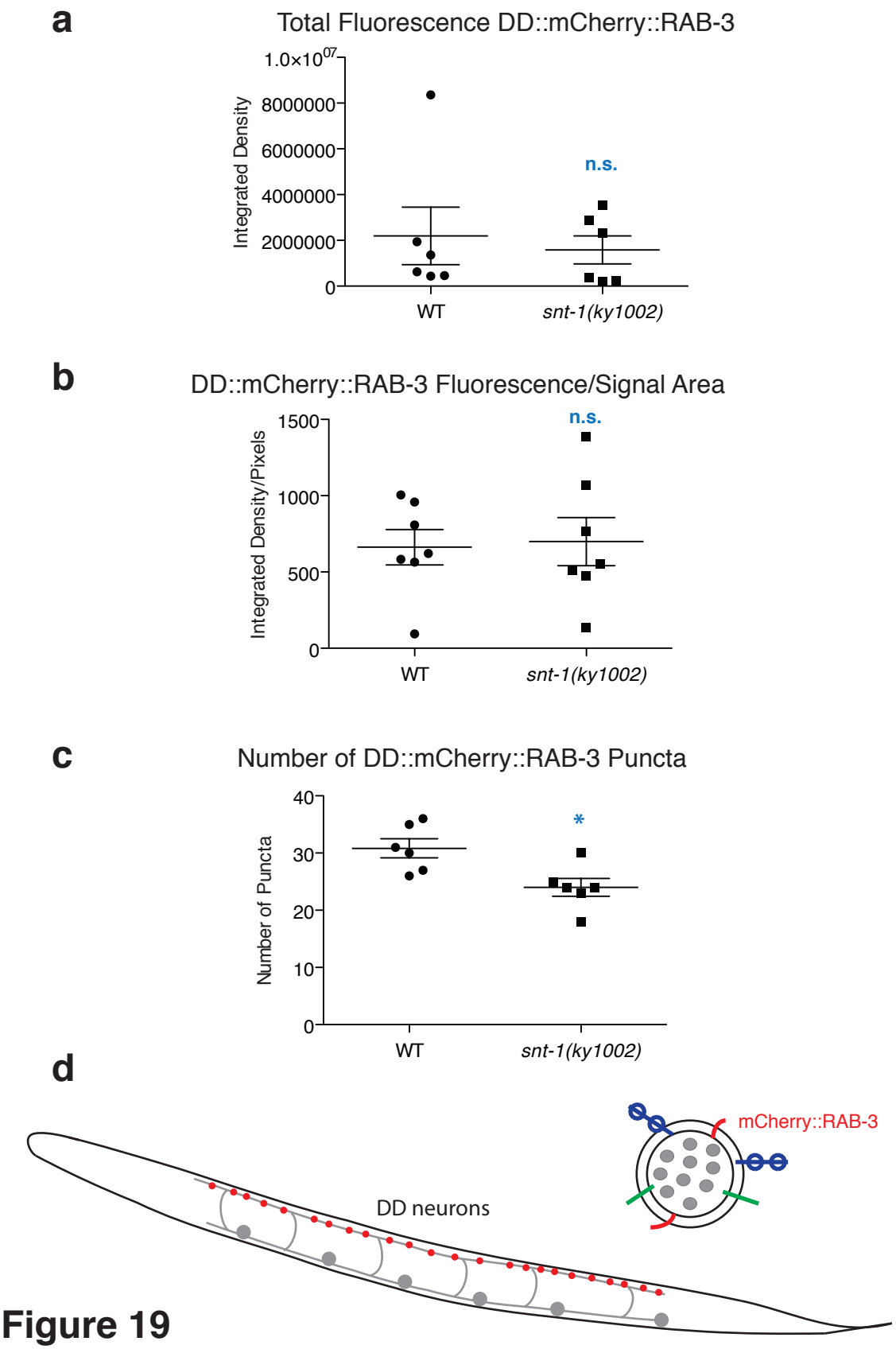
a
Total Fluorescence DD::mCherry::RAB-3
Integrated Density
1.0×10^07
8000000
6000000
4000000
2000000
0
n.s.
WT
snt-1(ky1002)
b
DD::mCherry::RAB-3 Fluorescence/Signal Area
Integrated Density/Pixels
1500
1000
500
0
n.s.
WT
snt-1(ky1002)
c
Number of DD::mCherry::RAB-3 Puncta
Number of Puncta
40
30
20
10
0
*
WT
snt-1(ky1002)
d
mCherry::RAB-3
DD neurons

Figure 19

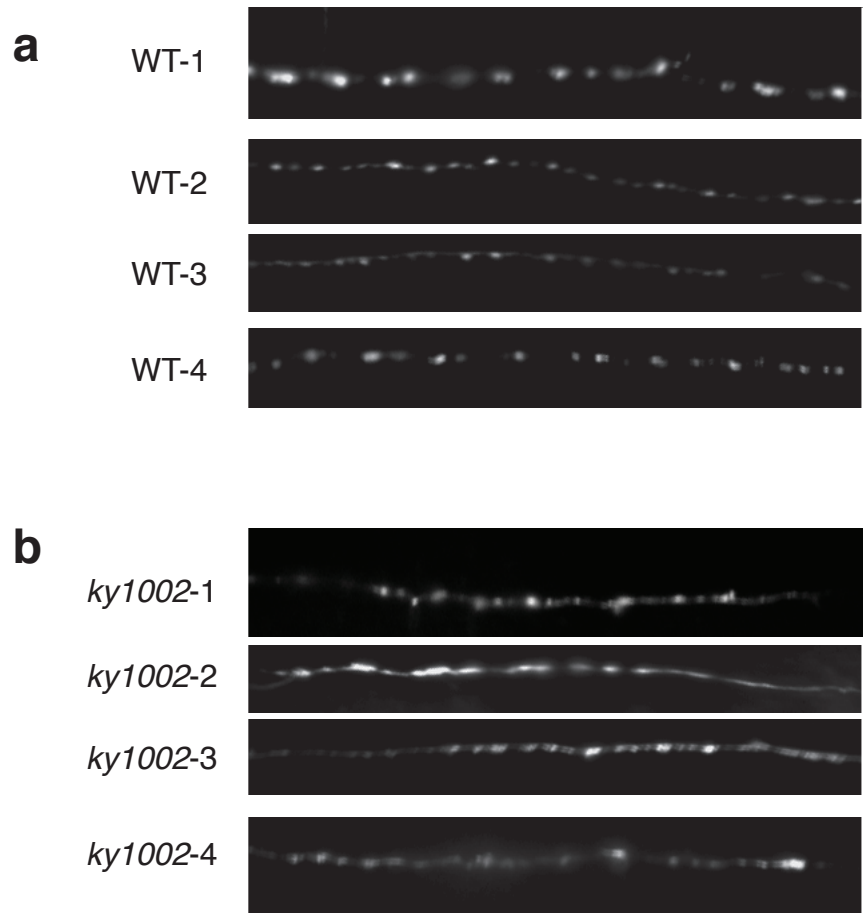

Figure 20. *snt-1(ky1002)* mutation causes mCherry::RAB-3 puncta to be less circular with a smaller interpunctal distance. (a) Four representative images of mCherry::RAB-3 in DD neurons in wildtype animals. (b) Four representative images of mCherry::RAB-3 in DD neurons in four *snt-1(ky1002)* mutant animals. All images at the same magnification.

Figure 21. *snt-1(ky1002)* effects on GFP::UNC-2 puncta number in DD neurons. (a) Total fluorescence in the region of interest in DD in each worm. (n.s., not statistically signficant) (b) Total fluorescence value divided by the number of pixels above the noise threshold, indicating the brightness of the fluorescent signal. (n.s., not statistically significant) (c) Number of fluorescent puncta in the region of interest in each worm. (n.s., not statistically significant) (d) Representation of GFP::UNC-2 puncta in DD neurons and model of GFP::UNC-2 subunit assembled into a Voltage-Gated Calcium Channel.

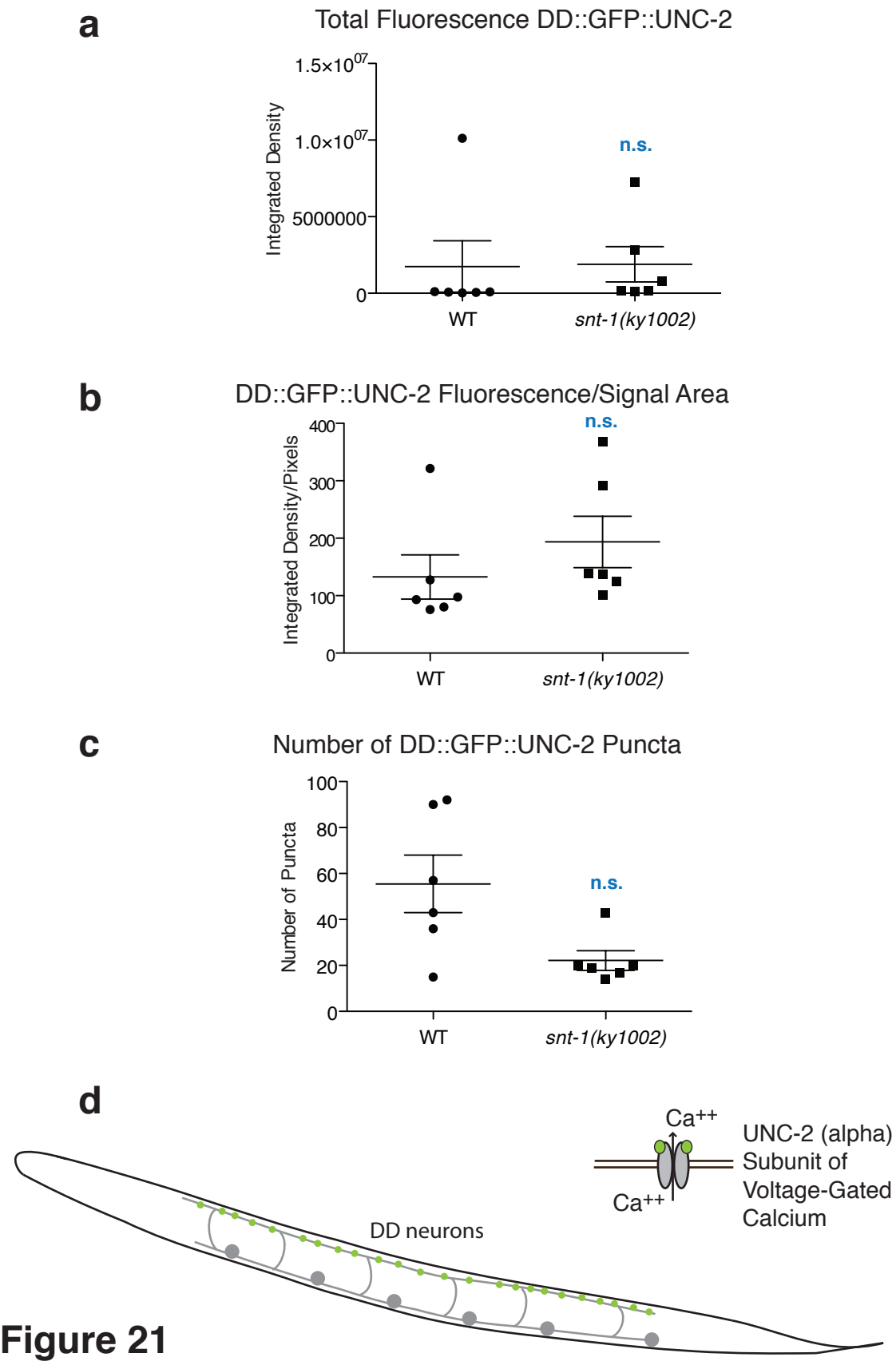
a
Total Fluorescence DD::GFP::UNC-2
Integrated Density
1.5×10^07
1.0×10^07
5000000
0
n.s.
WT
snt-1(ky1002)
b
DD::GFP::UNC-2 Fluorescence/Signal Area
Integrated Density/Pixels
400
300
200
100
0
n.s.
WT
snt-1(ky1002)
c
Number of DD::GFP::UNC-2 Puncta
Number of Puncta
100
80
60
40
20
0
n.s.
WT
snt-1(ky1002)
d
Ca++
Ca++
UNC-2 (alpha)
Subunit of
Voltage-Gated
Calcium
DD neurons

Figure 21

25::GFP::unc-2, which marks UNC-2 alpha subunit of a voltage-gated calcium channel (VGCC) in GABAergic neurons, including DD neurons; and *odr-1::mCherry,* a co-injection marker.

The *snt-1(ky1002)* mutant showed significant difference in the mCherry::RAB-3 puncta number, but did not significantly affect overall fluorescence or brightness in DD GABAergic neurons (Fig. 19) . This result indicates that *snt-1(ky1002)* affects motor neurons in addition to sensory neurons, suggesting that *snt-1(ky1002)* probably affects all of the neurons in which SNT-1A is produced. While the image quantification method detects some parameters of mCherry::RAB-3 puncta signal, it does not describe the roundness of the puncta or the interpunctal distance, both of which are strikingly affected by the *snt-1(ky1002)* mutation in DD neurons (Fig. 20). This qualitative result supports the idea that *snt-1(ky1002)* mutation affects many neurons, but with effects that vary in detail between different cell types.

There are fewer GFP::UNC-2 puncta in the DD neurons, but this result is not statistically significant, due to the small dataset (n=6) (Fig. 21). Furthermore, measuring GFP::UNC-2 puncta in the *kyIs476* background was technically difficult. A very dim signal that could not be detected by eye and required longer-than-usual exposure times, coupled with photobleaching problems and gut fluorescence proved rather challenging. Thus, these results do not support or refute the GFP::UNC-2 results seen in AWC.

Conclusion: *snt-1(ky1002) affects RAB-3 in multiple neurons.*

Table 3. Changes in RAB-3 fluorescent signal by cell type

Cell Type	Total Fluorescence	Puncta Brightness	Puncta Number
PQR	↓	↓	no change
AWC	↓	↓	↓
PVD	↓	no change	↓
DD	no change	no change	↓

In conclusion, in addition to reducing the YFP::RAB-3 signal in PQR, *snt-1(ky1002)* also affects RAB-3 signal in AWC, PVD, and DD neurons, indicating that *snt-1a* expression is critical in multiple neuron types throughout the body. Interestingly, the *snt-1(ky1002)* mutation caused an increase in GFP::UNC-2 total fluorescence in AWC, hinting at a homeostatic compensatory mechanism that is possibly conserved in other species. This result could not be confirmed in DD neurons due to technical difficulties.

To further investigate the potential synaptic homeostasis mechanisms in *C. elegans*, I examined the GFP::UNC-2 signal in a number of synaptic mutant backgrounds to determine if other endocytosis or exocytosis mutants showed an increase in GFP::UNC-2 expression (Supp. Fig. 4). An interesting result was obtained from *elks-1(tm1233)*, which knocks out the single *C. elegans* ELKS homolog. ELKS expression in *C. elegans* is restricted to the active zone, where exocytosis of synaptic vesicles occurs (Deken *et al.,* 2005). ELKS-1 is not essential for synaptic transmission; *elks-1* mutants have no aldicarb resistance or sensitivity compared to wildtype animals and closely resemble wildtype animals

in electrophysiology experiments (Deken *et al.,* 2005). ELKS interacts with UNC-10, but this interaction is not necessary for the proper localization of RIM to the active zone (Deker *et al.,* 2005). ELKS is proposed to act as a scaffold-like protein at the active zone. *unc-10* encodes the only RIM (Rab3 Interacting Molecule) protein in *C. elegans* (Koushika *et al.,* 2001). *elks-1(tm1233)* mutants had normal mCherry::RAB-3 signal in AWC, but a significant increase in GFP::UNC-2 total fluorescence. This effect is perhaps an indicator that in the absence of the organizing scaffold ELKS molecule, the active zone is less restricted within the axon, and an increased number of UNC-2-containing voltage-gated calcium channels must be generated to maintain synaptic signaling capacity. Thus, *elks-1* is a second example, with *unc-13*, of a mutant that increases synaptic UNC-2.

Another mutant examined was *unc-18(e234)*, in which exocytosis is severely blocked at the docking step. *unc-18(e234)* mutant animals showed significantly increased mCherry::RAB-3 brightness compared to wildtype animals, but did not differ from wildtype animals in terms of GFP::UNC-2 fluorescent signal. *dyn-1(ky51)* carries a mutation in the dynamin gene that is required for vesicle fission during endocytosis. *dyn-1(ky51)* animals had no mCherry:: RAB-3 defects, but had a significantly decreased GFP::UNC-2 fluorescent signal. This result hints that perhaps, when exocytosis is occurring at a rate that outpaces endocytic re-uptake of vesicles, the UNC-2-containing voltage-gated calcium channel is down-regulated, in an attempt to rebalance the exocytosis to a lower level.

UNC-10 is believed to play a role in the SV priming step of exocytosis, possibly through interactions with syntaxin-1 (Koushika *et al.,* 2001). In the case of the *unc-10(e102)* mutant animals, the GFP::UNC-2 total fluorescence and brightness of signal were significantly reduced compared to wildtype. This decreased GFP::UNC-2 signal is not surprising considering that the RIM proteins have been shown to bind to calcium channels and to recruit calcium channels to active zones in mice (Reviewed in Sudhof 2012b). This interaction between the *C.elegans* RIM UNC-10 and calcium channels may be conserved in the worm as well, and would account for the decreased GFP::UNC-2 signal seen in AWC in this experiment. Nonetheless, the results with *dyn-1* and *unc-10* should be interpreted with caution, since RAB-3 signal has a trend to lower levels. Therefore, like *dpy-23* and *unc-11* (shown in the next section), it is possible that *dyn-1* and *unc-10* cause a general down-regulation of synaptic markers.

Defining the role or roles of SNT-1 in the neurotransmission cycle

Endocytosis and exocytosis are highly correlated. Synaptic stimulation that causes increased vesicle exocytosis also causes correlated increased endocytosis; endocytosis ceases when exocytosis is blocked (Dittman and Ryan, 2009). SNT-1 has been implicated in both endocytosis and exocytosis in VD and DD neurons; we asked which of these processes leads to its effects in AWC neurons (Jorgensen *et al.,* 1995).

First, the *snt-1(md290)* phenotype was compared to known endocytosis and exocytosis mutants. To represent endocytosis mutants, *dpy-23(e840)* (AP2) and *unc-11(ky280)* (AP180) clathrin adaptor protein mutants were used. The exocytosis mutant *unc-13(e51)* (Munc-13) was employed for comparison. The *kyIs442* AWC-marked line was examined and quantified in each mutant background. *dpy-23, unc-11,* and *unc-13* mutants all displayed reduced mCherry::RAB-3 signal in AWC (Fig. 22). In every case, there were fewer and dimmer puncta, contributing to an overall mCherry::RAB-3 fluorescence reduction. GFP::UNC-2 signal was also reduced in these mutant backgrounds (Fig. 23). Both endocytosis mutants and the exocytosis mutant had reduced number of GFP::UNC-2 puncta and overall less total fluorescence. In addition the *unc-13(e51)* (Munc-13) exocytosis mutant and the *unc-11(ky280)* (AP180) endocytosis mutant had dimmer GFP::UNC-2 puncta than wildtype. The lack of delineation between endocytosis mutant phenotype and exocytosis mutant phenotype made this experiment difficult to interpret. In particular, the overall change in fluorescence could indicate that transgene expression was reduced in these strains for some reason.

As a next approach, we used genetics to ask where SNT-1 acts in the SV release and recycling pathway. There are three potential ways to decrease the number of synaptic vesicles in the axon. One is to decrease the number of vesicles made and trafficked to the active zone. Overactive exocytosis could also result in decreased SV number in the axon. Finally, defective endocytosis could

Figure 22. Endocytosis mutants and exocytosis mutants alike decrease mCherry::RAB-3 fluorescence in AWC. (a) Total fluorescence in the region of interest in AWC in each worm. (***p<0.001 versus wildtype, ANOVA with Tukey's Post Test). (b) Total fluorescence value divided by the number of pixels above the noise threshold, indicating the brightness of the fluorescent signal. (***p<0.001 versus wildtype, **p<0.01 versus wildtype, and n.s. not statistically significant ANOVA with Tukey's Post Test). (c) Number of fluorescent puncta in the region of interest in each worm.(*p<0.05 versus wildtype, n.s. not statistically significant Kruskal-Wallis ANOVA with Dunn's Multiple Comparisons Post Test) (d) Model of steps of neurotransmission with UNC-13, UNC-11, and DPY-23 shown at sites of action. Representation of mCherry::RAB-3 puncta in AWC neuron and model of mCherry::RAB-3 associated with a synaptic vesicle.

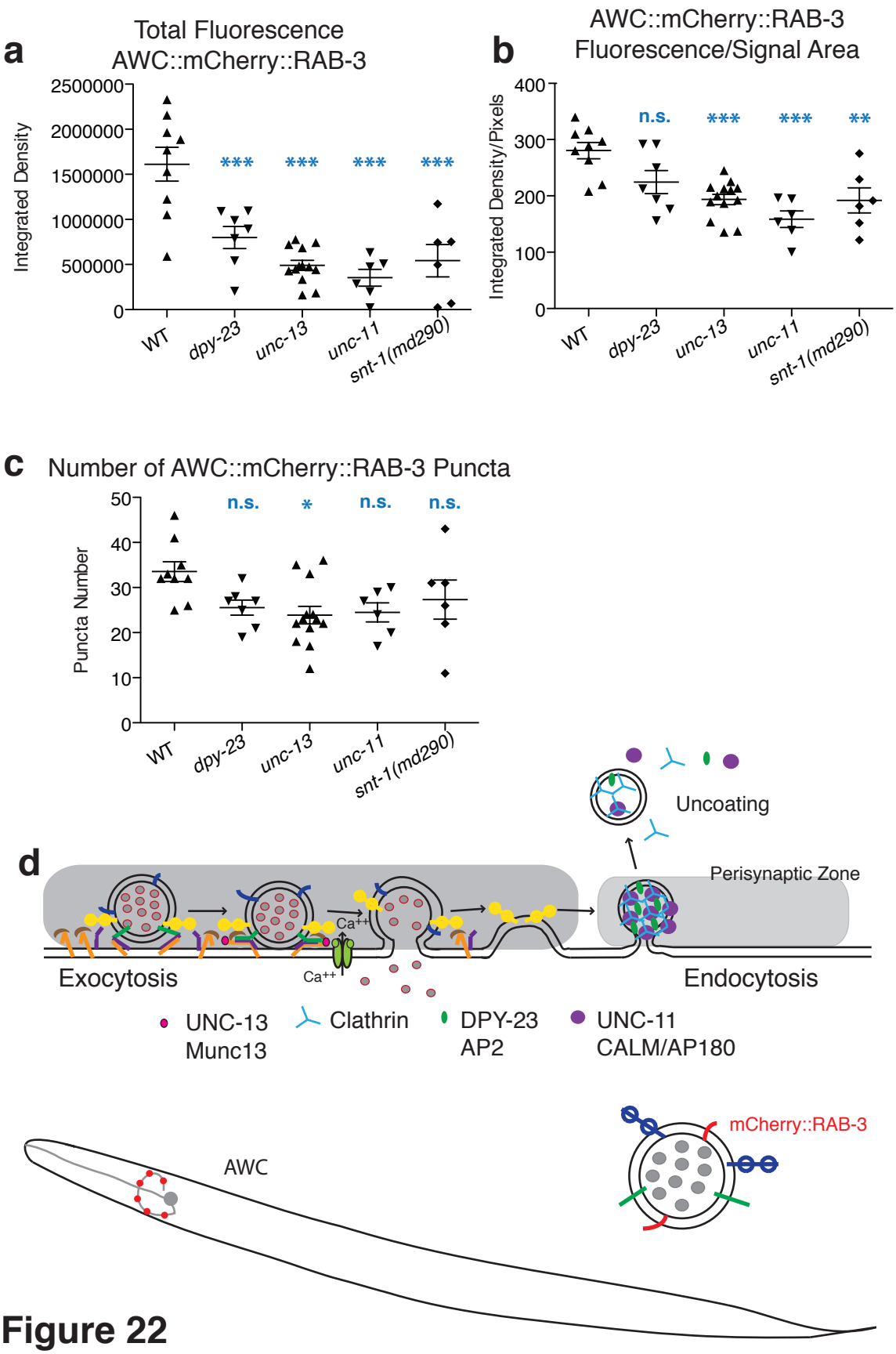
a
Total Fluorescence
AWC::mCherry::RAB-3
Integrated Density
2500000
2000000
1500000
1000000
500000
0
***
***
***
***
WT
dpy-23
unc-13
unc-11
snt-1(md290)
b
AWC::mCherry::RAB-3
Fluorescence/Signal Area
Integrated Density/Pixels
400
300
200
100
0
n.s.
***
***
**
WT
dpy-23
unc-13
unc-11
snt-1(md290)
c
Number of AWC::mCherry::RAB-3 Puncta
Puncta Number
50
40
30
20
10
0
n.s.
*
n.s.
n.s.
WT
dpy-23
unc-13
unc-11
snt-1(md290)
d
Uncoating
Perisynaptic Zone
Ca++
Ca++
Exocytosis
Endocytosis
UNC-13
Munc13
Clathrin
DPY-23
AP2
UNC-11
CALM/AP180
AWC
mCherry::RAB-3

Figure 22

Figure 23. Endocytosis mutants and exocytosis mutants alike have decreased GFP::UNC-2 fluorescence in AWC. (a) Total fluorescence in the region of interest in AWC in each worm. (**p<0.01 versus wildtype, n.s. not statistically significant Kruskal-Wallis ANOVA with Dunn's Multiple Comparisons Post Test) (b) Total fluorescence value divided by the number of pixels above the noise threshold, indicating the brightness of the fluorescent signal. (**p<0.01 versus wildtype, *p<0.05, and n.s. not statistically significant ANOVA with Tukey's Post Test). (c) Number of fluorescent puncta in the region of interest in each worm. (**p<0.01, n.s. not statistically significant ANOVA with Tukey's Post Test). (d) Model of steps of neurotransmission with UNC-13, UNC-11, and DPY-23 shown at sites of action. Representation of GFP::UNC-2 puncta in AWC neuron and model of GFP::UNC-2 subunit assembled into a Voltage-Gated Calcium Channel.

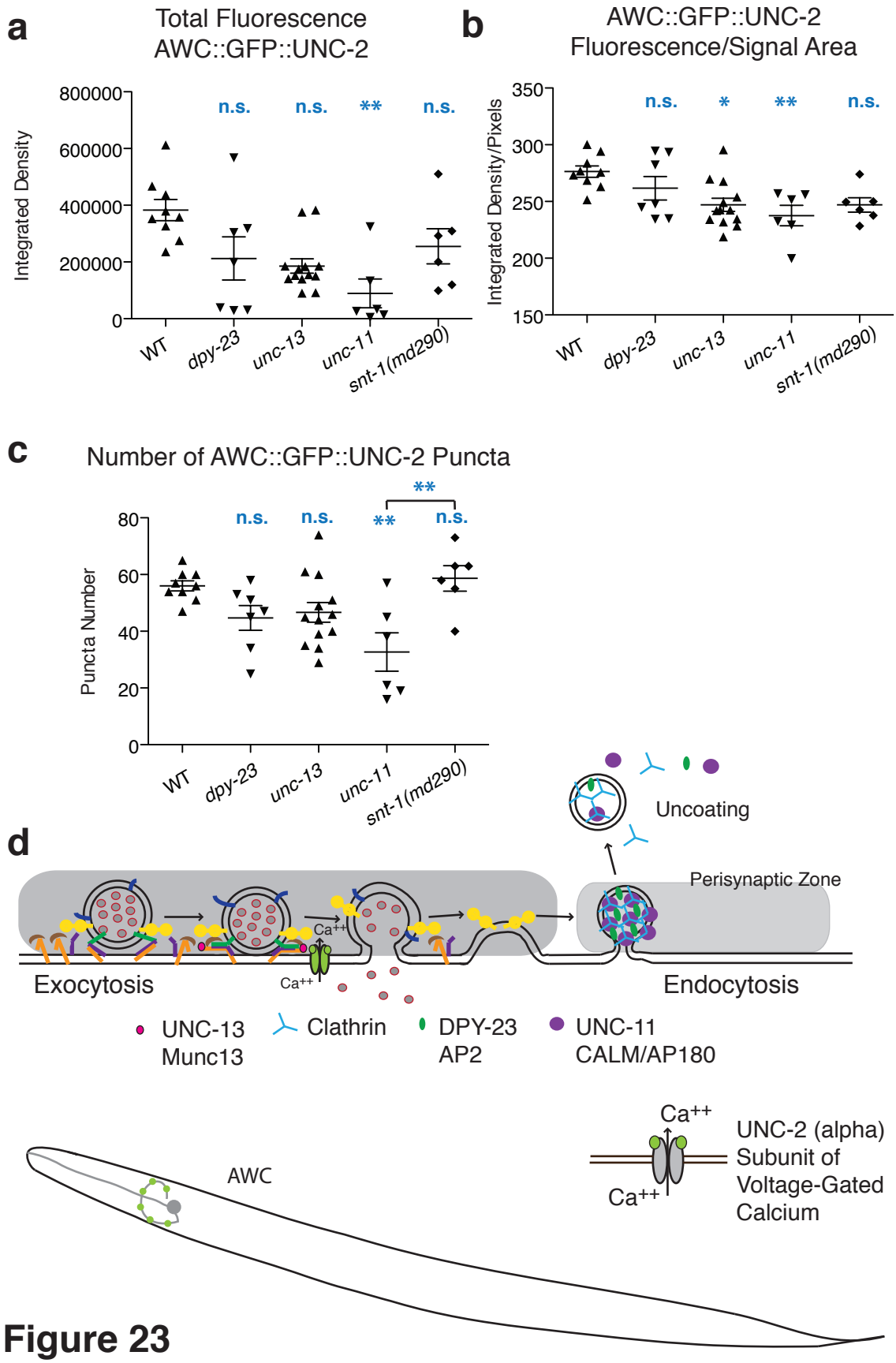
a
Total Fluorescence
AWC::GFP::UNC-2
Integrated Density
800000
600000
400000
200000
0
n.s.
n.s.
**
n.s.
WT
dpy-23
unc-13
unc-11
snt-1(md290)
b
AWC::GFP::UNC-2
Fluorescence/Signal Area
Integrated Density/Pixels
350
300
250
200
150
n.s.
*
**
n.s.
WT
dpy-23
unc-13
unc-11
snt-1(md290)
c
Number of AWC::GFP::UNC-2 Puncta
Puncta Number
80
60
40
20
0
**
n.s.
n.s.
**
n.s.
WT
dpy-23
unc-13
unc-11
snt-1(md290)
d
Uncoating
Perisynaptic Zone
Ca++
Ca++
Exocytosis
Endocytosis
UNC-13
Munc13
Clathrin
DPY-23
AP2
UNC-11
CALM/AP180
AWC
Ca++
Ca++
UNC-2 (alpha)
Subunit of
Voltage-Gated
Calcium

Figure 23

result in SV depletion after exocytosis that could not be recovered through subsequent endocytosis.

One experiment to address whether *snt-1* affects SV biogenesis used a null allele of *unc-18* (munc18). UNC-18 (Munc18) is an Sec1/Munc18 like or SM-protein, thought to play a key role in priming and/or docking of synaptic vesicles. Double mutant lines were generated that contained the *snt-1(md290)* null allele and an *unc-18(e234)* nonsense allele in the PQR-marked background. Because UNC-18 (Munc18) interacts with RAB-3 (Rab3B), the SV marker used was SNB-1::YFP. *snt-1(md290)* showed a significant reduction in SNB-1::YFP brightness compared to wildtype (Fig. 24), which is consistent with the result of *snt-1(ky1002)* reducing SNB-1::YFP signal (Fig. 14). *unc-18(e234)* did not significantly affect SNB-1::YFP compared to wildtype, indicating that while exocytosis was blocked in the *unc-18(e234)* background, SV-associated SNB-1::YFP was still being trafficked to the active zone at a normal level. When two *snt-1(md290); unc-18(e234)* double mutant lines 3G and 4E were examined, they most closely resembled wildtype and *unc-18(e234)* single mutant phenotypes. Notably, the *snt-1(md290); unc-18(e234)* 3G mutant line had significantly brighter SNB-1::YFP signal than the *snt-1(md290)* single mutant, suggesting suppression of the *snt-1(md290)* phenotype. However, the effect of *snt-1(md290)* in the experiment was small, and the suppression minimal, raising concerns about its reliability. These results overall indicated that SNB-1::YFP marker, which was introduced in the background by a chromosomal array, was not capable of

Figure 24. *unc-18* may suppress the *snt-1* defect in total synaptic SNB-1::YFP fluorescence. (a) Total fluorescence in the region of interest in PQR in each worm. (n.s. not statistically significant Kruskal-Wallis ANOVA with Dunn's Multiple Comparisons Post Test) (b) Total fluorescence value divided by the number of pixels above the noise threshold, indicating the brightness of the fluorescent signal. (*$p<0.05$ *snt-1* versus wildtype and *snt-1* versus double mutant, n.s., not statistically significant, ANOVA with Tukey's Post Test) (c) Number of fluorescent puncta in the region of interest in each worm. (n.s. not statistically significant Kruskal-Wallis ANOVA with Dunn's Multiple Comparisons Post Test) (d) Model of UNC-18 acting in exocytosis during docking and priming via interactions with syntaxin-1 and the SNARE complex. Representation of SNB-1::YFP puncta in PQR neuron and model of SNB-1::YFP associated with a synaptic vesicle.

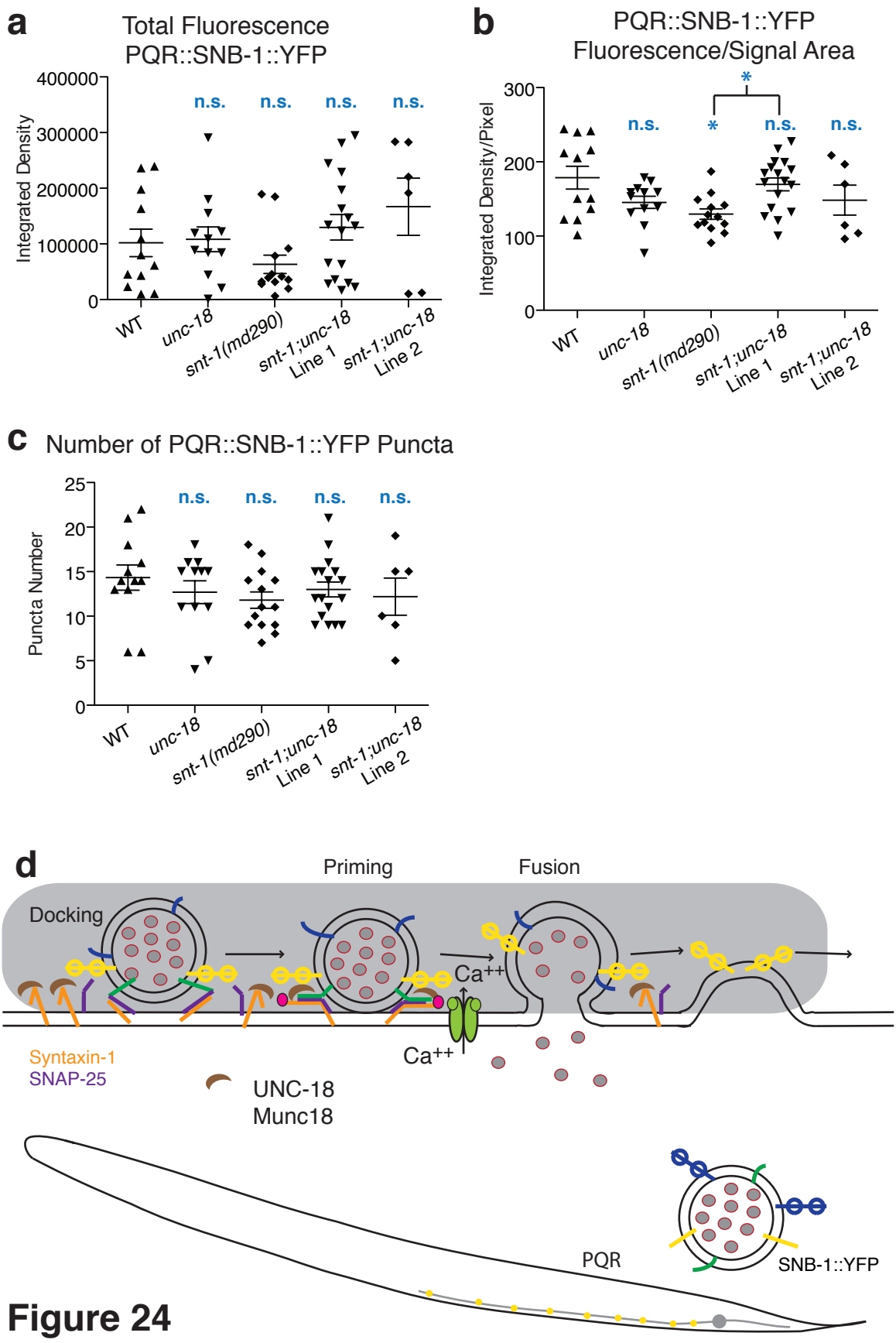
a
Total Fluorescence
PQR::SNB-1::YFP
Integrated Density
400000
300000
200000
100000
0
n.s.
n.s.
n.s.
n.s.
WT
unc-18
snt-1(md290)
snt-1;unc-18 Line 1
snt-1;unc-18 Line 2
b
PQR::SNB-1::YFP
Fluorescence/Signal Area
Integrated Density/Pixel
300
200
100
0
*
n.s.
*
n.s.
n.s.
WT
unc-18
snt-1(md290)
snt-1;unc-18 Line 1
snt-1;unc-18 Line 2
c
Number of PQR::SNB-1::YFP Puncta
Puncta Number
25
20
15
10
5
0
n.s.
n.s.
n.s.
n.s.
WT
unc-18
snt-1(md290)
snt-1;unc-18 Line 1
snt-1;unc-18 Line 2
d
Priming
Fusion
Docking
Ca++
Ca++
Syntaxin-1
SNAP-25
UNC-18
Munc18
PQR
SNB-1::YFP

Figure 24

providing strong evidence that blocking exocytosis suppresses the *snt-1* mutant phenotypes.

Next, a null allele of *unc-13/*munc13 was crossed into the *snt-1(md290)* mutant background. *unc-13* mutants are defective in most or all neurotransmission (Miller et al, 1996). In *C. elegans* UNC-13 plays a role in synaptic vesicle fusion in addition to its role in vesicle priming (Madison *et al.,* 2005). *unc-13(e51)* single mutant animals had significantly less YFP::RAB-3 fluorescence in their PQR puncta than wildtype, but the puncta number and brightness did not differ significantly from wildtype, suggesting that YFP::RAB-3 puncta may be slightly larger in *unc-13(e51)* mutants than in wildtype (Fig. 25). *snt-1(ky1002)* showed a reduction in YFP::RAB-3 brightness and total fluorescence compared to wildtype, but did not differ from wildtype in YFP::RAB-3 puncta number. *snt-1(ky1002)* single mutant animals differed significantly from *unc-13(e51)* animals in YFP::RAB-3 puncta number, brightness, and total fluorescence. *unc-13(e51); snt-1(ky1002)* double mutants more closely resembled *unc-13(e51)* mutants, and not *snt-1(ky1002)* mutants, in terms of YFP::RAB-3 brightness and total fluorescence. Thus, the *unc-13(e51)* mutation suppresses the *snt-1(ky1002)* phenotype, consistent with a *snt-1* defect in endocytosis, but also consistent with the possibility of SNT-1 acting downstream of UNC-13 in exocytosis. Furthermore, this result indicates that even in a *snt-1(ky1002)* background, synaptic vesicles marked with RAB-3 are still correctly assembled and trafficked to the active zone if their exocytosis is blocked by an

Figure 25 *unc-13* in PQR suppresses the effect of *snt-1* on total synaptic YFP::RAB-3 fluorescence. (a) Total fluorescence in the region of interest in PQR in each worm. (*p<0.05, **p<0.01, ***p<0.001, ANOVA with Tukey's Post Test) (b) Total fluorescence value divided by the number of pixels above the noise threshold, indicating the brightness of the fluorescent signal. (***p<0.001; n.s. not statistically significant, ANOVA with Tukey's Post Test) (c) Number of fluorescent puncta in the region of interest in each worm. (*p<0.05; n.s. not statistically significant Kruskal-Wallis ANOVA with Dunn's Multiple Comparisons Post Test). (d) Model of UNC-13 acting at the priming step of endocytosis. Representation of YFP::RAB-3 puncta in PQR neuron and model of YFP::RAB-3 associated with a synaptic vesicle.

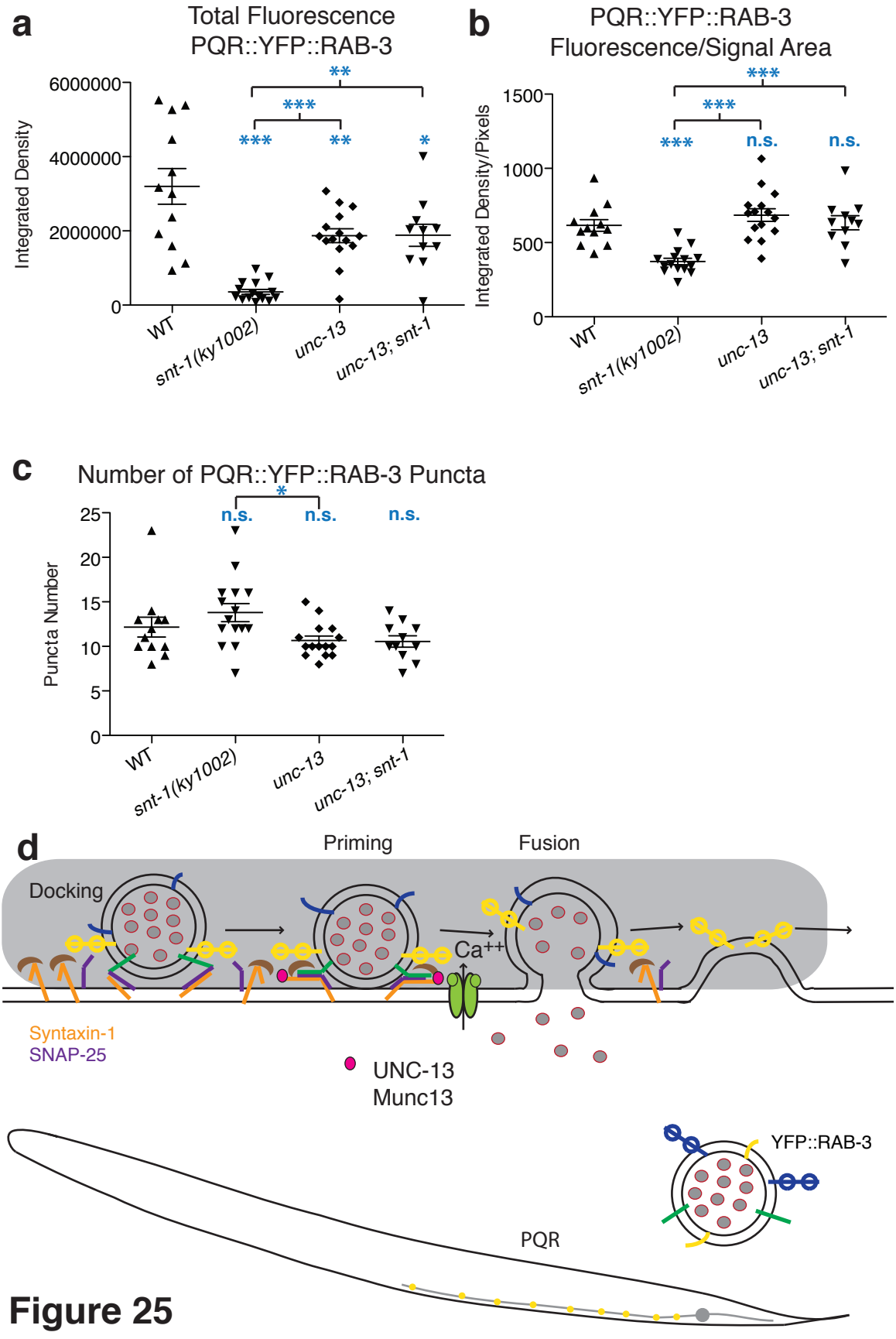
a
Total Fluorescence
PQR::YFP::RAB-3
Integrated Density
6000000
4000000
2000000
0
**
***
***
**
*
WT
snt-1(ky1002)
unc-13
unc-13; snt-1
b
PQR::YFP::RAB-3
Fluorescence/Signal Area
Integrated Density/Pixels
1500
1000
500
0
***
***
***
n.s.
n.s.
WT
snt-1(ky1002)
unc-13
unc-13; snt-1
c
Number of PQR::YFP::RAB-3 Puncta
Puncta Number
25
20
15
10
5
0
*
n.s.
n.s.
n.s.
WT
snt-1(ky1002)
unc-13
unc-13; snt-1
d
Priming
Fusion
Docking
Ca++
Syntaxin-1
SNAP-25
UNC-13
Munc13
YFP::RAB-3
PQR

Figure 25

unc-13 mutation, thus excluding the possibility that *snt-1* mutants are defective in earlier steps SV biogenesis.

Characterizing other synaptotagmin mutants

Similarities of *C. elegans* synaptotagmins to mammalian synaptotagmins:

There are seven synaptotagmin genes in the *C. elegans* genome. All of these molecules share common domains including C2A and C2B regions. SNT-1, SNT-2, SNT-4, SNT-5, SNT-6, and SNT-7 are predicted to be membrane-associated, whereas SNT-3 may not have a transmembrane domain. The exact orthologues within large gene families are not entirely clear, but with that caveat, using the TreeFam database for synaptotagmins (www.treefam.org, see methods), it was determined that *C. elegans snt-1* was most closely related to *C.elegans snt-3* and *Drosophila melanogaster syt-F3*. Both *C. elegans snt-1* and *snt-3* were related to mammalian Syt2, Syt1, and Syt5. *C. elegans snt-2* was somewhat related to *Homo sapiens syt8* and *Mus musculus syt8. C. elegans snt-4* and *snt-5* most closely resembled *Homo sapiens* Syt4 and Syt11, and were more distantly related to mammalian homologs of Syt9, Syt3, Syt6, and Syt10. *C. elegans snt-6* was related to the *Homo sapiens* Syt7, and *C. elegans snt-7* was related to mammalian Syt12, Syt13, Syt15, and *Homo sapiens* Syt17. All *C. elegans* synaptotagmin genes showed strong similarities to other worm species synaptotagmin homologs *e.g. C. briggsae and C. remanei,* but not to synaptotagmins of other model organisms.

In general, the gene size of the *snt* family member is between 4 and 6 kilobases, with spliced mRNAs between 798-1377 nucleotides and peptides ranging from 265 amino acids in length to 458 amino acids. The *snt-5* gene spans 18.4 kilobases, and is the largest *snt* gene; it also codes for the longest protein by six amino acids.

To understand what role other members of the synaptotagmin family might be playing in *C. elegans*, null mutant alleles of *snt-2(tm1711), snt-4(ok503), snt-5(ok3287),* and *snt-6(ok3496)* were crossed into a *kyIs403* background, and expression in PQR was examined (Fig. 26). *snt-2(tm1711)* showed slightly brighter YFP::RAB-3 puncta with a small, not statistically significant increase in total fluorescence compared to wildtype. *snt-4(ok503)* had significantly brighter YFP::RAB-3 puncta than wildtype and a significant increase in total fluorescence compared to wildtype. *snt-5(ok3287)* mutant animals had significantly brighter YFP::RAB-3 puncta than wildtype, but similar numbers of puncta and total fluorescence to wildtype. *snt-6(ok3496)* had slightly fewer YFP::RAB-3 puncta compared to wildtype; however, the YFP::RAB-3 puncta as bright as wildtype puncta and the total fluorescence was comparable to wildtype. The results of *snt-2(tm1711), snt-4(ok503),* and *snt-5(ok3287)* represented the first time a *C. elegans* synaptotagmin mutation was identified that increased synaptic vesicle markers in neurons. This type of phenotype would be predictably present if exocytosis of marked synaptic vesicles was decreased in PQR in *snt-2*, *snt-4*, and *snt-5* mutants.

Figure 26. Some synaptotagmin null mutations affect YFP::RAB-3 fluorescence in PQR. (a) Total fluorescence in the region of interest in PQR in each worm. (b) Total fluorescence value divided by the number of pixels above the noise threshold, indicating the brightness of the fluorescent signal. (c) Number of fluorescent puncta in the region of interest in each worm. (*$p<0.05$ versus wildtype, ***$p<0.001$ versus wildtype, n.s. not statistically significant; ANOVA with Tukey's Post Test) d) Representation of YFP::RAB-3 puncta in PQR neuron and model of YFP::RAB-3 associated with a synaptic vesicle.

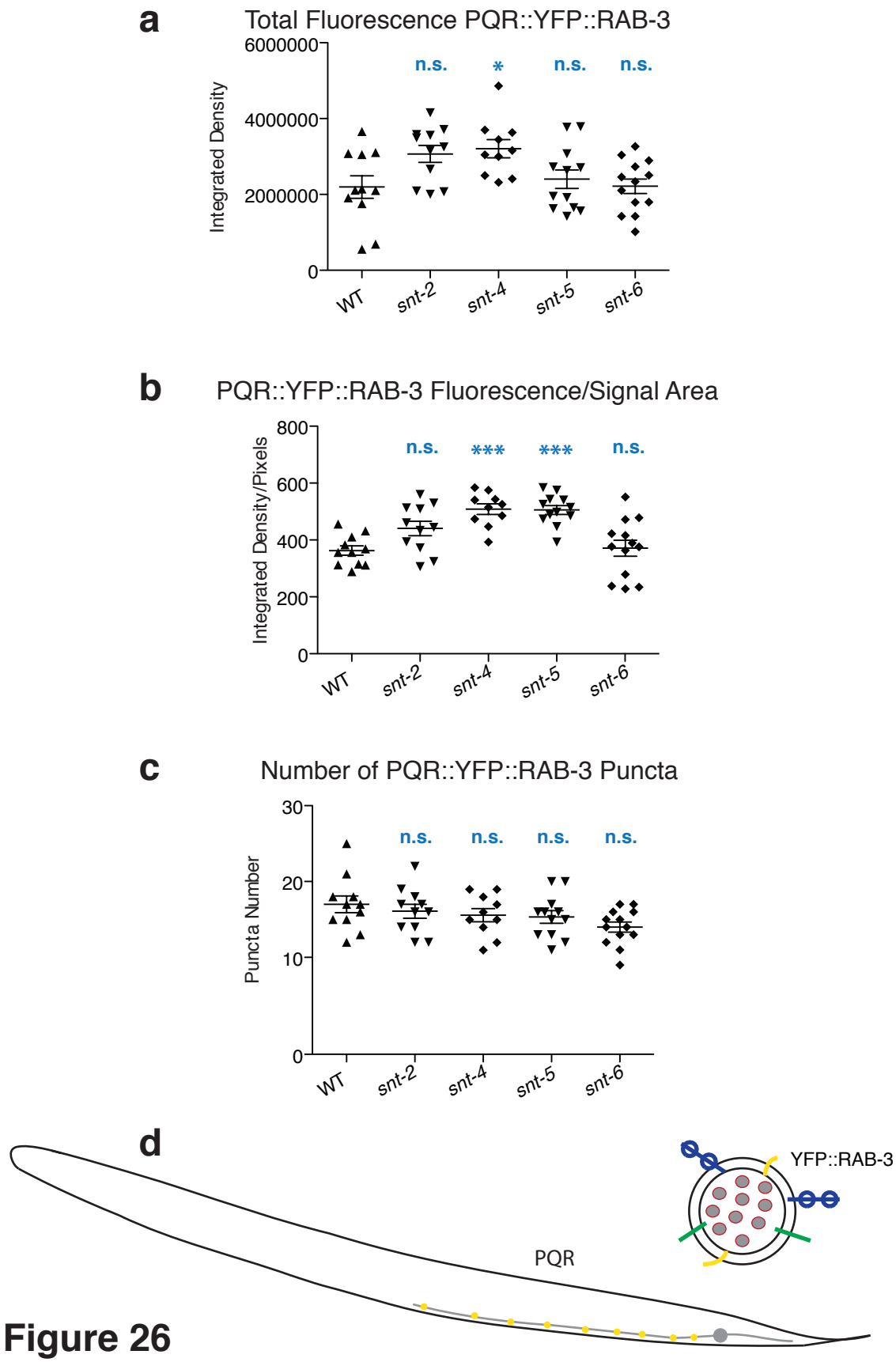
a
Total Fluorescence PQR::YFP::RAB-3
Integrated Density
6000000
4000000
2000000
0
n.s.
*
n.s.
n.s.
WT
snt-2
snt-4
snt-5
snt-6
b
PQR::YFP::RAB-3 Fluorescence/Signal Area
Integrated Density/Pixels
800
600
400
200
0
n.s.
***
***
n.s.
WT
snt-2
snt-4
snt-5
snt-6
c
Number of PQR::YFP::RAB-3 Puncta
Puncta Number
30
20
10
0
n.s.
n.s.
n.s.
n.s.
WT
snt-2
snt-4
snt-5
snt-6
d
YFP::RAB-3
PQR

Figure 26

Table 4. Changes in YFP::RAB-3 fluorescence in PQR

Synaptotagmin	Total Fluorescence	Puncta Brightness	Puncta Number
snt-2	Slight increase	Slight increase	no change
snt-4	↑	↑	no change
snt-5	no change	↑	no change
snt-6	no change	no change	Slight decrease

Null mutant alleles were also examined in AWC, using the *kyIs442* marker. Both *snt-2(tm1711)* and *snt-5(ok3287)* had slightly more mCherry::RAB-3 puncta than wildtype (Fig. 27). In *snt-5(ok3287)* mutant background, mCherry::RAB-3 puncta were also slightly brighter than wildtype puncta, contributing to a significantly higher overall total fluorescence of mcherry::RAB-3 signal in AWC. These results indicate that SNT-5 and perhaps SNT-2 play a role in synaptic vesicle exocytosis in AWC. Alternatively, SNT-2 and SNT-5 may play a role in controlling the size of the pool of vesicles docked in the active zone.

Table 5. Changes in mCherry::RAB-3 fluorescence in AWC

Synaptotagmin	Total Fluorescence	Puncta Brightness	Puncta Number
snt-2	no change	no change	Slight increase
snt-4	no change	no change	no change
snt-5	Slight increase	Slight increase	↑

The AWC GFP::UNC-2 fluorescent signal was also examined in *snt-2(tm1711)*, *snt-4(ok503),* and *snt-5(ok3287)* single mutant backgrounds (Fig. 28).

Figure 27. Mutations in some of the synaptotagmin family slightly affect mCherry::RAB-3 fluorescence in AWC. (a) Total fluorescence in the region of interest in AWC in each worm. (Kruskal-Wallis ANOVA with Dunn's Multiple Comparisons Post Test was used. n.s. not statistically significant compared to wildtype) (b) Total fluorescence value divided by the number of pixels above the noise threshold, indicating the brightness of the fluorescent signal. (Kruskal-Wallis ANOVA with Dunn's Multiple Comparisons Post Test was used. n.s. not statistically significant compared to wildtype) (c) Number of fluorescent puncta in the region of interest in each worm. (ANOVA with Tukey's post-test was used. **$p<0.01$ versus wildtype, n.s. not statistically significant) (d) Representation of mCherry::RAB-3 puncta in AWC neuron and model of mCherry::RAB-3 associated with a synaptic vesicle.

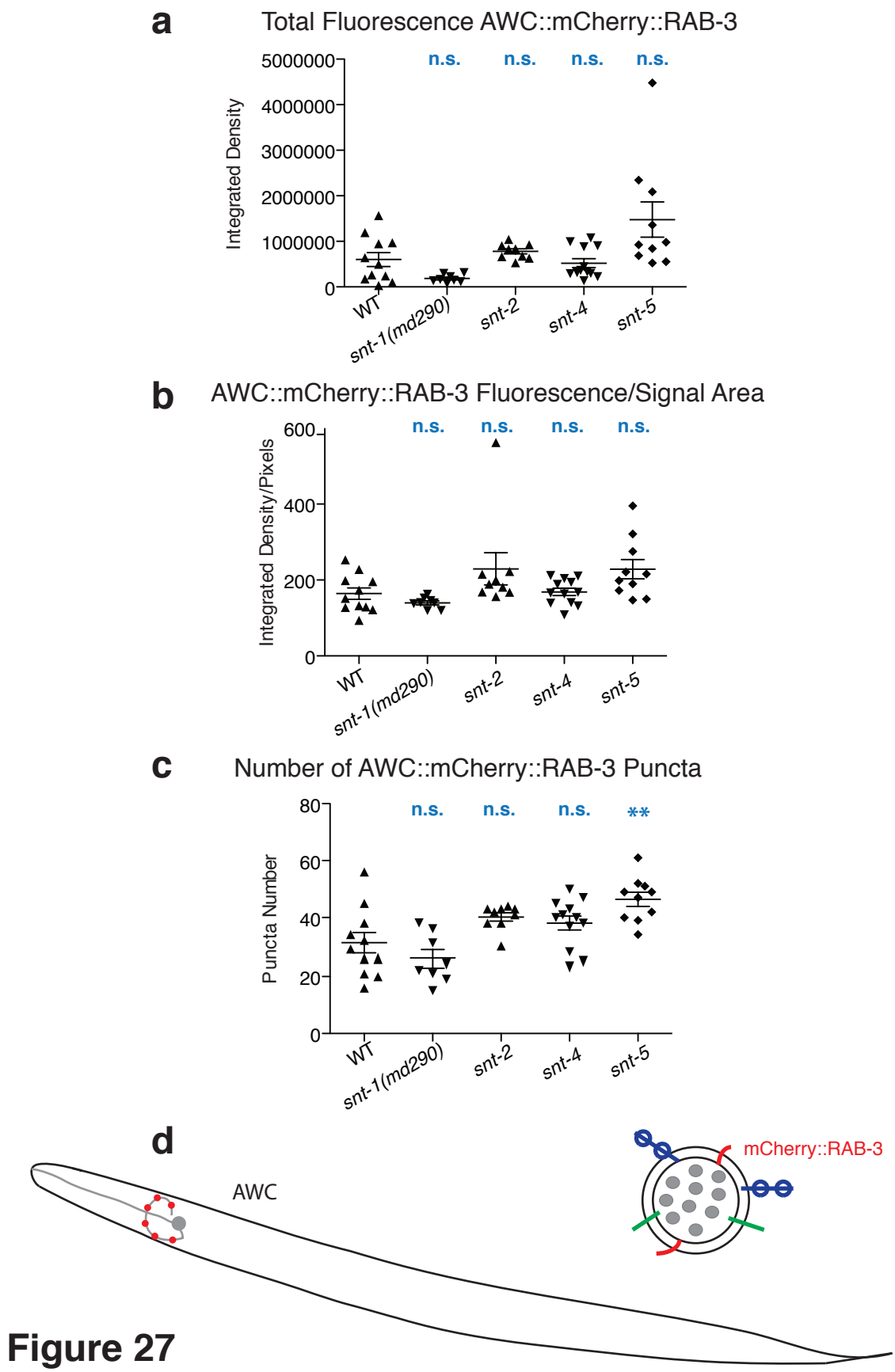
a
Total Fluorescence AWC::mCherry::RAB-3
Integrated Density
5000000
4000000
3000000
2000000
1000000
0
n.s.
n.s.
n.s.
n.s.
WT
snt-1(md290)
snt-2
snt-4
snt-5
b
AWC::mCherry::RAB-3 Fluorescence/Signal Area
Integrated Density/Pixels
600
400
200
0
n.s.
n.s.
n.s.
n.s.
WT
snt-1(md290)
snt-2
snt-4
snt-5
c
Number of AWC::mCherry::RAB-3 Puncta
Puncta Number
80
60
40
20
0
n.s.
n.s.
n.s.
**
WT
snt-1(md290)
snt-2
snt-4
snt-5
d
AWC
mCherry::RAB-3

Figure 27

Figure 28. Mutations in the synaptotagmin family genes do not significantly affect GFP::UNC-2 fluorescence in AWC. (a) Total fluorescence in the region of interest in AWC in each worm. (Kruskal-Wallis ANOVA with Dunn's Multiple Comparisons Post Test was used. n.s. not statistically significant compared to wildtype) (b) Total fluorescence value divided by the number of pixels above the noise threshold, indicating the brightness of the fluorescent signal. (Kruskal-Wallis ANOVA with Dunn's Multiple Comparisons Post Test was used. n.s. not statistically significant compared to wildtype) (c) Number of fluorescent puncta in the region of interest in each worm. (ANOVA with Tukey's Post Test was used. n.s. not statistically significant) (d) Representation of GFP::UNC-2 puncta in AWC neuron and model of GFP::UNC-2 subunit assembled into a Voltage-Gated Calcium Channel.

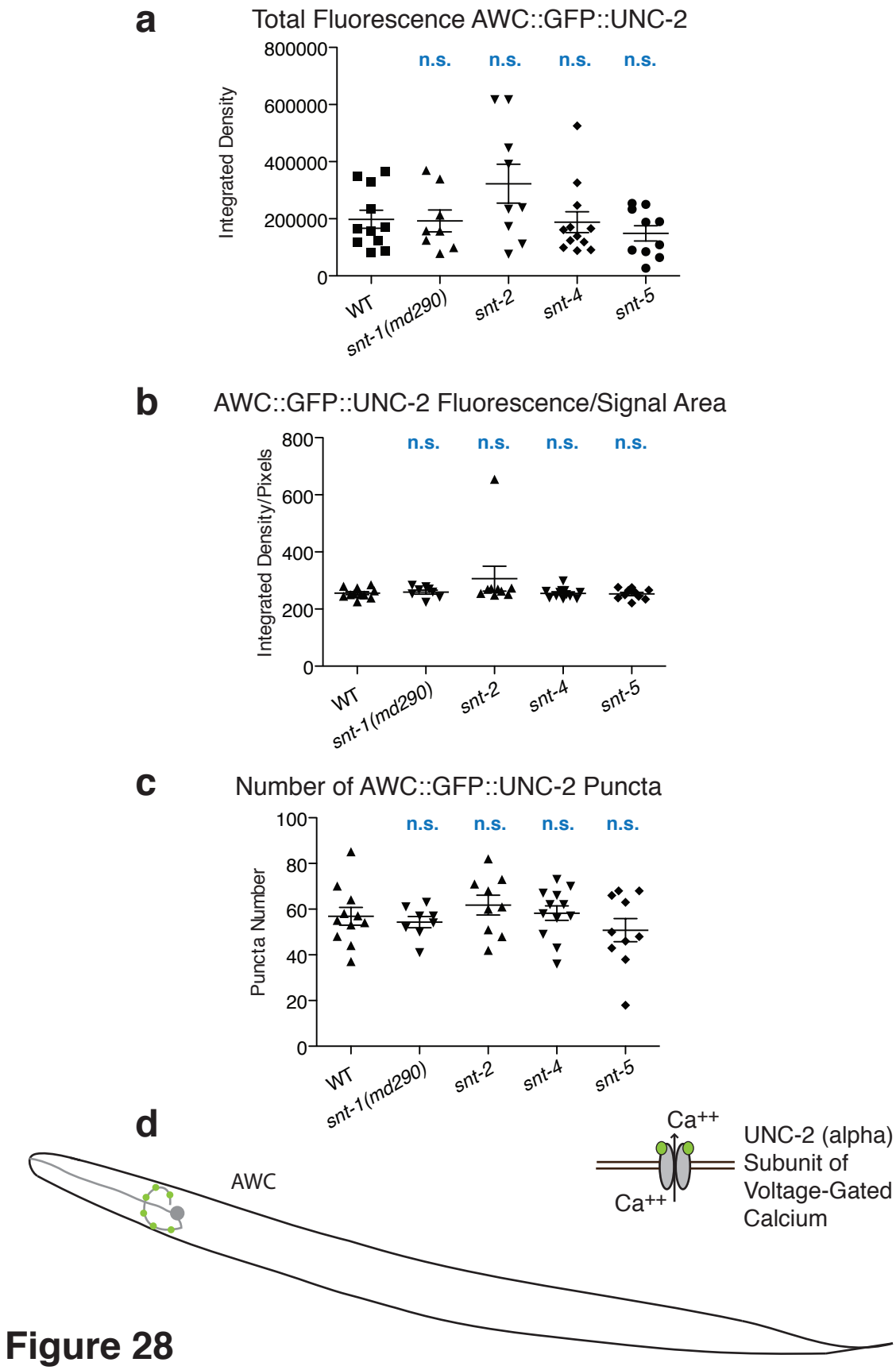
a
Total Fluorescence AWC::GFP::UNC-2
Integrated Density
800000
600000
400000
200000
0
n.s.
n.s.
n.s.
n.s.
WT
snt-1(md290)
snt-2
snt-4
snt-5
b
AWC::GFP::UNC-2 Fluorescence/Signal Area
Integrated Density/Pixels
800
600
400
200
0
n.s.
n.s.
n.s.
n.s.
WT
snt-1(md290)
snt-2
snt-4
snt-5
c
Number of AWC::GFP::UNC-2 Puncta
Puncta Number
100
80
60
40
20
0
n.s.
n.s.
n.s.
n.s.
WT
snt-1(md290)
snt-2
snt-4
snt-5
d
AWC
Ca++
Ca++
UNC-2 (alpha)
Subunit of
Voltage-Gated
Calcium

Figure 28

The single synaptotagmin mutants were not significantly altered compared to wildtype GFP::UNC-2 expression.

Analysis of *snt* Double Mutants

Phenotypic examination of double mutants is a genetic strategy to determine whether two genes function in the same pathway. In addition, reports in *Drosophila melanogaster* indicate that some synaptotagmins form homo- and hetero-oligomers, and act *in vivo* as oligomeric complexes (Perin *et al.,* 1991; Littleton *et al.,* 1994). To this end, double mutant lines were generated in the *kyIs403* PQR-marked background.

First, *snt-1(ky1002); snt-2(tm1711)* and *snt-1(md290); snt-2(tm1711)* phenotypes were examined (Fig. 29). The *snt-1(ky1002); snt-2(tm1711)* double mutant line had the same number of YFP::RAB-3 puncta on average as the *snt-1(ky1002)* and *snt-2(tm1711)* single mutant lines and the wildtype line, but in total fluorescence more closely resembled *snt-1(ky1002)* than either wildtype or *snt-2(tm1711)* alone. Puncta were dimmer in the *snt-1(ky1002); snt-2(tm1711)* double mutant than both the wild-type and the *snt-2(tm1711)* single mutant line but indistinguishable from the *snt-1(ky1002)* single mutant. The *snt-1(md290); snt-2(tm1711)* double mutant confirmed these results, with similar phenotypes for single and double mutants. The suppression of the *snt-2(tm1711)* phenotype by either *snt-1(ky1002)* or *snt-1(md290)* suggests that SNT-1A and possibly SNT-1B are epistatic to SNT-2 in their effect on RAB-3 puncta. In addition, this result

Figure 29. Mutations in *snt-1* are epistatic to *snt-2(tm1711)* in PQR. (a) Total fluorescence in the region of interest in PQR in each worm. (***p<0.001 versus wildtype, n.s. not statistically significant, ANOVA with Tukey's Post Test used to analyze both sets of experiments) (b) Total fluorescence value divided by the number of pixels above the noise threshold, indicating the brightness of the fluorescent signal. (For experiment with *snt-1(ky1002)* allele, Kruskal-Wallis ANOVA with Dunn's Multiple Comparisons Post Test was used. **p<0.01, n.s. not statistically significant; For experiment with *snt-1(md290)* allele, ANOVA with Tukey's Post Test was used. ***p<0.001, n.s. not statistically significant) (c) Number of fluorescent puncta in the region of interest in each worm. (For experiment with *snt-1(ky1002)* allele, Kruskal-Wallis ANOVA with Dunn's Multiple Comparisons Post Test was used. n.s. not statistically significant; For experiment with *snt-1(md290)* allele, ANOVA with Tukey's Post Test was used. n.s. not statistically significant) (d) Representation of YFP::RAB-3 puncta in PQR neuron and model of YFP::RAB-3 associated with a synaptic vesicle.

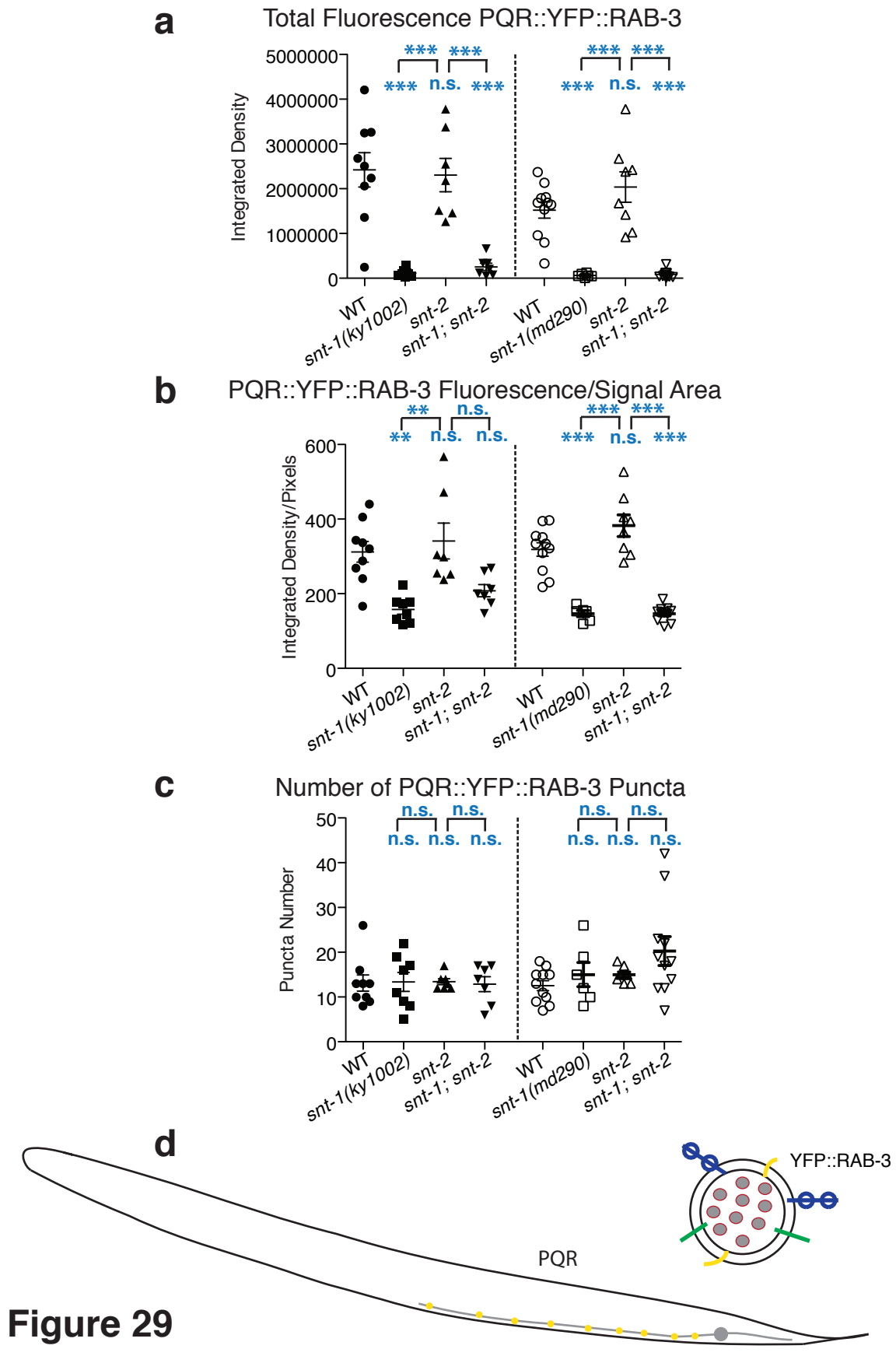
a
Total Fluorescence PQR::YFP::RAB-3
Integrated Density
5000000
4000000
3000000
2000000
1000000
0
***
***
***
n.s.
***
***
***
n.s.
***
WT
snt-1(ky1002)
snt-2
snt-1; snt-2
WT
snt-1(md290)
snt-2
snt-1; snt-2
b
PQR::YFP::RAB-3 Fluorescence/Signal Area
Integrated Density/Pixels
600
400
200
0
**
n.s.
**
n.s.
n.s.
***
***
***
n.s.
***
WT
snt-1(ky1002)
snt-2
snt-1; snt-2
WT
snt-1(md290)
snt-2
snt-1; snt-2
c
Number of PQR::YFP::RAB-3 Puncta
Puncta Number
50
40
30
20
10
0
n.s.
n.s.
n.s.
n.s.
n.s.
n.s.
n.s.
n.s.
n.s.
n.s.
n.s.
n.s.
WT
snt-1(ky1002)
snt-2
snt-1; snt-2
WT
snt-1(md290)
snt-2
snt-1; snt-2
d
YFP::RAB-3
PQR

Figure 29

indicates that SNT-1 and SNT-2 act on the same set of RAB-3-associated synaptic vesicles in PQR.

Next *snt-4(ok503); snt-1(ky1002)* and *snt-4(ok503); snt-1(md290)* double mutants phenotypes were examined in the PQR-marked background (Fig.30). Both *snt-1(ky1002)* and *snt-1(md290)* single mutants showed significantly reduced YFP::RAB-3 brightness and fluorescence compared to wildtype, but had no effect on the YFP::RAB-3 puncta number. *snt-4(ok503)* single mutant showed significantly increased YFP::RAB-3 total fluorescence compared to wildtype in both instances examined. In the experiment with *snt-1(ky1002)*, the *snt-4(ok503)* single mutant also had increased YFP::RAB-3 puncta number. A mutation in *snt-1*, either of the *md290* null allele or the *ky1002* allele, fully suppressed the *snt-4(ok503)* phenotype. This result suggests that SNT-1A and possibly SNT-1B are epistatic to SNT-4 in their effect on YFP::RAB-3 puncta. This result suggests that SNT-4 and SNT-1 act on the same subset of RAB-3-associated vesicles in PQR.

Finally, to determine whether SNT-2 and SNT-4 synaptotagmins were acting in a coordinated manner, *snt-4(ok503); snt-2(tm1711)* double mutants were examined in the PQR-marked background (Fig. 31). The *snt-4(ok503); snt-2(tm1711)* double mutant line showed an increase in total fluorescence that was as bright as the *snt-4(ok503)* single mutant. If SNT-2 and SNT-4 were acting in parallel pathways, the double mutant would have displayed an enhanced phenotype above either single mutant alone. Because the double mutant

Figure 30. Mutations in *snt-1* are epistatic to *snt-4(ok503)* in PQR. (a) Total fluorescence in the region of interest in PQR in each worm. (For experiment with *snt-1(ky1002)* allele, Kruskal-Wallis ANOVA with Dunn's Multiple Comparisons Post Test was used. **p<0.01 versus wildtype, *p<0.05 versus wildtype, n.s. not statistically significant, ***p<0.001; For experiment with *snt-1(md290)* allele, ANOVA with Tukey's Post Test was used. **p<0.01, ***p<0.001) (b) Total fluorescence value divided by the number of pixels above the noise threshold, indicating the brightness of the fluorescent signal. (***p<0.001 versus wildtype, n.s. not statistically significant, ANOVA with Tukey's Post Test used to analyze both sets of experiments) (c) Number of fluorescent puncta in the region of interest in each worm. (For experiment with *snt-1(ky1002)* allele, Kruskal-Wallis ANOVA with Dunn's Multiple Comparisons Post Test was used. n.s. not statistically significant For experiment with *snt-1(md290)* allele, ANOVA with Tukey's Post Test was used. n.s. not statistically significant) (d) Representation of YFP::RAB-3 puncta in PQR neuron and model of YFP::RAB-3 associated with a synaptic vesicle.

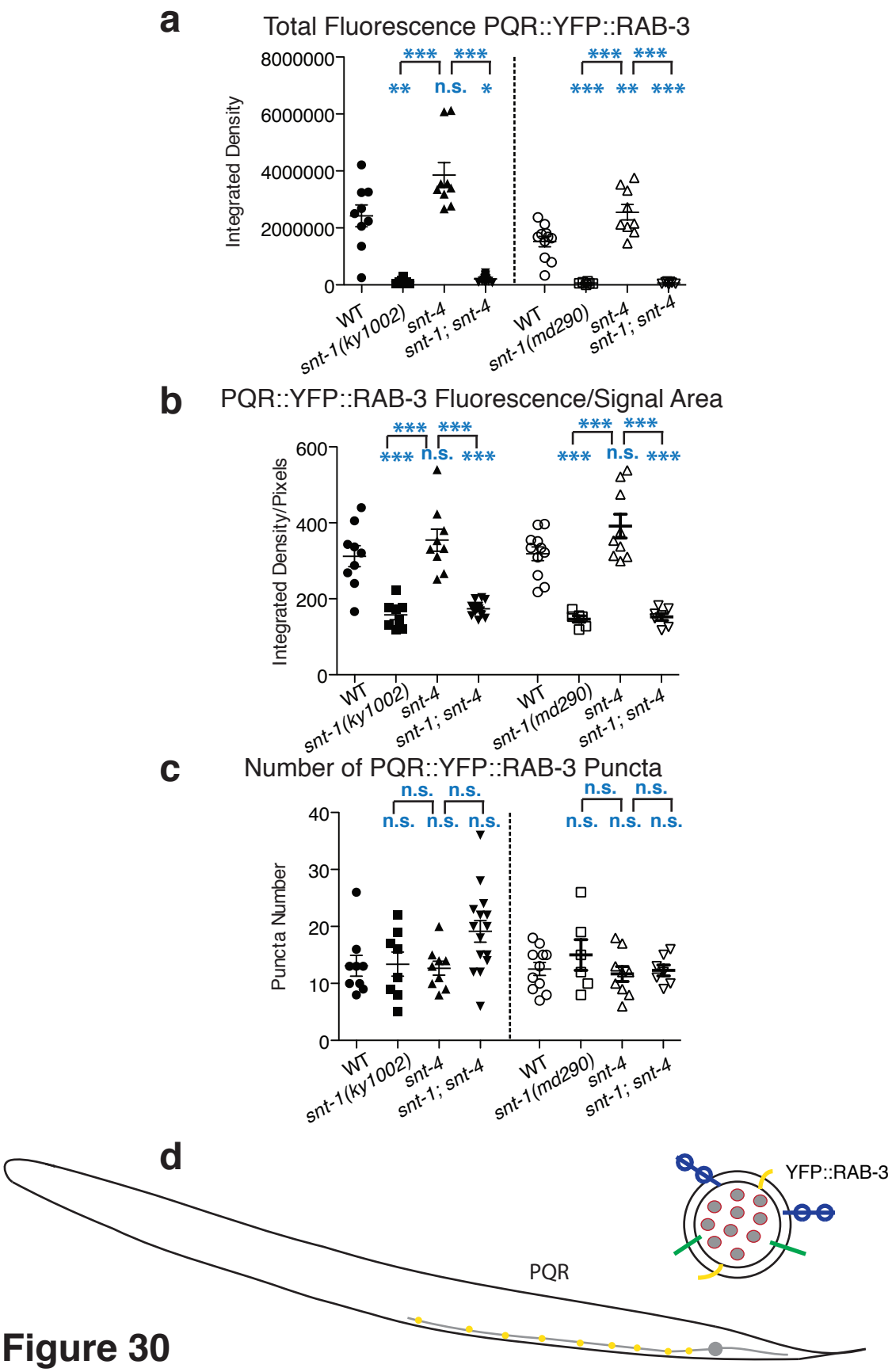
a
Total Fluorescence PQR::YFP::RAB-3
Integrated Density
8000000
6000000
4000000
2000000
0
***
***
**
n.s.
*
***
***
***
**
***
WT
snt-1(ky1002)
snt-4
snt-1; snt-4
WT
snt-1(md290)
snt-4
snt-1; snt-4
b
PQR::YFP::RAB-3 Fluorescence/Signal Area
Integrated Density/Pixels
600
400
200
0
c
Number of PQR::YFP::RAB-3 Puncta
Puncta Number
40
30
20
10
0
n.s.
d
YFP::RAB-3
PQR

Figure 30

Figure 31. Mutations in *snt-4(ok503)* and *snt-2(tm1711)* are not additive in PQR. (a) Total fluorescence in the region of interest in PQR in each worm. (***p<0.001 versus wildtype, **p<0.01 versus wildtype, *p<0.05, and n.s. not statistically significant ANOVA with Tukey's Post Test). (b) Total fluorescence value divided by the number of pixels above the noise threshold, indicating the brightness of the fluorescent signal. (n.s. not statistically significant ANOVA with Tukey's Post Test)(c) Number of fluorescent puncta in the region of interest in each worm. (n.s. not statistically significant Kruskal-Wallis ANOVA with Dunn's Multiple Comparisons Post Test) (d) Representation of YFP::RAB-3 puncta in PQR neuron and model of YFP::RAB-3 associated with a synaptic vesicle.

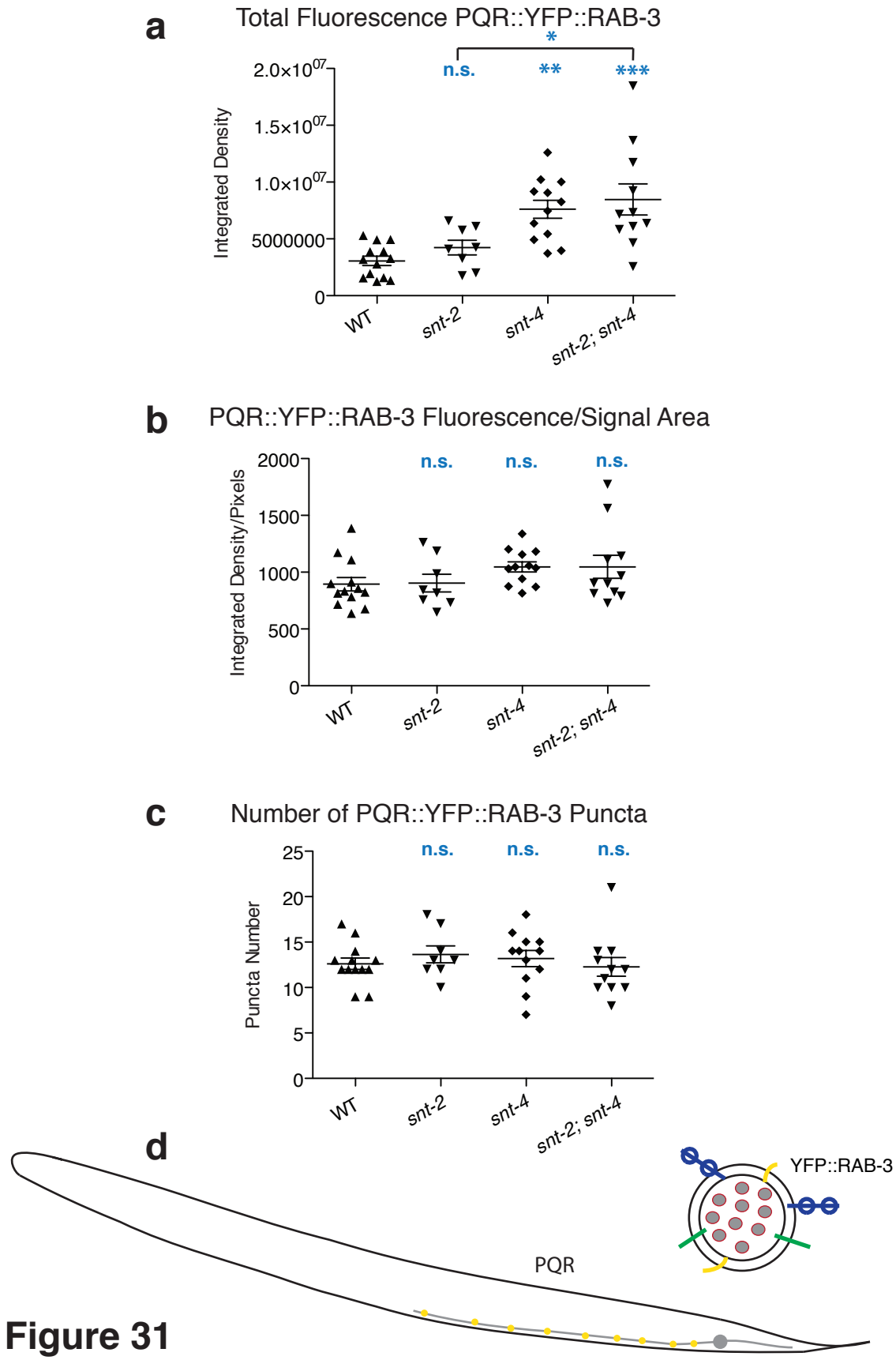
a
Total Fluorescence PQR::YFP::RAB-3
Integrated Density
2.0×10^07
1.5×10^07
1.0×10^07
5000000
0
n.s.
*
**
***
WT
snt-2
snt-4
snt-2; snt-4
b
PQR::YFP::RAB-3 Fluorescence/Signal Area
Integrated Density/Pixels
2000
1500
1000
500
0
n.s.
n.s.
n.s.
WT
snt-2
snt-4
snt-2; snt-4
c
Number of PQR::YFP::RAB-3 Puncta
Puncta Number
25
20
15
10
5
0
n.s.
n.s.
n.s.
WT
snt-2
snt-4
snt-2; snt-4
d
YFP::RAB-3
PQR

Figure 31

phenotype was only as severe as a single mutant, SNT-2 and SNT-4 may be acting in the same pathway in PQR, or on the same subset of synaptic vesicles.

Discussion and Future Direction

Summary of Results

Neurotransmission is a complex multi-step process. While the general steps and sequences of synaptic vesicle recycling are outlined, the details of exocytosis and endocytosis, and especially their regulation, remain to be understood. This thesis examined the contributions of the synaptotagmin family of proteins to neurotransmission in *C. elegans*.

My thesis work involved the identification of a novel allele of the *snt-1* gene, *ky1002* through a genetic screen for mutants with synaptic defects. The mutation in *ky1002* causes mis-splicing of the *snt-1A* transcript, resulting in a frameshift and an early stop codon. The *snt-1B* mRNA was still produced in the *ky1002* mutant. *snt-1(ky1002)* affects both SNB-1 and RAB-3 distribution in PQR, suggesting that SNT-1 alters synaptic vesicle distribution in PQR. *snt-1(ky1002)* mutant animals also displayed RAB-3 defects in AWC and PVD sensory neurons, as well as DD GABAergic motor neurons.

Previous studies of *snt-1* mutants had attempted to address whether SNT-1 was acting in the vesicle exocytosis or endocytosis steps, but no experiments had been performed to exclude the possibility of synaptic vesicle biogenesis defects. To address this question, I performed experiments in which I introduced a mutation that blocks synaptic vesicle exocytosis and then assayed whether the presence of synaptic vesicle markers increased or not. The results from these

experiments are consistent with *snt-1* being defective in endocytosis, and excluded defects in synaptic vesicle packaging and trafficking to the active zone as the sole defect in *snt-1* mutants.

The *C. elegans* genome contains seven identified synaptotagmin genes, six of which had been previously identified but heretofore uncharacterized. Because experiments performed in rat hippocampal neurons had showed that different synaptotagmins of those species displayed differing sub-cellular localizations, I examined available *C. elegans* synaptotagmin null alleles for synaptic vesicle defects. *snt-4* and *snt-5* mutant animals both showed significantly increased YFP::RAB-3 signal in PQR. In AWC sensory neurons, *snt-5* mutant animals also had significantly increased mCherry::RAB-3 puncta number. These results were consistent with SNT-4, SNT-5, and possibly SNT-2 acting as positive regulators of exocytosis or as negative regulators of synaptic vesicle endocytosis in PQR, AWC, or both sensory neurons.

Studies of synaptotagmins in other organisms had indicated that some synaptotagmin family members could rescue Syt1 deficiency. Also, synaptotagmin proteins may form hetero-oligomers. I examined whether introducing a second synaptotagmin null mutation to *snt-1* mutant background either enhanced the *snt-1* mutant phenotype, indicating that SNT-1 and the synaptotagmin in question functioned in parallel to control neurotransmission; suppressed the *snt-1* mutant phenotype, suggesting that the synaptotagmin in question played a role in a step of neurotransmission preceding the endocytosis

controlled by SNT-1; or displayed a phenotype identical to *snt-1* mutants, indicating that SNT-1 is epistatic to the synaptotagmin in question. I tested *snt-1; snt-2* double mutants and *snt-4; snt-1* double mutants. Both showed phenotypes that closely resembled *snt-1* mutant phenotype, indicating that SNT-1 is epistatic to SNT-2 and SNT-4. A *snt-4; snt-2* double mutant line was also generated to asses whether SNT-2 and SNT-4 act in the same pathway or parallel pathways. The *snt-4; snt-2* double mutant was as severe as the *snt-4* single mutant, suggesting that SNT-2 and SNT-4 act in the same pathway in PQR or on the same subset of RAB-3-associated vesicles in PQR.

Future Directions

A more rigorous rescue experiment should be performed in which the two isoforms, SNT-1A and SNT-1B, are introduced into *snt-1* mutant backgrounds. For example, in the case of *snt-1(ky1002)* mutants, rescuing SNT-1A using an endogenous *snt-1* promoter and assaying the synaptic distribution of RAB-3 and SNB-1 in several neurons would be informative. Furthermore, expressing SNT-1A using cell-specific promoters and seeing rescue of synaptic phenotypes would also indicate that SNT-1A acts cell autonomously to affect synaptic vesicle distribution.

To rule out the possibility that mutations in *snt-1* affect the *gcy-36* promoter driving expression in PQR, additional analysis was performed on the *kyIs403* marked lines. Briefly, measurements were taken of the YFP::RAB-3 puncta

fluorescence where the synaptic vesicles were localized in PQR, designated as the “peak” fluorescence areas; and measurements were taken of the spaces between the YFP::RAB-3 puncta within the PQR neuron, designated as the “cord” (Supp. Fig. 3). If mutations in *snt-1* were affecting the transcription of the integrated transgene, we would expect the peak value and the cord value to be decreased in *snt-1* mutants, but the peak-to-cord ratio to be comparable to wildtype. While there was a large reduction in the peak values in *snt-1* mutants, and a moderate reduction in the cord values as well, the peak-to-cord ratio was severely diminished in the *snt-1* mutants compared to wildtype, indicating that any transcriptional defect is small compared to the defect in YFP::RAB-3 overall fluorescence.

Additional analysis confirmed that the distribution of YFP::RAB-3 puncta along the axon in *snt-1* mutants closely resembles the wildtype distribution (Supp. Fig. 3d). Also, the width of the YFP::RAB-3 puncta in wildtype and *snt-1* mutants is roughly identical (Supp. Fig. 3e).

snt-1(ky1002) mutants also displayed a surprising effect on UNC-2 voltage-gated calcium channel subunit in AWC (Fig. 16). To extend this result, a rescue experiment should be performed in which *snt-1* expression is restored in AWC, to demonstrate that lack of a functional SNT-1A protein in AWC initiates a compensatory mechanism of synaptic modulation that is mediated through the UNC-2 protein in a cell-autonomous manner. Restoration of functional SNT-1A

under the AWC-specific promoter is predicted to result in expression of UNC-2 at wildtype levels.

We cannot conclude from the experiments in this thesis whether or not the synaptic homeostasis mechanisms evident in other model organisms are also present in *C. elegans*, but an experiment in which a post-synaptic neuron of AWC has an impaired neurotransmitter receptor could provide further and more conclusive evidence. If the homeostatic mechanism is indeed conserved, in the presence of such a receptor mutation, we would expect to see an increased GFP::UNC-2 signal and perhaps to see interesting electrophysiological effects. For example, if the post-synaptic neuron's receptor could be acutely impaired on a temporal scale with an agonist, we might see a decrease in AWC signaling for a short time until the homeostatic mechanisms were activated, similar to results seen in *Drosophila melanogaster* (Frank *et al.,* 2006). Such an experiment would also confirm the timescale of synaptic homeostasis mechanisms in another invertebrate model organism.

Continuing the Analysis of Synaptotagmin Family Members

The null alleles of *snt-2, snt-4, snt-5,* and *snt-6* were only studied in two sensory neurons, AWC and PQR. No mutant phenotype was detected in *snt-6(ok3496)* animals, and a mutant phenotype was identified in *snt-4(ok503)* in PQR, but not in AWC. The lack of a mutant phenotype can be explained if *snt-6* is not expressed in AWC or PQR and *snt-4* is not expressed in PQR. It is also possible that SNT-6, for example, acts on dense core vesicles or a vesicle type

that is not associated with RAB-3. To address this possibility, the cellular expression patterns and sub-cellular localization of each synaptotagmin protein should be determined. One method of assessing cellular expression patterns is to create a reporter plasmid with a promoter region of a *snt* gene fused to a fluorophore such as GFP. A strategy to determine the subcellular localization of various SNT proteins would be to genetically fuse the pH sensitive GFP protein, pHluorin, to the predicted luminal end of each synaptotagmin isoform (Dean *et al.,* 2012a). Recently, a library of recombineered fosmids was generated covering 73% of the *C. elegans* proteome. Briefly, fosmid transgenes were made containing genes tagged at the C terminus with GFP and 3xFLAG. These fosmids allow for the study of subcellular localization of a protein and a cellular expression pattern, as the transgene expression is under the control of the endogenous promoter (Sarov, *et al.* 2012).

It is important to note that rescue experiments for the *snt-2, snt-4,* and *snt-5* mutant phenotypes were not performed. Thus, the phenotypic effects present in the mutant backgrounds were not proved to be caused by mutations in these genes. Performing rescue experiments using endogenous promoters would prove that mutations in *snt-2, snt-4,* and *snt-5* indeed affect RAB-3 distribution in PQR and/or AWC. Performing rescue experiments using cell-specific promoters driving expressing in either PQR or AWC would also demonstrate that these synaptotagmins act cell-autonomously to affect RAB-3 expression.

Both *snt-5* and *snt-6* have two null alleles available, and this thesis work only made use of one of these alleles for each gene. Testing the second allele could confirm the phenotypes that I've already identified (in the case of *snt-5*), or the second allele may be a larger deletion of the gene, resulting in a more severe phenotype. A future study could involve generating mutations in *snt-3* and *snt-7*, which currently have no mutant alleles identified.

To assay which synaptotagmins are affecting exocytosis or endocytosis, we could use synaptopHlourin, which is a fusion protein of the pH-sensitive pHluorin to the luminal domain of synaptobrevin (Dittman and Kaplan, 2006). Exocytosis mutants, such as *unc-13*, *unc-18*, and *unc-64*(syntaxin) all reduce synaptopHluorin on the surface of cholinergic motor neurons; endocytosis mutants, such as *unc-11*, *dpy-23*, and *dyn-1*(dynamin) all increase synaptopHluorin on the surface of cholinergic motor neurons. This experiment hinges on each synaptotagmin tested being endogenously expressed in the cholinergic motor neurons where the measurements are taken.

Structure-Function Analyses

Although many EMS- and ENU-induced mutations in *C. elegans* have been sequenced, to date, only one structure function analysis has been performed on a synaptotagmin protein in *C. elegans*: the VIL domain in the fifth exon in SNT-1 is necessary for correctly trafficking SNT-1 from the cell body to the active zone (Mathews *et al.,* 2007). While we know where the C2A and C2B domains are in SNT-1, we do not know which residues are calcium-binding residues. A crystal

structure for the C2A domain of rat Syt1 showed that three aspartic acid residues act as the key calcium interaction amino acids in the C2A domain (Sutton *et al.,* 1995), and NMR results revealed that the C2B domain of Syt1 binds two calcium ions (reviewed in Rizo *et al., 2012*). Knowing which SNT proteins bind calcium and which do not would aid in their analysis. A calcium-binding SNT would be hypothesized to play a role in exocytosis. Furthermore the calcium-binding residues could be mutated in SNT proteins to potentially parse the roles of that SNT in neurotransmission. When the calcium binding residues of mouse syt1 were mutated, the resulting Syt1 protein was still trafficked to the presynaptic bouton, but fast vesicle exocytosis was severely diminished (Yao, *et al.,* 2012b). The endocytosis rates were also assayed in the presence of the non-calcium-binding mouse Syt1, and found to be slower, hinting that the endocytic defects characterized in *snt-1* mutant backgrounds may be conserved. Mutating the calcium-binding residues of C2A, C2B, or both domains in SNT-1 may provide insight into which domains are required for endocytosis, which for exocytosis, and which for both steps of neurotransmission. Conversely, mutating the calcium-binding domains to enhance their calcium affinity could potentially increase exocytosis speed or endocytosis rates and provide information about the necessity of calcium binding in both endocytosis and exocytosis.

Replacing the C2B calcium-binding domain of mouse Syt1 with the calcium-binding C2B domain of mouse Syt7 renders Syt1 unable to mediate fast neurotransmitter release in neuronal cell culture, indicating that not all calcium-

binding domains are equivalent and hinting that some calcium binding domains may have other interactions (Xue, *et al.,* 2010). In mammals, the C2B domain is considered the main mediator of Syt1 interaction with the SNARE complex, as it is thought to bind to two membranes simultaneously: the plasma membrane and bilayers containing SNARES, e.g. vesicles with complexed SNARES (Arac *et al.,* 2006). Two arginines in the C2B domain of the mammalian Syt1 are critical for this interaction with two membranes (Reviewed in Rizo *et al.,* 2012). Perhaps this function of the C2B domain is conserved in *C. elegans*. To investigate this, the corresponding arginines in SNT-1 could be mutated, and then animals expressing this mutated SNT-1 could be assayed for exocytosis, locomotion, and number of docked vesicles in an active zone. In addition, a pulldown assay with C2B as bait could be performed and a yeast two-hybrid assay could be executed. Furthermore, *in vitro* binding assays could done with *C. elegans* homologs of syntaxin, AP2, and neurexin adhesion molecules, which have been shown to interact with synatptotagmin in other organisms. The PIP_2-binding domains would also be useful to identify, as PIP_2 binding to rat Syt1 increases the calcium affinity of the C2B domain 40-fold *in vitro* (van den Bogaart *et al.,* 2012). Manipulating the PIP_2-binding domains could provide a useful tool for dissecting the calcium requirements for the steps of neurotransmission in *C. elegans*. Moreover, *in vitro* results indicate that $PI(4,5)P_2$ and SNAP-25 compete for binding with the rat Syt1 C2B domain, indicating that Syt1 must sequentially interact with various partners (Parisotto *et al.,* 2012). Identifying the phospholipid-binding domains, the

calcium-binding domains, and any protein-binding domains of the SNT proteins could thus provide insight in the sequence of events required for neurotransmission.

Further Endocytosis Examinations

To further confirm that SNT-1 critically acts in the endocytosis of synaptic vesicles, the distribution of endocytic proteins should be examined. For example, APS-2::GFP is thought to mark clathrin coated pits and vesicles, GFP::RAB-5 is associated with early endosomes, and GFP::RAB-11 marks recycling endosomes (Troulinaki and Tavernarakis, 2012). A reduction in one or all of these proteins in the *snt-1* mutant background would further support the conclusion that SNT-1 plays a role in endocytosis.

On the same note, examining the distribution of UNC-57::GFP may be useful. *unc-57* encodes endophilin, an endocytosis protein. In *unc-18* and *unc-13* exocytosis mutants, UNC-57::GFP puncta fluorescence is significantly increased. If *snt-1* mutations only affect exocytosis, then in a *snt-1* mutant background, UNC-57::GFP fluorescence should increase. Conversely, a decrease in UNC-57::GFP fluorescence would indicate that mutating *snt-1* results in increased exocytosis, similar to the UNC-57::GFP decrease seen in *tom-1* (tomosyn) mutant backgrounds. (Bai *et al.*, 2010).

Another way to separate the roles of synaptotagmins in endocytosis and exocytosis involves retargeting the synaptotagmin to the plasma membrane in the active zone. Yao and colleagues showed that fusing the cytoplasmic C2A-

C2B domain of Syt1 to an N-terminal 20 amino-acid segment of GAP-43, which is anchored to the plasma membrane in neurons, created a fusion protein capable of rescuing exocytosis in mouse syt1 knockout neurons, but incapable of rescuing the slow rates of endocytosis in syt1 knockout neurons. Creating a similar fusion protein with SNT-1 and a membrane-anchored protein could provide further information about neurotransmission in *C. elegans.* This anchored SNT should still be able to act in exocytosis, which could be confirmed using electrophysiology and synaptopHlourin. Endocytosis rates could also be monitored using the synaptopHluorin. If the rates of endocytosis in the presence of the tethered SNT are comparable to wildtype, it would suggest that that particular SNT is not involved in regulating endocytosis. If the rate of endocytosis is slower than wildtype rates, it would suggest that that particular SNT is involved in regulating endocytosis (Yao *et al.,* 2012a).

unc-41 encodes an adaptor protein known as stonin. Stonin 2 contains an evolutionarily conserved β strand that interacts with the cytoplasmic domain of rat Syt1. Stonin 2 also directly binds to AP2, a part of the endocytosis machinery. Thus Stonin 2 is an endocytic adaptor protein that mediates an indirect interaction between the AP2 complex and Syt1, presumably during the sorting step of SV recycling (Jung *et al.,* 2007). UNC-41 has been shown to recruit SNT-1 to endocytic sites in the sublateral nerve cord of *C. elegans*, and overexpression of SNT-1 does not rescue locomotion defects of *unc-41* mutant animals (Mullen *et al.,* 2012). This combination of a functional SNT-1 in a mutant

unc-41 background could provide an interesting background for studying the exocytosis functions of SNT-1 without the functional endocytosis pathway.

It is possible that other SNT family members could rescue endocytic defects in a *snt-1* mutant background. Mouse Syt1 may play a role in calcium-sensing during clathrin-mediated endocytosis, specifically at the fission step of vesicle budding. This is mediated by the Syt1-AP2 interaction. In Syt1 knockout cultures, calcium-independent fission still occurs, possibly aided by other synaptotagmin isoforms that don't bind calcium (Yao *et al.,* 2012b). Overexpressing synaptotagmin family members or driving expression of a synaptotagmin in neurons where it is not endogenously expressed may provide further insight to the binding domain requirements of the endocytic machinery.

Materials and Methods

Strains used:

Wild type nematodes were *C. elegans* Bristol variety N2. Strains were cultured using standard techniques at 20-23°C.

CB4856 C. elegans wild type, CB subclone of HA-8(Tc1 pattern IX)

Synaptotagmin Mutants: *NM204 snt-1(md290) II, FX01711 snt-2(tm1711)III, RB737 snt-4(ok503)I, RB2402 snt-5(ok3287)V, RB2520 snt-6(ok3496)*

PQR-marked lines: *CX11472 kyIs512 [gcy-36::ptp-3A::spGFP11 2 ng μl^{-1}, gcy-36::mCherry::rab-3 0.4 ng μl^{-1}, flp-18::nlg-1::spGFP1-10 10ng μl^{-1}, pSM 50ng μl^{-1}, flp-17::mCherry 2ng μl^{-1}]*

CX1002 snt-1(ky1002); kyIs512 [gcy-36::ptp-3A::spGFP11 2 ng μl^{-1}, gcy-36::mCherry::rab-3 0.4 ng μl^{-1}, flp-18::nlg-1::spGFP1-10 10ng μl^{-1}, pSM 50ng μl^{-1}, flp-17::mCherry 2ng μl^{-1}]

CX13911 unc-104(e1265) II; kyIs512 X[gcy-36::ptp-3A::spGFP11 2 ng μl^{-1}, gcy-36::mCherry::rab-3 0.4 ng μl^{-1}, flp-18::nlg-1::spGFP1-10 10ng μl^{-1}, pSM 50ng μl^{-1}, flp-17::mCherry 2ng μl^{-1}]

CX7726 kyIs403 [odr-1::DsRed2; flp-18::unc-43g::DsRed2; gcy-36::YFP::rab-3; gcy-36::myrCFP]

CX13716 kyIs403; snt-1(ky1002) [odr-1::DsRed2; flp-18::unc-43g::DsRed2; gcy-36::YFP::rab-3; gcy-36::myrCFP]

CX15269 kyIs403 I; snt-1(md290) II [odr-1::DsRed2; flp-18::unc-43g::DsRed2; gcy-36::YFP::rab-3; gcy-36::myrCFP]

CX14127 kyIs403 I; snt-6(ok3496) II [odr-1::DsRed2; flp-18::unc-43g::DsRed2; gcy-36::YFP::rab-3; gcy-36::myrCFP]

CX14128 kyIs403 I; snt-5(ok3287) V [odr-1::DsRed2; flp-18::unc-43g::DsRed2; gcy-36::YFP::rab-3; gcy-36::myrCFP]

CX14130 kyIs403, snt-4(ok503) I [odr-1::DsRed2; flp-18::unc-43g::DsRed2; gcy-36::YFP::rab-3; gcy-36::myrCFP]

CX15267 kyIs403; snt-2(tm1711) III [odr-1::DsRed2; flp-18::unc-43g::DsRed2; gcy-36::YFP::rab-3; gcy-36::myrCFP]

CX14165 kyIs403 I; snt-1(ky1002) II; kyEx4425. [odr-1::DsRed2; flp-18::unc-43g::DsRed2; gcy-36::YFP::rab-3; gcy-36::myrCFP] [2ng fosmid WRM0625cD08, 10ng unc-122::GFP]

CX14167 kyIs403 I; snt-1(md290)II; kyEx4425 [odr-1::DsRed2; flp-18::unc-43g::DsRed2; gcy-36::YFP::rab-3; gcy-36::myrCFP] [2ng fosmid WRM0625cD08, 10ng unc-122::GFP]

CX15252 kyIs403 unc-13(e51) I [odr-1::DsRed2; flp-18::unc-43g::DsRed2; gcy-36::YFP::rab-3; gcy-36::myrCFP]

CX15255 kyIs403 unc-13(e51) I; snt-1(ky1002) II [odr-1::DsRed2; flp-18::unc-43g::DsRed2; gcy-36::YFP::rab-3; gcy-36::myrCFP]

CX15496 kyIs403 I; snt-1(ky1002) II; snt-2(tm1711) III [odr-1::DsRed2; flp-18::unc-43g::DsRed2; gcy-36::YFP::rab-3; gcy-36::myrCFP]

CX15527 kyIs403 I; snt-1(md290) II; snt-2(tm1711) III [odr-1::DsRed2; flp-18::unc-43g::DsRed2; gcy-36::YFP::rab-3; gcy-36::myrCFP]

CX15522 kyIs403, snt-4(ok503) I; snt-1(ky1002) II [odr-1::DsRed2; flp-18::unc-43g::DsRed2; gcy-36::YFP::rab-3; gcy-36::myrCFP]

CX15525 kyIs403, snt-4(ok503) I; snt-1(md290) II; [odr-1::DsRed2; flp-18::unc-43g::DsRed2; gcy-36::YFP::rab-3; gcy-36::myrCFP]

CX15264 kyIs403, snt-4(ok503) I; snt-2(tm1711) III [odr-1::DsRed2; flp-18::unc-43g::DsRed2; gcy-36::YFP::rab-3; gcy-36::myrCFP]

CX7042 kyEx802 [odr-1::DsRed; gcy-36::snb-1::YFP]

CX15233 unc-18(e234) X; kyEx802[odr-1::Dsred; gcy-36::snb-1::YFP]

CX15230 snt-1(md290); unc-18(e234) kyEx802 (line 3G) [odr-1::DsRed; gcy-36::snb-1::YFP]

CX15231 snt-1(md290); unc-18(e234) kyEx802 (line 4E) [odr-1::DsRed; gcy-36::snb-1::YFP]

AWC-marked lines: *CX10060 kyIs442 [odr-3::GFP::unc-2cDNA with synthetic intron 100ng μl^{-1}, odr-3::mCherry::rab-3 1ng μl^{-1}, unc-122::DsRed 5ng μl^{-1}]*

CX13714 kyIs442; snt-1(ky1002) [odr-3::GFP::unc-2cDNA with synthetic intron 100ng μl^{-1}, odr-3::mCherry::rab-3 1ng μl^{-1}, unc-122::DsRed 5ng μl^{-1}]

CX15286 kyIs442; snt-1(md290) II [odr-3::GFP::unc-2cDNA with synthetic intron 100ng μl^{-1}, odr-3::mCherry::rab-3 1ng μl^{-1}, unc-122::DsRed 5ng μl^{-1}]

CX15281 kyIs442; snt-2(tm1711) III [odr-3::GFP::unc-2cDNA with synthetic intron 100ng µl^{-1}, odr-3::mCherry::rab-3 1ng µl^{-1}, unc-122::DsRed 5ng µl^{-1}]

CX15284 kyIs442, snt-4(ok503) I [odr-3::GFP::unc-2cDNA with synthetic intron 100ng µl^{-1}, odr-3::mCherry::rab-3 1ng µl^{-1}, unc-122::DsRed 5ng µl^{-1}]

CX15283 kyIs442 I; snt-5(ok3287) V [odr-3::GFP::unc-2cDNA with synthetic intron 100ng µl^{-1}, odr-3::mCherry::rab-3 1ng µl^{-1}, unc-122::DsRed 5ng µl^{-1}]

CX9471 kyIs442; unc-11(ky280)I [odr-3::GFP::unc-2cDNA with synthetic intron 100ng µl^{-1}, odr-3::mCherry::rab-3 1ng µl^{-1}, unc-122::DsRed 5ng µl^{-1}]

CX9654 kyIs442; unc-13(e51)I [odr-3::GFP::unc-2cDNA with synthetic intron 100ng µl^{-1}, odr-3::mCherry::rab-3 1ng µl^{-1}, unc-122::DsRed 5ng µl^{-1}]

CX9472 kyIs442; dpy-23(e840)X [odr-3::GFP::unc-2cDNA with synthetic intron 100ng µl^{-1}, odr-3::mCherry::rab-3 1ng µl^{-1}, unc-122::DsRed 5ng µl^{-1}]

CX15786 kyIs442; unc-18(e234)X [odr-3::GFP::unc-2cDNA with synthetic intron 100ng µl^{-1}, odr-3::mCherry::rab-3 1ng µl^{-1}, unc-122::DsRed 5ng µl^{-1}]

CX11416 kyIs442; dyn-1(ky51)X [odr-3::GFP::unc-2cDNA with synthetic intron 100ng µl^{-1}, odr-3::mCherry::rab-3 1ng µl^{-1}, unc-122::DsRed 5ng µl^{-1}]

CX9337 kyIs442; unc-10(e102)X [odr-3::GFP::unc-2cDNA with synthetic intron 100ng µl^{-1}, odr-3::mCherry::rab-3 1ng µl^{-1}, unc-122::DsRed 5ng µl^{-1}]

CX9272 kyIs439 [odr-3::GFP::unc-2cDNA with synthetic intron 100ng µl^{-1}, odr-3::mCherry::rab-3 1ng µl^{-1}, unc-122::DsRed 5ng µl^{-1}]

CX9549 kyIs439; elks-1(tm1233)IV [odr-3::GFP::unc-2cDNA with synthetic intron 100ng µl^{-1}, odr-3::mCherry::rab-3 1ng µl^{-1}, unc-122::DsRed 5ng µl^{-1}]

PVD-marked lines: *CX9797 kyIs445 [des-2::mCherry::rab-3* injected at 0.5 ng μl^{-1}*, des-2::sad-1::GFP* 2 ng μl^{-1}*, odr-1::DsRed* 30 ng μl^{-1}*]*

CX13715 snt-1(ky1002); kyIs445 [des-2::mCherry::rab-3 injected at 0.5 ng μl^{-1}*, des-2::sad-1::GFP* 2 ng μl^{-1}*, odr-1::DsRed* 30 ng μl^{-1}*]*

VD/DD-marked lines: *CX10413 kyIs476 [unc-25::GFP::unc-2cDNA with synthetic intron 100ng* μl^{-1}*, unc-25::mCherry::rab-3 5ng* μl^{-1}*, odr-1P::mCherry 20 ng* μl^{-1}*]*

CX15185 snt-1(ky1002) I; kyIs476 X [unc-25::GFP::unc-2cDNA with synthetic intron 100ng μl^{-1}*, unc-25::mCherry::rab-3 5ng* μl^{-1}*, odr-1P::mCherry 20 ng* μl^{-1}*]*

Microscopy Methods

PQR Microscopy: Young adult hermaphrodites carrying the integrated *kyIs403* array were mounted on a 2% agarose pad (dissolved in sterilized distilled water) within a 0.02% drop of tetramisole in M9 buffer. A 40X objective on a Zeiss Axioplan2 microscope with a Hamamatsu Photonics C2400 CCD camera and Metamorph software was used to capture the PQR neuron axon. Z-planes were separated by 1 micron; each stack was collected using as many planes as necessary to capture the whole axon (usually 20-25 slices). Later, during image analysis and compression, extraneous slices with no axon signal were discarded.

In the *kyIs403* lines, the exposure times used for each flurophore were as follows: CFP 300 msec, YFP 400 msec, mCherry 200 msec.

In the *kyEx802* lines, the exposure time for YFP was 400 msec. The 40X objective on the same Zeiss Axioplan2 microscope setup described above was used, as was a 2% agarose pad with 0.02% tetramisole in M9.

AWC Microscopy: Young adult hermaphrodites carrying the integrated *kyIs442* array were placed on a 4% agarose pad, within a drop of 400 μM tetramisole dissolved in M9 buffer. For the experiments characterizing *ky1002*, the same Zeiss Axioplan2 setup with the Hamamatsu CCD camera as described above was used. For the experiments characterizing *unc-13, unc-11,* and *dpy-23,* a Zeiss Axpioplan2 microscope setup with a Hamamatsu Photonics C2400 CCD camera and Metamorph software was used. Additionally, for the experiments characterizing the synaptotagmin mutants *snt-2, snt-4, snt-5,* and *snt-6,* the Hamamatsu Photonics C2400 CCD camera was used.

PVD Microscopy: Young adult hermaphrodites carrying the integrated *kyIs445* marker were mounted on a 2% agarose pad (dissolved in sterilized distilled water) within a drop of 400 μM tetramisole dissolved in M9 buffer. A 40X objective on a Zeiss Axioplan2 microscope with a Hamamatsu Photonics C2400 CCD camera and Metamorph software was used to capture the PQR neuron axon. Z-planes were separated by 1 micron; each stack was collected using as many planes as necessary to capture the whole axon (usually 20-25 slices). Later, during image analysis and compression, extraneous slices with no axon

signal were discarded. In the *kyIs442* lines, the exposure times used for each flurophore were as follows: mCherry 500 msec and GFP 500 msec.

VD/DD Microscopy: Young adults carrying the integrated *kyIs476* array were placed on a 4% agarose pad, within a drop of 400 μM tetramisole dissolved in M9 buffer. After 20-30 minutes stored in a humidified chamber, an eyelash was used to straighten or uncurl paralyzed worms, and a coverslip was carefully placed over the worms on the agarose pad. Additional tetramisole was added as needed to prevent desiccation. Slight pressure was applied to the coverslip and a sliding motion was used to turn the paralyzed worms onto their ventral sides, leaving the dorsal DD neurons in a single plane. A Zeiss Axioplan2 microscope with a Hamamatsu Photonics C2400 CCD camera and Metamorph software was used. A single slice was taken of the DD axon fluorescence i.e. no z-stacks were obtained, the exposure times used for each flurophore were as follows: mCherry 300 msec and GFP 500 msec.

Image Analysis:

To quantify fluorescence intensities, puntcal brightness, and number of puncta, ImageJ (US National Institutes of Health) software was used. Z-stacks were compressed into a single plane using the maximum projection function. The background intensity was determined by measuring the mean integrated density of three areas adjacent to the fluorescent puncta, then averaging these three values. This average background intensity was subtracted from the whole image

and pixels with a signal above an arbitrary threshold and within the axon were measured for total fluorescence intensity and total signal area. The same arbitrary threshold was used across genotypes within a single experiment; each arbitrary threshold was chosen based on which value allowed for the most signal quantification with the least amount of noise inclusion.

The fluorescence intensity values were summed for each animal, as were the signal areas. Dividing the total fluorescence intensity per animal by the sum of its signal area gave an indication of the "brightness" of the puncta. The number of puncta per animal was counted by eye, using the maximum projected Z-stack after the background had been subtracted.

Additional Methods

Generation of *snt-1(ky1002)*: The *CX11472* line was mutagenized with Ethyl methanesulfonate according to standard protocols (Anderson, 1995).

Generation and analysis of cDNAs:

snt-1 cDNA primers:

snt-1-cDNA-L-NheI:5'-TATTGCTAGCATGGTGAAATTAGACTTTTCGTC-3'

snt-1-cDNA-R-KpnI:5'-

GGCGGGTACCGGTTTCTTATCATCTTTCTTATCACCTTC-3'

snt-1-exon6-sequencingL:5'-TGGACGTCGGTGGTTTATCAG-3'

RNA was isolated from N2 and a line carrying the *snt-1(ky1002)* mutation using a Trizol reagent. The SuperScript™ III First-Strand Synthesis System for RT-PCR was used to generate cDNA libraries from the isolated RNA.

Transgenic methods: Fosmid rescue lines were generated by microinjection of 2ng μL^{-1} of the fosmid 065cD08 into the gonad of both *kyIs403; snt-1(md290)* and *kyIs403; snt-1(ky1002).* The injection mix for creating transgenic lines was 2ng μL^{-1} of fosmid 065cD08, 10 ng μL^{-1-} coel::GFP, 88 ng μL^{-1} PSM. Animals carrying the coel::GFP were presumed to also be carrying the fosmid.

Comparison of gene homology: Using the tree families database (http://www.treefam.org), a search was performed using the *C. elegans snt-1* gene to determine whether any of the mammalian synaptotagmins were closely related to *C. elegans* synaptotagmins.

Statistical Analysis: GraphPad Prism 5 software was used to perform statistics on all data. Data that did not fit a normal distribution as determined by the Kolmogorov-Smirnov test for normality were analyzed using Kruskal-Wallis ANOVA with Dunn's Mutliple Comparisons Post Test. Data that fit a normal distribution were analyzed using Student's Unpaired t-test (if only two datasets were being compared i.e. wildtype vs. *snt-1(ky1002)*) or ANOVA with Tukey's Post Test for Multiple Comparisons.

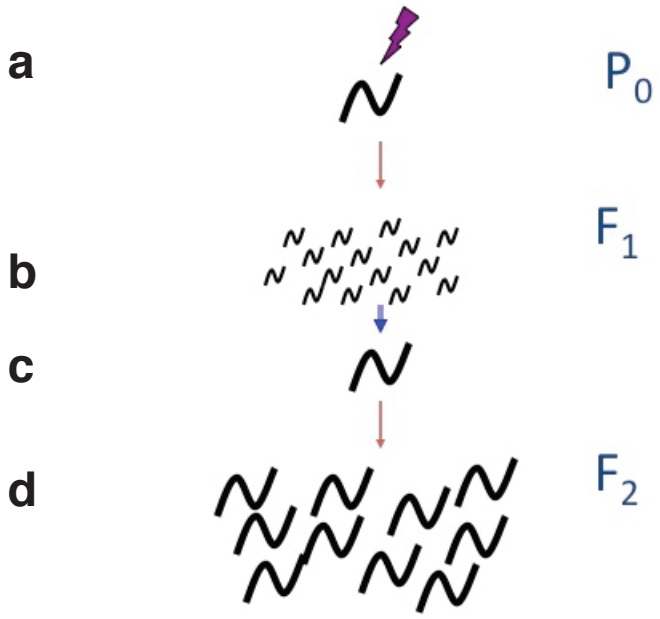

Supplementary Figure 1. Schematic of the Clonal Screen (a) The P0 animals were mutagenized with EMS. (b) L1 animals were prepared for long term freezing and aliquotted into 100 vials. (c) L1 animals were thawed and single animals were picked to plates to segregate progeny. (d) The progeny of 500 F1 worms were examined for defects in GRASP signal or mCherry::RAB-3 signal.

Supplementary Figure 2. Image processing steps to analyze fluorescent puncta in axons. First, a Z-stack is obtained of the puncta in the axon (not shown) Using the ImageJ program, slices without puncta are removed from the beginning and/or the end of the stack. The remaining slices are compressed into a single plane using the maximum projection function. The background signal is calculated and subtracted from the image. (a) In the image with the background subtracted, the number of puncta in the axon region are counted by eye. (b) The region of interest containing the fluorescent puncta is designated in ImageJ, using the polygon tool. (c) Using the Threshold function in ImageJ, every sample in an experiment is converted into a binary image in which pixels with a fluorescence value over an arbitrary threshold are considered signal (white regions). The arbitrary minimum threshold changes from experiment to experiment, but never changes from sample-to-sample within an experiment. From this point, only the pixels determined to be signal by the thresholding are included in further measurements. Only signal pixels within the region of interest designated in step (b) are used in the measurements. The fluorescence value of signal pixels within the region of interest is determined in ImageJ and imported into Microsoft Excel for tabulation. In addition, the area of the signal, which is given in pixels, is also imported into Microsoft Excel. For each sample, the total fluorescence value i.e. the integrated density is summed, as is the number of signal pixels. To determine the average signal brightness, the total integrated density of a sample is divided by the total signal area.

Count Puncta Number
Select region of axon where fluorescent sig

a

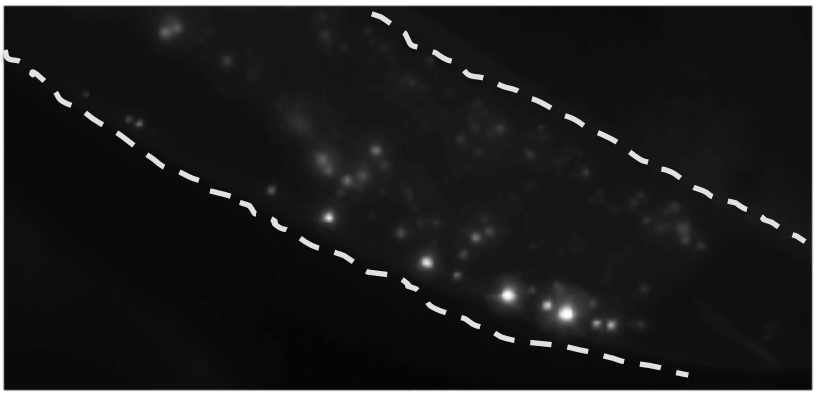

Measurement 1:
YFP::RAB-3 puncta counted by eye

b

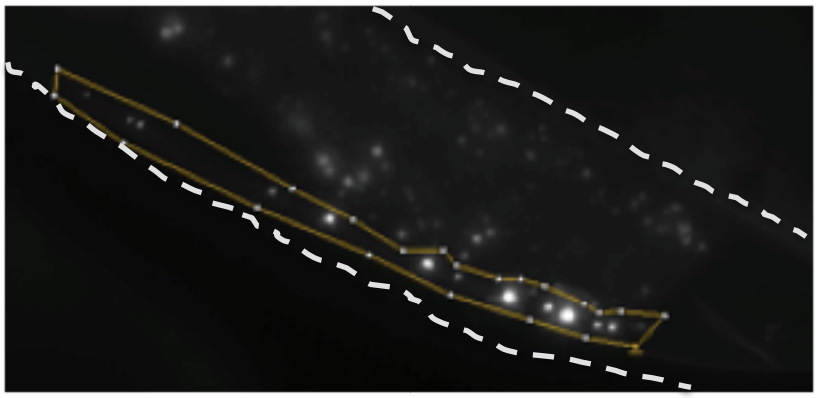

Select region of axon where fluorescent signal is.

c

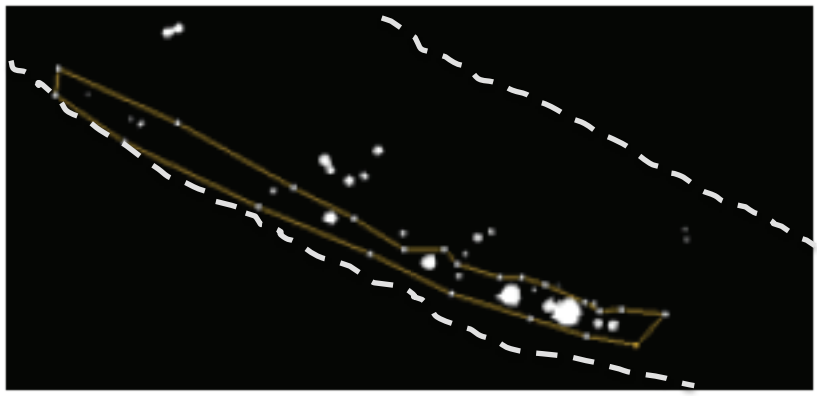

Threshold image:
White=Signal pixels
Black= background

Measurement 2:
Number of “signal” pixels
Measurement 3:
Sum of Fluorescence Value of “signal” pixels
Calculation:
Total Fluorescence divided by area of signal to give average signal brightness

Supplementary Figure 2

Supplementary Figure 3. Mutations in *snt-1* do not severely affect transcription in PQR (a) Average fluorescence of puncta in PQR, normalized to wildtype. (b) Average fluorescence of areas between puncta within PQR axon, normalized to wildtype. (c) Punctal fluorescence compared to background cord fluorescence, normalized to wildtype. d) Distribution of fluorescent puncta along region of interest in PQR, measured as density of puncta in region of interest. e) Width of puncta in PQR axon. (Figure generated by Jeremy Dittman)

PQR Summary

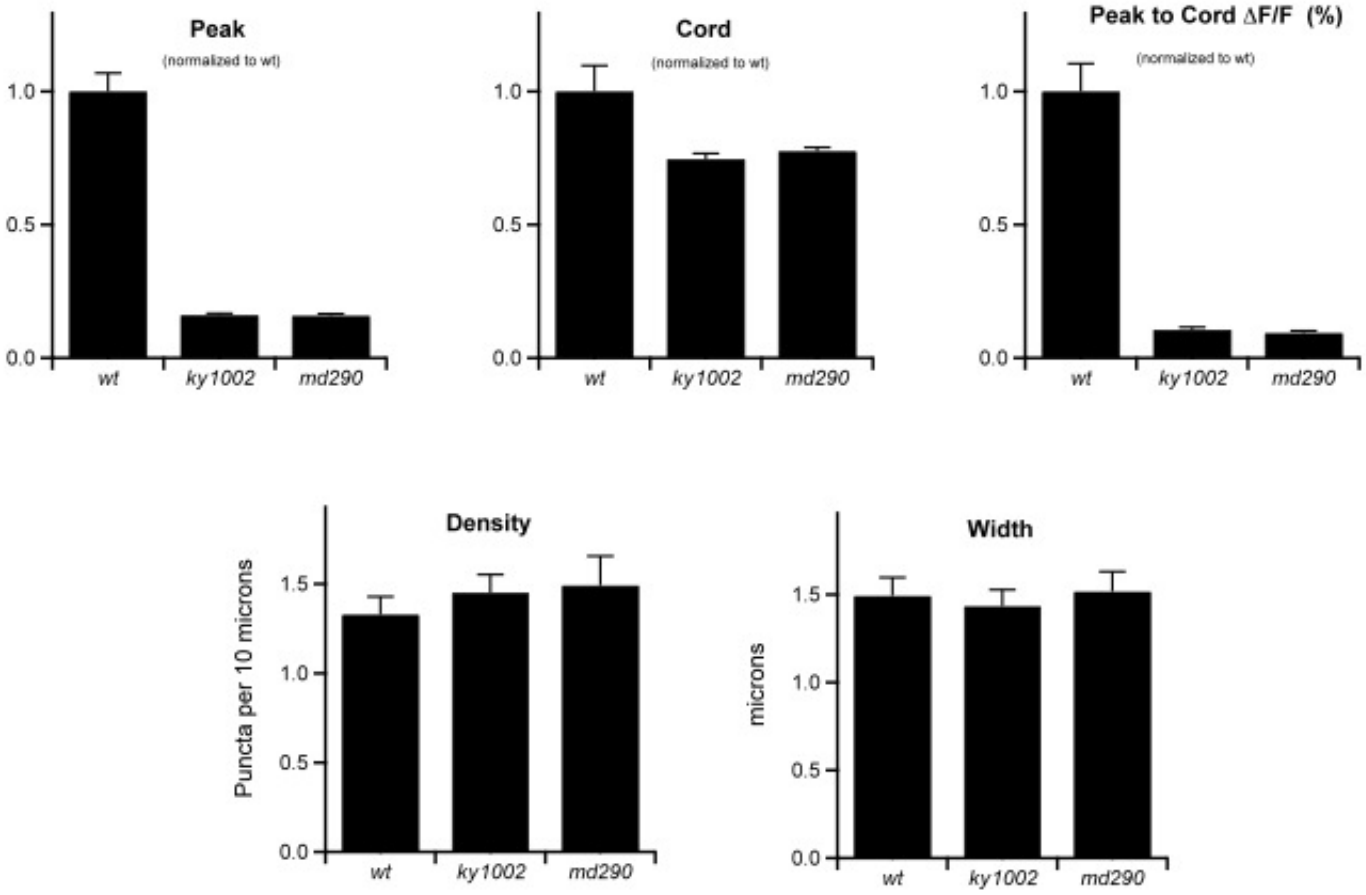
Peak
(normalized to wt)
1.0
0.5
0.0
wt
ky1002
md290
Cord
(normalized to wt)
1.0
0.5
0.0
wt
ky1002
md290
Peak to Cord ΔF/F (%)
(normalized to wt)
1.0
0.5
0.0
wt
ky1002
md290
Density
Puncta per 10 microns
1.5
1.0
0.5
0.0
wt
ky1002
md290
Width
microns
1.5
1.0
0.5
0.0
wt
ky1002
md290

Supplementary Figure 4. Some endocytosis mutants and exocytosis mutants show effects in mCherry::RAB-3 and GFP::UNC-2 fluorescence in AWC. (a) Total mCherry::RAB-3 fluorescence in the region of interest in AWC in each worm. (n.s. not statistically significant, t-test for *elks-1*; n.s. not statistically significant, Kruksal-Wallis ANOVA with Dunn's Multiple Comparisons Post Test for other mutants). (b) Total GFP::UNC-2 fluorescence in the region of interest in AWC in each worm. (*p<0.05 versus wildtype, t-test for *elks-1*; ***p<0.001 versus wildtype, *p<0.05 versus wildtype, and n.s. not statistically significant Kruksal-Wallis ANOVA with Dunn's Multiple Comparisons Post Test for other mutants). (c) Total fluorescence value divided by the number of pixels above the noise threshold, indicating the brightness of the fluorescent signal. (n.s. not statistically significant, t-test for *elks-1*; **p<0.01 versus wildtype and n.s. not statistically significant Kruksal-Wallis ANOVA with Dunn's Multiple Comparisons Post Test for other mutants). (d) Total fluorescence value divided by the number of pixels above the noise threshold, indicating the brightness of the fluorescent signal. (**p<0.01 versus wildtype and n.s. not statistically significant Kruksal-Wallis ANOVA with Dunn's Multiple Comparisons Post Test for all columns, each mutant compared to its wildtype counterpart). (e) Representation of mCherry::RAB-3 and GFP::UNC-2 puncta in AWC neuron, model of mCherry::RAB-3 associated with a synaptic vesicle, and model of UNC-2 subunit-containing voltage-gated calcium channel.

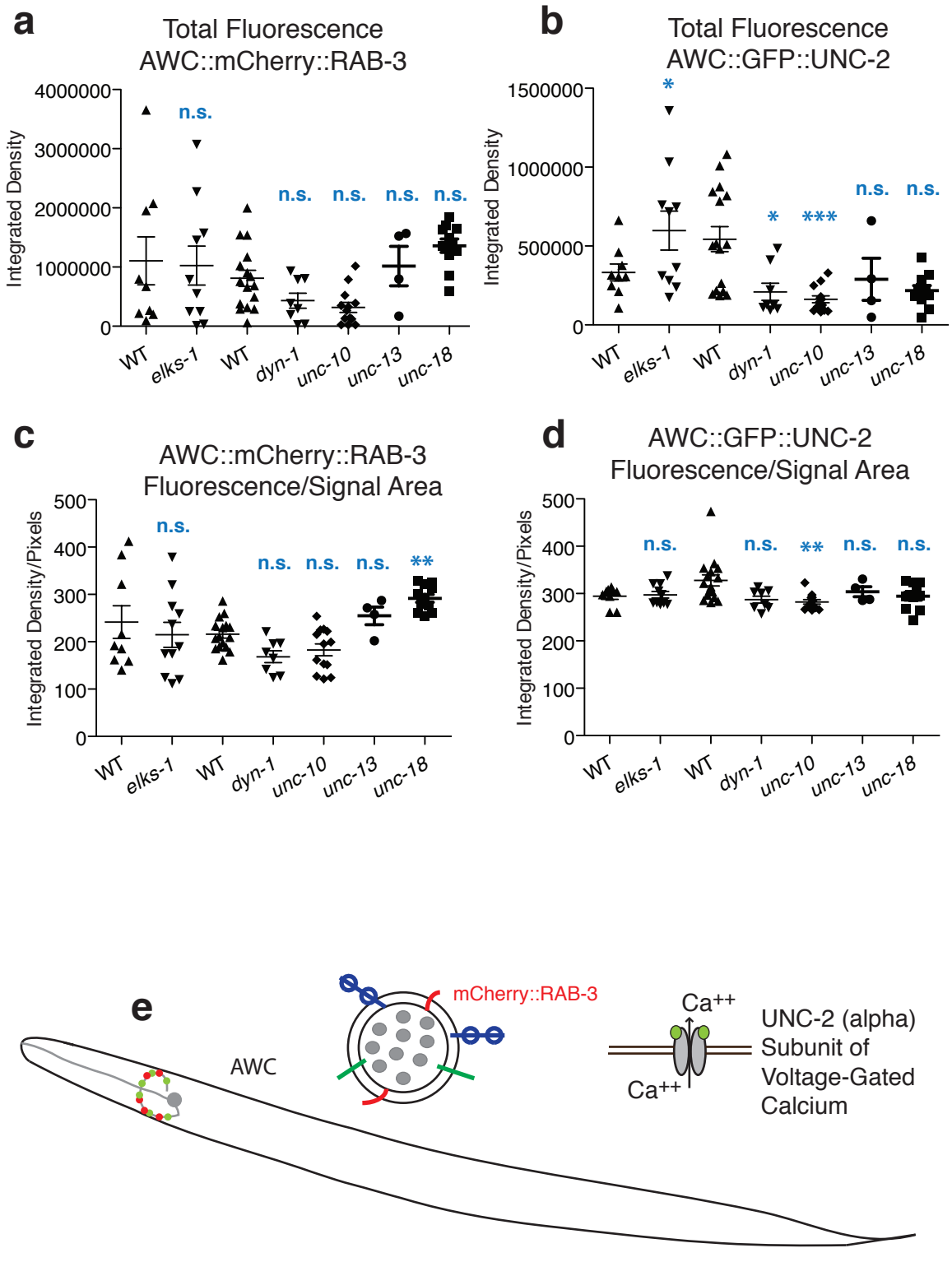

Supplementary Figure 4

References:

Abraham C, Bai L, Leube RE (2011) Synaptogyrin-dependent modulation of synaptic neurotransmission in Caenorhabditis elegans. Neuroscience 190:75-88.

Anderson P (1995) Mutagenesis. Methods in cell biology 48:31-58.

Arac D, Chen X, Khant HA, Ubach J, Ludtke SJ, Kikkawa M, Johnson AE, Chiu W, Sudhof TC, Rizo J (2006) Close membrane-membrane proximity induced by Ca(2+)-dependent multivalent binding of synaptotagmin-1 to phospholipids. Nature structural & molecular biology 13:209-217.

Arimoto M, Koushika SP, Choudhary BC, Li C, Matsumoto K, Hisamoto N (2011) The Caenorhabditis elegans JIP3 protein UNC-16 functions as an adaptor to link kinesin-1 with cytoplasmic dynein. The Journal of neuroscience : the official journal of the Society for Neuroscience 31:2216-2224.

Arthur CP, Dean C, Pagratis M, Chapman ER, Stowell MH (2010) Loss of synaptotagmin IV results in a reduction in synaptic vesicles and a distortion of the Golgi structure in cultured hippocampal neurons. Neuroscience 167:135-142.

Augustin I, Rosenmund C, Sudhof TC, Brose N (1999) Munc13-1 is essential for fusion competence of glutamatergic synaptic vesicles. Nature 400:457-461.

Augustine GJ, Santamaria F, Tanaka K (2003) Local calcium signaling in neurons. Neuron 40:331-346.

Avery L (1993) The genetics of feeding in Caenorhabditis elegans. Genetics 133:897-917.

Bai J, Hu Z, Dittman JS, Pym EC, Kaplan JM (2010) Endophilin functions as a membrane-bending molecule and is delivered to endocytic zones by exocytosis. Cell 143:430-441.

Balaji J, Armbruster M, Ryan TA (2008) Calcium control of endocytic capacity at a CNS synapse. The Journal of neuroscience : the official journal of the Society for Neuroscience 28:6742-6749.

Baram D, Adachi R, Medalia O, Tuvim M, Dickey BF, Mekori YA, Sagi-Eisenberg R(1999) Synaptotagmin II negatively regulates Ca2+-triggered exocytosis of lysosomes in mast cells. The Journal of experimental medicine 189:1649-1658.

Barclay JW, Morgan A, Burgoyne RD (2012) Neurotransmitter release mechanisms studied in Caenorhabditis elegans. Cell calcium.

Berton F, Cornet V, Iborra C, Garrido J, Dargent B, Fukuda M, Seagar M, Marqueze B (2000) Synaptotagmin I and IV define distinct populations of neuronal transport vesicles. The European journal of neuroscience 12:1294-1302.

Betz A, Okamoto M, Benseler F, Brose N (1997) Direct interaction of the rat unc-13 homologue Munc13-1 with the N terminus of syntaxin. The Journal of biological chemistry 272:2520-2526.

Blasi J, Chapman ER, Link E, Binz T, Yamasaki S, De Camilli P, Sudhof TC, Niemann H, Jahn R (1993) Botulinum neurotoxin A selectively cleaves the synaptic protein SNAP-25. Nature 365:160-163.

Blasi J, Chapman ER, Yamasaki S, Binz T, Niemann H, Jahn R (1993) Botulinum neurotoxin C1 blocks neurotransmitter release by means of cleaving HPC-1/syntaxin. The EMBO journal 12:4821-4828

Brenner S (1974) The genetics of Caenorhabditis elegans. Genetics 77:71-94.

Brodin L, Shupliakov O (2006) Giant reticulospinal synapse in lamprey: molecular links between active and periactive zones. Cell and tissue research 326:301-310.

Brose N, Hofmann K, Hata Y, Sudhof TC (1995) Mammalian homologues of Caenorhabditis elegans unc-13 gene define novel family of C2-domain proteins. The Journal of biological chemistry 270:25273-25280.

Brose N, Petrenko AG, Sudhof TC, Jahn R (1992) Synaptotagmin: a calcium sensor on the synaptic vesicle surface. Science 256:1021-1025.

Brose N, Rosenmund C, Rettig J (2000) Regulation of transmitter release by Unc-13 and its homologues. Current opinion in neurobiology 10:303-311.

Burkhardt P, Hattendorf DA, Weis WI, Fasshauer D (2008) Munc18a controls SNARE assembly through its interaction with the syntaxin N-peptide. The EMBO journal 27:923-933.

Burns DJ, Bell RM (1991) Protein kinase C contains two phorbol ester binding domains. The Journal of biological chemistry 266:18330-18338.

Cao P, Maximov A, Sudhof TC (2011) Activity-dependent IGF-1 exocytosis is controlled by the Ca(2+)-sensor synaptotagmin-10. Cell 145:300-311.

Ch'ng Q, Sieburth D, Kaplan JM (2008) Profiling synaptic proteins identifies regulators of insulin secretion and lifespan. PLoS genetics 4:e1000283.

Chicka MC, Hui E, Liu H, Chapman ER (2008) Synaptotagmin arrests the SNARE complex before triggering fast, efficient membrane fusion in response to Ca2+. Nature structural & molecular biology 15:827-835.

Craxton M (2001) Genomic analysis of synaptotagmin genes. Genomics 77:43-49.

Crump JG, Zhen M, Jin Y, Bargmann CI (2001) The SAD-1 kinase regulates presynaptic vesicle clustering and axon termination. Neuron 29:115-129.

de Wit H, Walter AM, Milosevic I, Gulyas-Kovacs A, Riedel D, Sorensen JB, Verhage M (2009) Synaptotagmin-1 docks secretory vesicles to syntaxin-1/SNAP-25 acceptor complexes. Cell 138:935-946.

Dean C, Dunning FM, Liu H, Bomba-Warczak E, Martens H, Bharat V, Ahmed S, Chapman ER (2012a) Axonal and dendritic synaptotagmin isoforms revealed by a pHluorin-syt functional screen. Molecular biology of the cell 23:1715-1727.

Dean C, Liu H, Dunning FM, Chang PY, Jackson MB, Chapman ER (2009) Synaptotagmin-IV modulates synaptic function and long-term potentiation by regulating BDNF release. Nature neuroscience 12:767-776.

Dean C, Liu H, Staudt T, Stahlberg MA, Vingill S, Buckers J, Kamin D, Engelhardt J, Jackson MB, Hell SW, Chapman ER (2012b) Distinct subsets of Syt-IV/BDNF vesicles are sorted to axons versus dendrites and recruited to synapses by activity. The Journal of neuroscience : the official journal of the Society for Neuroscience 32:5398-5413.

Deken SL, Vincent R, Hadwiger G, Liu Q, Wang ZW, Nonet ML (2005) Redundant localization mechanisms of RIM and ELKS in Caenorhabditis elegans. The Journal of neuroscience : the official journal of the Society for Neuroscience 25:5975-5983.

Diril MK, Wienisch M, Jung N, Klingauf J, Haucke V (2006) Stonin 2 is an AP-2-dependent endocytic sorting adaptor for synaptotagmin internalization and recycling. Developmental cell 10:233-244.

Dittman J, Ryan TA (2009) Molecular circuitry of endocytosis at nerve terminals. Annual review of cell and developmental biology 25:133-160.

Dittman JS, Kaplan JM (2006) Factors regulating the abundance and localization

of synaptobrevin in the plasma membrane. Proceedings of the National Academy of Sciences of the United States of America 103:11399-11404.

Feinberg EH, Vanhoven MK, Bendesky A, Wang G, Fetter RD, Shen K, Bargmann CI (2008) GFP Reconstitution Across Synaptic Partners (GRASP) defines cell contacts and synapses in living nervous systems. Neuron 57:353-363.

Fernandez-Alfonso T, Kwan R, Ryan TA (2006) Synaptic vesicles interchange their membrane proteins with a large surface reservoir during recycling. Neuron 51:179-186.

Fernandez-Alfonso T, Ryan TA (2008) A heterogeneous "resting" pool of synaptic vesicles that is dynamically interchanged across boutons in mammalian CNS synapses. Brain cell biology 36:87-100.

Fischer von Mollard G, Sudhof TC, Jahn R (1991) A small GTP-binding protein dissociates from synaptic vesicles during exocytosis. Nature 349:79-81.

Frank CA, Kennedy MJ, Goold CP, Marek KW, Davis GW (2006) Mechanisms underlying the rapid induction and sustained expression of synaptic homeostasis. Neuron 52:663-677.

Frank CA, Pielage J, Davis GW (2009) A presynaptic homeostatic signaling system composed of the Eph receptor, ephexin, Cdc42, and CaV2.1 calcium channels. Neuron 61:556-569.

Fukuda M, Ibata K, Mikoshiba K (2001) A unique spacer domain of synaptotagmin IV is essential for Golgi localization. Journal of neurochemistry 77:730-740.

Fukuda M, Kanno E, Mikoshiba K (1999) Conserved N-terminal cysteine motif is essential for homo- and heterodimer formation of synaptotagmins III, V, VI, and X. The Journal of biological chemistry 274:31421-31427.

Gauer JW, Sisk R, Murphy JR, Jacobson H, Sutton RB, Gillispie GD, Hinderliter A (2012) Mechanism for calcium ion sensing by the C2A domain of synaptotagmin I. Biophysical journal 103:238-246.

Geppert M, Goda Y, Hammer RE, Li C, Rosahl TW, Stevens CF, Sudhof TC (1994) Synaptotagmin I: a major Ca2+ sensor for transmitter release at a central synapse. Cell 79:717-727.

Gracheva EO, Maryon EB, Berthelot-Grosjean M, Richmond JE (2010)

Differential Regulation of Synaptic Vesicle Tethering and Docking by UNC-18 and TOM-1. Frontiers in synaptic neuroscience 2:141.

Graham ME, Handley MT, Barclay JW, Ciufo LF, Barrow SL, Morgan A, Burgoyne RD (2008) A gain-of-function mutant of Munc18-1 stimulates secretory granule recruitment and exocytosis and reveals a direct interaction of Munc18-1 with Rab3. The Biochemical journal 409:407-416.

Gu M, Schuske K, Watanabe S, Liu Q, Baum P, Garriga G, Jorgensen EM (2008) Mu2 adaptin facilitates but is not essential for synaptic vesicle recycling in Caenorhabditis elegans. The Journal of cell biology 183:881-892.

Hall DH, Hedgecock EM (1991) Kinesin-related gene unc-104 is required for axonal transport of synaptic vesicles in C. elegans. Cell 65:837-847.

Hammarlund M, Palfreyman MT, Watanabe S, Olsen S, Jorgensen EM (2007) Open syntaxin docks synaptic vesicles. PLoS biology 5:e198.

Han W, Rhee JS, Maximov A, Lin W, Hammer RE, Rosenmund C, Sudhof TC (2005) C-terminal ECFP fusion impairs synaptotagmin 1 function: crowding out synaptotagmin 1. The Journal of biological chemistry 280:5089-5100.

Harris TW, Hartwieg E, Horvitz HR, Jorgensen EM (2000) Mutations in synaptojanin disrupt synaptic vesicle recycling. The Journal of cell biology 150:589-600.

Harris TW, Schuske K, Jorgensen EM (2001) Studies of synaptic vesicle endocytosis in the nematode C. elegans. Traffic 2:597-605.

Hata Y, Slaughter CA, Sudhof TC (1993) Synaptic vesicle fusion complex contains unc-18 homologue bound to syntaxin. Nature 366:347-351.

Hosono R, Kamiya Y (1991) Additional genes which result in an elevation of acetylcholine levels by mutations in Caenorhabditis elegans. Neuroscience letters 128:243-244.

Hui E, Bai J, Wang P, Sugimori M, Llinas RR, Chapman ER (2005) Three distinct kinetic groupings of the synaptotagmin family: candidate sensors for rapid and delayed exocytosis. Proceedings of the National Academy of Sciences of the United States of America 102:5210-5214.

Ibata K, Fukuda M, Hamada T, Kabayama H, Mikoshiba K (2000) Synaptotagmin IV is present at the Golgi and distal parts of neurites. Journal of neurochemistry 74:518-526.

Jahn R, Fasshauer D (2012) Molecular machines governing exocytosis of synaptic vesicles. Nature 490:201-207.

Jakubowski J, Kornfeld K (1999) A local, high-density, single-nucleotide polymorphism map used to clone Caenorhabditis elegans cdf-1. Genetics 153:743-752.

Jorgensen EM, Hartwieg E, Schuske K, Nonet ML, Jin Y, Horvitz HR (1995) Defective recycling of synaptic vesicles in synaptotagmin mutants of Caenorhabditis elegans. Nature 378:196-199.

Jung N, Wienisch M, Gu M, Rand JB, Muller SL, Krause G, Jorgensen EM, Klingauf J, Haucke V (2007) Molecular basis of synaptic vesicle cargo recognition by the endocytic sorting adaptor stonin 2. The Journal of cell biology 179:1497-1510.

Kaibuchi K, Fukumoto Y, Oku N, Takai Y, Arai K, Muramatsu M (1989) Molecular genetic analysis of the regulatory and catalytic domains of protein kinase C. The Journal of biological chemistry 264:13489-13496.

Kee Y, Scheller RH (1996) Localization of synaptotagmin-binding domains on syntaxin. The Journal of neuroscience : the official journal of the Society for Neuroscience 16:1975-1981.

Kim JS, Lilley BN, Zhang C, Shokat KM, Sanes JR, Zhen M (2008) A chemical-genetic strategy reveals distinct temporal requirements for SAD-1 kinase in neuronal polarization and synapse formation. Neural development 3:23.

Kim JY, Choi BK, Choi MG, Kim SA, Lai Y, Shin YK, Lee NK (2012) Solution single- vesicle assay reveals PIP2-mediated sequential actions of synaptotagmin-1 on SNAREs. The EMBO journal 31:2144-2155.

Koch M, Holt M (2012) Coupling exo- and endocytosis: An essential role for PIP(2) at the synapse. Biochimica et biophysica acta 1821:1114-1132.

Koushika SP, Richmond JE, Hadwiger G, Weimer RM, Jorgensen EM, Nonet ML (2001) A post-docking role for active zone protein Rim. Nature neuroscience 4:997-1005.

Koushika SP, Schaefer AM, Vincent R, Willis JH, Bowerman B, Nonet ML (2004) Mutations in Caenorhabditis elegans cytoplasmic dynein components reveal specificity of neuronal retrograde cargo. The Journal of neuroscience : the official journal of the Society for Neuroscience 24:3907-3916.

Lee HK, Yang Y, Su Z, Hyeon C, Lee TS, Lee HW, Kweon DH, Shin YK, Yoon TY (2010) Dynamic Ca2+-dependent stimulation of vesicle fusion by membrane-anchored synaptotagmin 1. Science 328:760-763.

Li C, Ullrich B, Zhang JZ, Anderson RG, Brose N, Sudhof TC (1995) Ca(2+)-dependent and -independent activities of neural and non-neural synaptotagmins. Nature 375:594-599.

Liewald JF, Brauner M, Stephens GJ, Bouhours M, Schultheis C, Zhen M, Gottschalk A (2008) Optogenetic analysis of synaptic function. Nature methods 5:895-902.

Link E, Edelmann L, Chou JH, Binz T, Yamasaki S, Eisel U, Baumert M, Sudhof TC, Niemann H, Jahn R (1992) Tetanus toxin action: inhibition of neurotransmitter release linked to synaptobrevin proteolysis. Biochemical and biophysical research communications 189:1017-1023.

Littleton JT, Bellen HJ, Perin MS (1993a) Expression of synaptotagmin in Drosophila reveals transport and localization of synaptic vesicles to the synapse. Development 118:1077-1088.

Littleton JT, Stern M, Perin M, Bellen HJ (1994) Calcium dependence of neurotransmitter release and rate of spontaneous vesicle fusions are altered in Drosophila synaptotagmin mutants. Proceedings of the National Academy of Sciences of the United States of America 91:10888-10892.

Littleton JT, Stern M, Schulze K, Perin M, Bellen HJ (1993b) Mutational analysis of Drosophila synaptotagmin demonstrates its essential role in Ca(2+)-activated neurotransmitter release. Cell 74:1125-1134.

Lonart G, Sudhof TC (2000) Assembly of SNARE core complexes prior to neurotransmitter release sets the readily releasable pool of synaptic vesicles. The Journal of biological chemistry 275:27703-27707.

Mackler JM, Drummond JA, Loewen CA, Robinson IM, Reist NE (2002) The C(2)B Ca(2+)-binding motif of synaptotagmin is required for synaptic transmission in vivo. Nature 418:340-344.

Madison JM, Nurrish S, Kaplan JM (2005) UNC-13 interaction with syntaxin is required for synaptic transmission. Current biology : CB 15:2236-2242.

Maruyama IN, Brenner S (1991) A phorbol ester/diacylglycerol-binding protein encoded by the unc-13 gene of Caenorhabditis elegans. Proceedings of the

National Academy of Sciences of the United States of America 88:5729-5733.

Mathews EA, Mullen GP, Crowell JA, Duerr JS, McManus JR, Duke A, Gaskin J, Rand JB (2007) Differential expression and function of synaptotagmin 1 isoforms in Caenorhabditis elegans. Molecular and cellular neurosciences 34:642-652.

Matteoli M, Takei K, Cameron R, Hurlbut P, Johnston PA, Sudhof TC, Jahn R, De Camilli P (1991) Association of Rab3A with synaptic vesicles at late stages of the secretory pathway. The Journal of cell biology 115:625-633.

Meinrenken CJ, Borst JG, Sakmann B (2003) Local routes revisited: the space and time dependence of the Ca2+ signal for phasic transmitter release at the rat calyx of Held. The Journal of physiology 547:665-689.

Mendez JA, Bourque MJ, Fasano C, Kortleven C, Trudeau LE (2011) Somatodendritic dopamine release requires synaptotagmin 4 and 7 and the participation of voltage-gated calcium channels. The Journal of biological chemistry 286:23928-23937.

Miesenbock G, De Angelis DA, Rothman JE (1998) Visualizing secretion and synaptic transmission with pH-sensitive green fluorescent proteins. Nature 394:192-195.

Miller KG, Alfonso A, Nguyen M, Crowell JA, Johnson CD, Rand JB (1996) A genetic selection for Caenorhabditis elegans synaptic transmission mutants. Proceedings of the National Academy of Sciences of the United States of America 93:12593-12598.

Misura KM, Scheller RH, Weis WI (2000) Three-dimensional structure of the neuronal-Sec1-syntaxin 1a complex. Nature 404:355-362.

Mullen GP, Grundahl KM, Gu M, Watanabe S, Hobson RJ, Crowell JA, McManus JR, Mathews EA, Jorgensen EM, Rand JB (2012) UNC-41/Stonin Functions with AP2 to Recycle Synaptic Vesicles in Caenorhabditis elegans. PloS one 7:e40095.

Nagai Y, Tadokoro S, Sakiyama H, Hirashima N (2011) Effects of synaptotagmin 2 on membrane fusion between liposomes that contain SNAREs involved in exocytosis in mast cells. Biochimica et biophysica acta 1808:2435-2439.

Nakhost A, Houeland G, Blandford VE, Castellucci VF, Sossin WS (2004) Identification and characterization of a novel C2B splice variant of synaptotagmin I. Journal of neurochemistry 89:354-363.

Neher E (1998) Vesicle pools and Ca2+ microdomains: new tools for understanding their roles in neurotransmitter release. Neuron 20:389-399.

Nonet ML (1999) Visualization of synaptic specializations in live C. elegans with synaptic vesicle protein-GFP fusions. Journal of neuroscience methods 89:33-40.

Nonet ML, Grundahl K, Meyer BJ, Rand JB (1993) Synaptic function is impaired but not eliminated in C. elegans mutants lacking synaptotagmin. Cell 73:1291-1305.

Nonet ML, Saifee O, Zhao H, Rand JB, Wei L (1998) Synaptic transmission deficits in Caenorhabditis elegans synaptobrevin mutants. The Journal of neuroscience : the official journal of the Society for Neuroscience 18:70-80.

Nonet ML, Staunton JE, Kilgard MP, Fergestad T, Hartwieg E, Horvitz HR, Jorgensen EM, Meyer BJ (1997) Caenorhabditis elegans rab-3 mutant synapses exhibit impaired function and are partially depleted of vesicles. The Journal of neuroscience : the official journal of the Society for Neuroscience 17:8061-8073.

Pang ZP, Shin OH, Meyer AC, Rosenmund C, Sudhof TC (2006) A gain-of-function mutation in synaptotagmin-1 reveals a critical role of Ca2+-dependent soluble N-ethylmaleimide-sensitive factor attachment protein receptor complex binding in synaptic exocytosis. The Journal of neuroscience : the official journal of the Society for Neuroscience 26:12556-12565.

Pang ZP, Sudhof TC (2010) Cell biology of Ca2+-triggered exocytosis. Current opinion in cell biology 22:496-505.

Parisotto D, Malsam J, Scheutzow A, Krause JM, Sollner TH (2012) SNAREpin assembly by Munc18-1 requires previous vesicle docking by synaptotagmin 1. The Journal of biological chemistry 287:31041-31049.

Perin MS, Johnston PA, Ozcelik T, Jahn R, Francke U, Sudhof TC (1991) Structural and functional conservation of synaptotagmin (p65) in Drosophila and humans. The Journal of biological chemistry 266:615-622.

Pieribone VA, Shupliakov O, Brodin L, Hilfiker-Rothenfluh S, Czernik AJ, Greengard P (1995) Distinct pools of synaptic vesicles in neurotransmitter release. Nature 375:493-497.

Piggott BJ, Liu J, Feng Z, Wescott SA, Xu XZ (2011) The neural circuits and synaptic mechanisms underlying motor initiation in C. elegans. Cell 147:922-933.

Raizen DM, Lee RY, Avery L (1995) Interacting genes required for pharyngeal excitation by motor neuron MC in Caenorhabditis elegans. Genetics 141:1365-1382.

Rand, J.B. Acetylcholine (January 30, 2007), *WormBook*, ed. The *C. elegans* Research Community, WormBook, doi/10.1895/wormbook.1.131.1, http://www.wormbook.org.

Richmond, J. Synaptic function (December 7, 2007), *WormBook*, ed. The *C. elegans* Research Community, WormBook, doi/10.1895/wormbook.1.69.1, http://www.wormbook.org.

Richmond JE, Davis WS, Jorgensen EM (1999) UNC-13 is required for synaptic vesicle fusion in C. elegans. Nature neuroscience 2:959-964.

Ringstad N, Nemoto Y, De Camilli P (1997) The SH3p4/Sh3p8/SH3p13 protein family: binding partners for synaptojanin and dynamin via a Grb2-like Src homology 3 domain. Proceedings of the National Academy of Sciences of the United States of America 94:8569-8574.

Robinson IM, Ranjan R, Schwarz TL (2002) Synaptotagmins I and IV promote transmitter release independently of Ca(2+) binding in the C(2)A domain. Nature 418:336-340.

Sara Y, Virmani T, Deak F, Liu X, Kavalali ET (2005) An isolated pool of vesicles recycles at rest and drives spontaneous neurotransmission. Neuron 45:563-573.

Sarov M, Murray JI, Schanze K, Pozniakovski A, Niu W, Angermann K, Hasse S, Rupprecht M, Vinis E, Tinney M, Preston E, Zinke A, Enst S, Teichgraber T, Janette J, Reis K, Janosch S, Schloissnig S, Ejsmont RK, Slightam C, Xu X, Kim SK, Reinke V, Stewart AF, Snyder M, Waterston RH, Hyman AA (2012) A genome-scale resource for in vivo tag-based protein function exploration in C. elegans. Cell 150:855-866.

Schafer WR, Kenyon CJ (1995) A calcium-channel homologue required for adaptation to dopamine and serotonin in Caenorhabditis elegans. Nature 375:73-78.

Schiavo G, Benfenati F, Poulain B, Rossetto O, Polverino de Laureto P, DasGupta BR, Montecucco C (1992) Tetanus and botulinum-B neurotoxins block neurotransmitter release by proteolytic cleavage of synaptobrevin. Nature 359:832-835.

Schiavo G, Gmachl MJ, Stenbeck G, Sollner TH, Rothman JE (1995) A possible

docking and fusion particle for synaptic transmission. Nature 378:733-736.

Schuske KR, Richmond JE, Matthies DS, Davis WS, Runz S, Rube DA, van der Bliek AM, Jorgensen EM (2003) Endophilin is required for synaptic vesicle endocytosis by localizing synaptojanin. Neuron 40:749-762.

Sieburth D, Ch'ng Q, Dybbs M, Tavazoie M, Kennedy S, Wang D, Dupuy D, Rual JF, Hill DE, Vidal M, Ruvkun G, Kaplan JM (2005) Systematic analysis of genes required for synapse structure and function. Nature 436:510-517.

Sollner T, Bennett MK, Whiteheart SW, Scheller RH, Rothman JE (1993) A protein assembly-disassembly pathway in vitro that may correspond to sequential steps of synaptic vesicle docking, activation, and fusion. Cell 75:409-418.

Stahl B, Chou JH, Li C, Sudhof TC, Jahn R (1996) Rab3 reversibly recruits rabphilin to synaptic vesicles by a mechanism analogous to raf recruitment by ras. The EMBO journal 15:1799-1809.

Staunton J, Ganetzky B, Nonet ML (2001) Rabphilin potentiates soluble N-ethylmaleimide sensitive factor attachment protein receptor function independently of rab3. The Journal of neuroscience : the official journal of the Society for Neuroscience 21:9255-9264.

Steger KA, Shtonda BB, Thacker C, Snutch TP, Avery L (2005) The C. elegans T- type calcium channel CCA-1 boosts neuromuscular transmission. The Journal of experimental biology 208:2191-2203.

Stevens CF, Tsujimoto T (1995) Estimates for the pool size of releasable quanta at a single central synapse and for the time required to refill the pool. Proceedings of the National Academy of Sciences of the United States of America 92:846-849.

Sudhof TC (2012a) Calcium control of neurotransmitter release. Cold Spring Harbor perspectives in biology 4:a011353.

Sudhof TC (2012b) The presynaptic active zone. Neuron 75:11-25.

Sudhof TC, Rizo J (2011) Synaptic vesicle exocytosis. Cold Spring Harbor perspectives in biology 3.

Sudhof TC, Rothman JE (2009) Membrane fusion: grappling with SNARE and SM proteins. Science 323:474-477.

Sugita S, Shin OH, Han W, Lao Y, Sudhof TC (2002) Synaptotagmins form a

hierarchy of exocytotic Ca(2+) sensors with distinct Ca(2+) affinities. The EMBO journal 21:270-280.

Sutton RB, Davletov BA, Berghuis AM, Sudhof TC, Sprang SR (1995) Structure of the first C2 domain of synaptotagmin I: a novel Ca2+/phospholipid-binding fold. Cell 80:929-938.

Sutton RB, Ernst JA, Brunger AT (1999) Crystal structure of the cytosolic C2A-C2B domains of synaptotagmin III. Implications for Ca(+2)-independent snare complex interaction. The Journal of cell biology 147:589-598.

Troulinaki K, Tavernarakis N (2012) Endocytosis and intracellular trafficking contribute to necrotic neurodegeneration in C. elegans. The EMBO journal 31:654-666.

van den Bogaart G, Meyenberg K, Diederichsen U, Jahn R (2012) Phosphatidylinositol 4,5-bisphosphate increases Ca2+ affinity of synaptotagmin-1 by 40-fold. The Journal of biological chemistry 287:16447-16453.

von Poser C, Ichtchenko K, Shao X, Rizo J, Sudhof TC (1997) The evolutionary pressure to inactivate. A subclass of synaptotagmins with an amino acid substitution that abolishes Ca2+ binding. The Journal of biological chemistry 272:14314-14319.

Wang CT, Grishanin R, Earles CA, Chang PY, Martin TF, Chapman ER, Jackson MB (2001) Synaptotagmin modulation of fusion pore kinetics in regulated exocytosis of dense-core vesicles. Science 294:1111-1115.

Weimer RM, Richmond JE (2005) Synaptic vesicle docking: a putative role for the Munc18/Sec1 protein family. Current topics in developmental biology 65:83-113.

Weimer RM, Richmond JE, Davis WS, Hadwiger G, Nonet ML, Jorgensen EM (2003) Defects in synaptic vesicle docking in unc-18 mutants. Nature neuroscience 6:1023-1030.

White JG, Southgate E, Thomson JN, Brenner S (1986) The structure of the nervous system of the nematode Caenorhabditis elegans. Philosophical transactions of the Royal Society of London Series B, Biological sciences 314:1-340.

Xu J, Mashimo T, Sudhof TC (2007) Synaptotagmin-1, -2, and -9: Ca(2+) sensors for fast release that specify distinct presynaptic properties in subsets of neurons. Neuron 54:567-581.

Xue M, Craig TK, Shin OH, Li L, Brautigam CA, Tomchick DR, Sudhof TC, Rosenmund C, Rizo J (2010) Structural and mutational analysis of functional differentiation between synaptotagmins-1 and -7. PloS one 5.

Xue L, Zhang Z, McNeil BD, Luo F, Wu XS, Sheng J, Shin W, Wu LG (2012) Voltage-dependent calcium channels at the plasma membrane, but not vesicular channels, couple exocytosis to endocytosis. Cell reports 1:632-638.

Yao J, Kwon SE, Gaffaney JD, Dunning FM, Chapman ER (2012) Uncoupling the roles of synaptotagmin I during endo- and exocytosis of synaptic vesicles. Nature neuroscience 15:243-249.

Yao LH, Rao Y, Varga K, Wang CY, Xiao P, Lindau M, Gong LW (2012) Synaptotagmin 1 is necessary for the Ca2+ dependence of clathrin-mediated endocytosis. The Journal of neuroscience : the official journal of the Society for Neuroscience 32:3778-3785.

Zhang G, Bai H, Zhang H, Dean C, Wu Q, Li J, Guariglia S, Meng Q, Cai D (2011a) Neuropeptide exocytosis involving synaptotagmin-4 and oxytocin in hypothalamic programming of body weight and energy balance. Neuron 69:523-535.

Zhang JZ, Davletov BA, Sudhof TC, Anderson RG (1994) Synaptotagmin I is a high affinity receptor for clathrin AP-2: implications for membrane recycling. Cell 78:751-760.

Zhang X, Rizo J, Sudhof TC (1998) Mechanism of phospholipid binding by the C2A- domain of synaptotagmin I. Biochemistry 37:12395-12403.

Zhang Y, Kubiseski TJ (2010) Caenorhabditis elegans wsp-1 regulation of synaptic function at the neuromuscular junction. The Journal of biological chemistry 285:23040-23046.

Zhang Z, Wu Y, Wang Z, Dunning FM, Rehfuss J, Ramanan D, Chapman ER, Jackson MB (2011b) Release mode of large and small dense-core vesicles specified by different synaptotagmin isoforms in PC12 cells. Molecular biology of the cell 22:2324-2336.